

Development of Screening Platforms  
for Discovery of Ice Nucleators

by

Yuki Kamijo

A thesis submitted in partial fulfillment of the requirements for the degree of

Master of Science

Department of Chemistry  
University of Alberta

© Yuki Kamijo, 2019

## **Abstract**

In this thesis, I describe the development and demonstration of a screening platform for the discovery of ice-nucleators. Ice nucleating agents (INAs) have been used to control the temperature of ice nucleation within a narrow range at high temperature. They play an important role in atmospheric ice formation and plant pathogenesis. However, the relationship between surface chemical structure and ice nucleation activity remains elusive. In the first chapter of this thesis, I briefly reviewed the current INA study and its experimental methods, and challenges.

The primary focus within Chapter 2 is the development of Freeze-float selection system that is designed to screen the stronger ice-nucleating substances by buoyancy-based separation. This system employed the density-based separation of the sample encapsulated into droplets, so that allows the identification of the molecules that can cause ice-nucleation at different temperatures and separate from others. The system showed the correlation of the droplet freezing temperature and the INA concentration of the sample droplets.

To extend the screening system of the freeze-float selection and improve the efficiencies and accuracies, in Chapter 3, I investigated the introduction of automated droplets generation system and uniform controlled-rate cooling system to the freeze-float selection. The new platform successfully improved the capacity of the droplet numbers (from 50 to theoretically 1920 droplets) and sample numbers (from 1 cuvette to 48 vials) that can be tested at once. To confirm the accuracy of

the screening system, I investigated the detection threshold of the INA concentration. At the threshold concentration, controlled-rate cooling system showed better differentiation accuracies ( $p = 4.4 \times 10^{-7}$ ) compared to the commodity freezer ( $p = 0.83$ ). The enlarged screening setup can lead to comprehensive research for the ice-binding study.

Finally, I described the screening of ice-binding glycans by combining ice-affinity purification technique “ice-shell purification” and genetically-encoded glycan library; Liquid glycan array. The glycan library was screened and separated into the ice-included and ice-excluded phase and the ice enriched glycans were identified by the deep-sequencing. Further validation of the potential hit was done by plaque forming assay of the colorimetric phage. This platform will complement with different genetically modified library to identify ice-binding molecules.

In summary, I tested a methodology to screen the ice-binding glycans that were chemically conjugated to phage. The LiGA array of genetically encoded glycans permitted the screening against immobilized and slowly growing ice surface. We showed the first demonstration of the ice-binding glycan screening result analysis and validation test of the LiGA. However the screening validation results were not reproducible, and hit discovery was inconclusive. Further optimization of the screening platform or library with different glycan modification is needed. Although the result was inconclusive, preliminary screening of ice-binding protein demonstrated the feasibility of affinity-based screening. I believe

this platform can be easily adapted for the screening of different modifications, genetically-encoded libraries for further ice-binding molecule discoveries.

## Preface

**Chapter 1** is an original brief review of current ice nucleator study and the methods, and has not been published. I reviewed the current ice-nucleator studies, wrote the manuscript and created the figures and tables with advice from R. Derda.

**Chapter 2** is based on published work from Y. Kamijo and R. Derda, “Freeze–Float Selection of Ice Nucleators”, *Langmuir* 2019, 35 (2), 359-364. R. Derda initiated the project and I was responsible for the optimization and validation of the selection system.

**Chapter 3** is based on non-published work initiated by R. Derda. I was responsible for collecting and organizing the experimental data as well as modification of the system and validation test. The operation program directing the Biomek 3000 was written by Mr. Troy Locke in Molecular Biology Service Unit.

**Chapter 4** is based on non-published work initiated by R. Derda. J. Wickware optimized the Ice-shell purification screening condition, and purified AFP-GFP. I was responsible for optimization of Liquid Glycan Array screening conditions, optimization of DNA extraction and PCR conditions, data analysis, with advice from R. Derda. I am also responsible for the chemical modification of glycans on phage, and validation of the selected glycans based on the screenings. J. Maghera developed and constructed the Liquid Glycan Array. S. Sarkar, J. Maghera and M. Sojitra isolated, amplified and glycosylated the phage clones. M. Sojitra

constructed the R script for the sequencing visualization script. N. Bennet cloned and amplified fluorescent phage clones mNeonGreen and mCherry.

## Acknowledgements

I am deeply thankful to my supervisor, Professor Ratmir Derda for accepting me in his group, and his continuous support and guidance throughout my research. He is the most enthusiastic, knowledgeable and inspiring person in my life, and he provided me a good basis for my research career.

I am thankful to Professor Robert Campbell and Professor Jed Harrison for being my committee members and for providing constructive advice during my program. I would also like to thank Professor Peichun Amy Tsai for accepting being arm's length examiner.

I would like to thank Professor Steven Lindow at the University of California, Berkeley for the sample of *P. syringae* and generous advice on the INA experiment. I am thankful to Jessica Wickware, who has initiated this INA screening project and gave me critical advices. I am thankful to Professor Bart Hazes in Department of Biochemistry at University of Alberta for advice on the *P. syringae* ice nucleating protein.

I would like to acknowledge the fellowship support from the Faculty of Graduate Studies and Research from the University of Alberta, and financial support from my advisor Ratmir Derda. This accomplishment would not have been possible without these supports.

I would like to express my sincere gratitude to my colleagues and my friends who have supported me and given me a lot of encouragement during my years.

Finally, I want to thank all my family members, my mother Atsuko, my sister Rina, my grandmother Setsuko, and my grandfather Kenji, for their continuous supports and encouragements. I owe everything to my family for giving me the opportunities and experiences that have made me who I am.



## Table of Contents

Abstract.....	ii
Preface.....	v
Acknowledgements.....	vii
Table of Contents.....	ix
List of Tables.....	xii
List of Figures.....	xiii
List of Abbreviations.....	xv
Chapter 1: Introduction.....	1
1.1 Physical Foundation of Homogeneous and Heterogeneous Ice Nucleation.....	1
1.2 Ice nucleators.....	6
1.2.1 Organic and inorganic molecules.....	8
1.2.2 Ice nucleating protein.....	9
1.3 Application of Ice-nucleators.....	14
1.4 Current methods to study ice-nucleators.....	17
1.4.1 Microscopic method.....	17
1.4.2 Cloud Chambers.....	18
1.4.3 Continuous Flow Diffusion Chamber.....	18
1.4.4 Droplets freezing assay.....	19
1.4.5 Molecular dynamics simulation.....	20
1.5 Tools for molecular studies of Ice-binders.....	21
1.5.1 Splat assay.....	22
1.5.2 Nanoliter osmometer.....	23
1.5.3 Ice affinity purification.....	23
1.6 Thesis overview.....	25
Chapter 2: Freeze-float selection of Ice nucleator.....	27
2.1 Introduction.....	27
2.2 Experimental Design.....	30
2.3 Results and discussion.....	32
2.3.1 Establishment of Freeze-float selection system.....	32

2.3.2. Statistical testing of Freeze-float selection .....	38
2.3.3. Freeze-float selection validation testing .....	41
2.4 Conclusions.....	44
2.5 Experimental procedures .....	47
2.5.1 Materials and general information.....	47
2.5.2 Freeze-float selection system in organic buoyant layer.....	47
2.5.3 Freeze-float selection system in silicone oil buoyant layer.....	48
2.5.4 Freeze-float selection procedure.....	48
2.5.5 Monitoring of the temperature of freeze-float system.....	49
2.5.6 Thermal gradient simulation calculation .....	49
2.5.7 Culture of <i>P. syringae</i> .....	50
2.5.8 Validation testing of the Freeze-float selection.....	51
Chapter 3: System for achieving enhanced throughput and quality for Freeze-float selection .....	52
3.1 Introduction.....	52
3.2 Experimental Design.....	54
3.3 Results and Discussion .....	57
3.3.1 Automated droplets generation.....	57
3.3.2 Asymptote VIA freezer.....	65
3.4 Conclusion .....	69
3.5 Experimental Procedures .....	72
3.5.1 Materials and general information.....	72
3.5.2 Automated droplets generation and droplet dispersion measurement.....	72
3.5.3 Asymptote VIA Freezer Freeze-float system .....	73
Chapter 4: Selection of the Ice-binding Glycans using Genetically Encoded Fragment-based Discovery by Ice Affinity Purification.....	75
4.1 Introduction.....	75
4.2 Experimental design.....	77
4.3 Results and Discussion .....	80
4.3.1 Validation of Ice shell screening.....	80
4.3.2 Screening assay to select ice-binding carbohydrate.....	82

4.3.3 Analysis of Illumina sequencing.....	82
4.3.4 Validation of the potential hit .....	89
4.4 Conclusion .....	92
4.5 Experimental procedures .....	93
4.5.1 Materials and general information.....	93
4.5.2 Ice-shell purification validation test using AFP-GFP .....	94
4.5.2.1 Amplification of AFP-GFP (performed by J. Wickware) .....	94
4.5.2.2 Purification of AFP-GFP (performed by J. Wickware).....	94
4.5.2.3 Ice-shell screening procedure .....	95
4.5.3 LiGA construction .....	96
4.5.4 Ice-shell purification of ice-binding glycans .....	100
4.5.5 Preparation for Illumina sequencing.....	101
4.5.6 Analysis of the deep-sequencing data.....	102
4.5.7 Construction of glycan modified phage.....	102
4.5.8 Construction of glycan modified mCherry phage.....	103
4.5.9 Construction of mNeonGreen phage .....	104
4.5.10 Analysis of glycosylation of phage by MALDI-TOF MS.....	105
4.5.11 Validation of the potential hit glycan.....	105
Chapter 5: Conclusion and outlook.....	107
5.1 Conclusion .....	107
5.2 Future directions .....	108
Reference .....	110
Appendix A: Supporting information for Chapter 2.....	124
Appendix B: Supporting information for Chapter 3 .....	127
Appendix C: Supporting information for Chapter 4.....	145

## **List of Tables**

Table 1-1. The component of the INA and freezing temperature.....	13
Table 4-1. SDB id and glycan modifications.....	84
Table 4-2. Silent barcodes of LiGA library .....	85
Table 4-3. Post-selection analysis on LiGA in ice-affinity purification. ....	89

## List of Figures

Figure 1-1. Contact angle of the ice nuclei on an INA surface described by the young's equation. ....	6
Figure 1-2. Molecular composition of INA surfaces. ....	7
Figure 1-3. Consensus repeat of ice nucleating protein from bacteria. ....	11
Figure 1-4. The available technique to study ice nucleators. ....	17
Figure 2-1. The design of freeze-float selection system. ....	32
Figure 2-2. Thermal gradient of the cuvettes. ....	37
Figure 2-3. Validation of freeze-float system with INA positive and negative droplets. ....	38
Figure 2-4. Optimization of the cooling rate. ....	40
Figure 2-5. Ice-nucleating activity and concentration. ....	41
Figure 2-6. Validation of freeze-float system with various concentration of INA droplets. ....	42
Figure 2-7. Optimization of the cooling rate with various concentration of INA droplets. ....	44
Figure 3-1. Automated droplets generation system using Biomek 3000. ....	60
Figure 3-2. Thermal gradient in Biomek 3000 deep well system. ....	61
Figure 3-3. Comparison of droplet freezing temperature dispersions by Kolmogorov-Smirnov test. ....	63
Figure 3-4. Thermal gradient in Asymptote system. ....	66
Figure 3-5. Comparison of droplet freezing temperature dispersions by Kolmogorov-Smirnov test. ....	67
Figure 3-6. Droplet freezing temperatures of serial dilution of INA solution. ....	69
Figure 3-7. Comparison of droplet freezing temperature dispersion. ....	71
Figure 4-1. Ice-shell purification strategy. ....	79
Figure 4-2. Ice-shell purification validation test. ....	81
Figure 4-3. Glycan structures of LiGA library. ....	86

Figure 4-4. Analysis of ice-binding preferences of glycans from ice-shell purification using LiGA.....	88
Figure 4-5. Validation experiment of glycosylated phage by ice-affinity purification.....	91
Figure 4-6. Phage-INP conjugation strategy.....	92

## List of Abbreviations

AFP	Antifreeze protein
CFDC	Continuous flow diffusion chamber
CFU	Colony forming unit
<i>E. coli</i>	<i>Escherichia coli</i>
Da	Dalton
DFA	Droplet freezing assay
DNA	Deoxyribonucleic acid
DSC	Differential scanning calorimetry
dNTP	Deoxynucleotide
GFP	Green fluorescent protein
HTS	High-throughput screening
IBP	Ice-binding protein
INA	Ice-nucleating agents
INP	Ice-nucleating protein
IPTG	Isopropyl $\beta$ -D-1-thiogalactopyranoside
IRI	Ice recrystallization inhibition
LiGA	Liquid Glycan Array
MALDI	matrix-assisted laser desorption/ionization
MDS	Molecular dynamics simulation

PBS	Phosphate buffered saline
PCR	Polymerase chain reaction
PFU	Plaque forming unit
<i>P. syringae</i>	<i>Pseudomonas syringae</i>
rpm	Revolutions per minute
RT	Room temperature
ssDNA	Single-stranded DNA
TH	Thermal hysteresis



## **Chapter 1: Introduction**

### **1.1 Physical Foundation of Homogeneous and Heterogeneous Ice Nucleation**

0 °C is a well-known temperature at which melting of ice occurs at 1 atm. It is often incorrectly referred to as “freezing” temperature, but the ice formation without any foreign substances, so-called homogeneous ice nucleation, is not happening spontaneously at 0 °C or temperatures that are near 0 °C. In fact, true homogeneous nucleation is postulated to occur only at temperatures about -38 °C,<sup>1, 2</sup> and this difference between freezing temperature and melting temperature is referred to as thermal hysteresis (TH). Freezing of droplets of pure water is entropically disfavored event that requires the formation of ice nuclei.<sup>3, 4</sup> Once the ice nuclei size reach to a critical size, they become thermodynamically stable and ice growing becomes spontaneous. The critical size of the ice nuclei of homogeneous nucleation is temperature dependent and postulated to be inversely proportional to temperature; the critical radius of ice is around 9 nm at -10 °C, and around 2 nm at -38 °C.<sup>5</sup>

Since the homogeneous ice nucleation is a stochastic process, nucleation event is a time and volume dependent event with fixed probability of occurrence. This probability value is referred to as a nucleation rate and the principal parameter is temperature. This leads to the two observations; freezing temperature dependence on the water volume at a constant cooling rate, and freezing time

dependence on the volume at a fixed temperature. Bigg and co-workers first reported that the mean freezing temperature shows linear dependence on the logarithm of droplets volume, for example mean freezing temperature of diameter of 10  $\mu\text{m}$  droplets is  $-37.5\text{ }^\circ\text{C}$ , that of 1 mm droplets is  $-23.8\text{ }^\circ\text{C}$ , and that of 10 cm droplets is  $-10\text{ }^\circ\text{C}$ .<sup>6</sup> Leisner and co-worker observed that the droplets of two different radii (49 and 19  $\mu\text{m}$ ) showed different freezing rate ( $1.35\text{ s}^{-1}$  and  $8.2\times 10^{-2}\text{ s}^{-1}$  respectively) at a constant temperature ( $-35\text{ }^\circ\text{C}$ ).<sup>7</sup> This observation is in a good agreement with the volume-nucleation rate theory; freezing rate is proportional to the droplet volume.<sup>4, 8</sup> Mason and co-worker showed the volume dependent freezing temperature at the constant cooling rate, which gives  $-35.3\text{ }^\circ\text{C}$  for droplets of 100  $\mu\text{m}$  diameter and  $-41.2\text{ }^\circ\text{C}$  for droplets of 1  $\mu\text{m}$  diameter.<sup>9</sup> One nuclei can be defined as the minimum amount required for phase transition, therefore the formation of one nuclei is the rate determining step in transition of all water molecules into ice.<sup>10</sup>

To describe the freezing process, classical nucleation theory has been used as the most common theory.<sup>11</sup> For the homogeneous nucleation to happen, the formation of an ice embryo is required. The Gibbs free energy required to create the cluster of water molecules of a critical size (ice embryo) can be described as the difference between the free energy of a bulk and that of the surface.

$$\Delta G_{hom} = \frac{4}{3}\pi r^3 \Delta g + 4\pi r^2 \sigma$$

where  $r$  is the radius of the sphere of nucleus,  $\Delta g$  is the difference in free energy per unit volume, and  $\sigma$  is the surface tension of the interface of the nucleus and liquid.  $\Delta G$  of the homogeneous nucleation at 220 K is calculated to be  $\sim 18 k_B T$  by the MD simulation.<sup>12</sup> Because of the energy barrier associated with the surface energy, homogeneous ice nucleation is not spontaneous until the embryo reaches to the critical radius.

The rate of nucleation  $R$  is expressed as

$$R = N_S Z j \exp(-\Delta G^*/k_B T)$$

where  $N_S$  is the number of nucleation sites,  $Z$  is the Zeldovich factor,  $j$  is the rate at which molecules attach to the nucleus causing to grow,  $\Delta G^*$  is the free energy cost of forming the critical nucleus,  $k_B$  is the Boltzmann constant and  $T$  is the absolute temperature.<sup>13</sup> This expression for the rate is defined as the number of nucleus formed per unit volume in unit time, and it is consisted of two factors; the average number of ice nucleus that have critical size ( $N_S \exp(-\Delta G^*/k_B T)$ ), and probability of the ice nuclei with critical size to grow diffusively and complete ice formation by the incoming water molecules ( $Zj$ ).

Ice nucleation in nature practically occurs at much higher temperatures due to the presence of foreign substances. Homogeneous ice nucleation is thus a rare event and majority of ice formation around us does not occur through a homogeneous mechanism. To increase the nucleation rate by the substances in contact with water, surface of some (but not all) foreign substances in contact with

the liquid water can lower the free energy barrier of the nucleation and affect the number of nucleation sites.<sup>14-16</sup> A general property of such surface is described as wetting by water and ice. Blohm and co-workers experimented using water-repellent surface to test the impact of substrate that have low wettabilities.<sup>17</sup> They showed that the low contact angle of the substrate reduced the energy barrier and probability of forming a single ice nucleus. The wetting factor  $f$  is the parameter that describes how much the foreign surface reduces the energy barrier for the formation of ice embryo compared to homogeneous nucleation.<sup>18, 19</sup>

$$\Delta G = f(\theta) \times \Delta G_{hom}$$

From the volume of the sphere-cap ice nucleus and change in volume energy  $\Delta G$ ,  $f$  is derived as follows:<sup>20</sup>

$$f(\theta) = \frac{(2 + \cos\theta)(1 - \cos\theta)^2}{4}$$

The angle  $\theta$  (Figure 1-1) is the contact angle, which is the tangential angle between the ice embryo on the foreign surface and the liquid water phase, and it has a value between 0 and 180°. The contact angle is determined from the interfacial energies by the Young's equation:

$$\gamma_{sl} = \gamma_{is} + \gamma_{il}\cos\theta$$

The force acting on an ice embryo on INA surface is associated with this contact angle. Theoretically, when the contact angle on the foreign surface is close to 0°, nucleation is more promoted.<sup>21</sup> For instance the surface that have  $\theta = \sim 25^\circ$  is about

117 times lower  $\Delta G$  compared to that have  $\theta = \sim 110^\circ$ , which results in the higher nucleation rate.<sup>22</sup> The contact angle of homogeneous nucleation is described as  $180^\circ$ , then  $f(\theta)$  becomes 1 so that free energy will be equal to  $\Delta G_{hom}$ . Contact angle of the nuclei on the solid surface has been studied by using molecular dynamic simulations,<sup>22</sup> or a direct measurement system on nearly molecular scale, and the relationship between the observed contact angle and the nucleation rate was examined.<sup>23</sup> While these definitions are important, quantitative validity of the atom-scale and molecular requirements of the nucleation process are not confirmed. All molecular scale investigation of heterogeneous nucleation is top-down and they start from known substances or surface that has been empirically observed to act as a nucleator. It is not known how to relate the atomic composition of an interface and its ability to influence the  $\Delta G$  to act as ice nucleator.

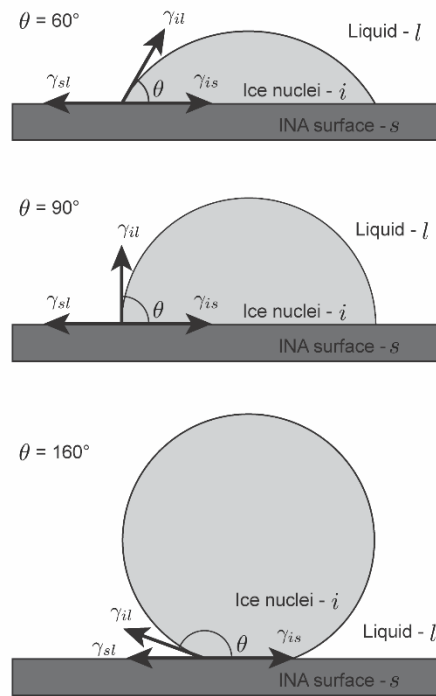


**Figure 1-1.** Contact angle of the ice nuclei on an INA surface described by the young's equation.

$\gamma_{sl}$  is the surface tension for INA surface-liquid,  $\gamma_{il}$  is the surface tension for ice-liquid, and  $\gamma_{is}$  is the surface tension of ice-INA surface. Three surface tensions  $\gamma_{sl}$ ,  $\gamma_{il}$ , and  $\gamma_{is}$  are at the equilibrium at the contact angle  $\theta$  between the nucleating phase and the surface. Theoretically the lower the contact angle, the better the surface ability to promote ice nucleation.

## 1.2 Ice nucleators

The foreign substances that can induce heterogeneous ice nucleation at subzero temperatures are specifically called ice nucleating agents (INAs). It is proposed that the ice-binding surface of the strong nucleators act as a template to

organize water molecules into the ice-like confirmations and form ice embryo. The relationship between the chemical composition of INA surface and its ability to induce ice nucleation has been intensively studied.<sup>24</sup>

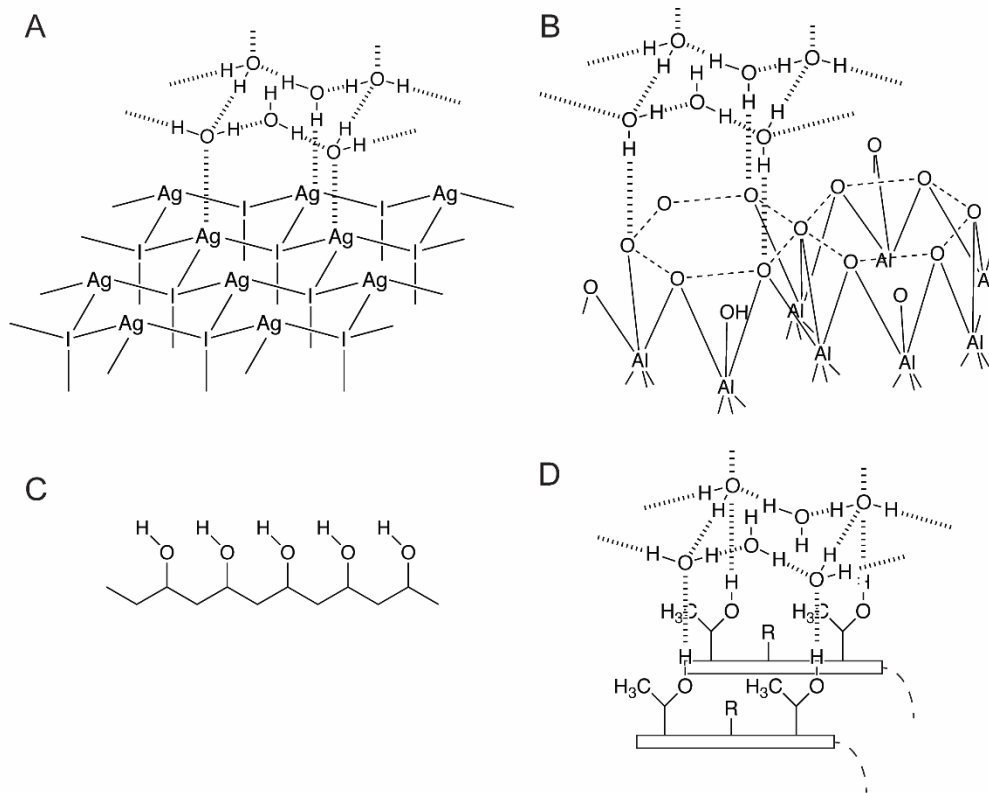


**Figure 1-2.** Molecular composition of INA surfaces. (A) Inorganic INA AgI crystal surface with Ag exposure surface.<sup>25</sup> (B) Mineral INA Kaolinite surface.<sup>26</sup> (C) Synthetic polymer INA poly(vinyl) alcohol (PVA).<sup>27</sup> (D) Ice nucleating protein InaZ of *P. syringae*.<sup>28</sup>

### 1.2.1 Organic and inorganic molecules

A soluble synthetic polymer poly(vinyl) alcohol (PVA) (Figure 1-2C) is known to have ice-nucleating activity<sup>27</sup>, however, the structural resemblance to the structure of ice is not obvious. MD simulation suggested that PVA is able to promote ice-nucleation by increasing the nucleation rate of homogeneous mechanisms.<sup>29</sup> Wang and co-workers suggested that by reducing the density of hydroxyl group on the PVA, ice-nucleating efficiency was improved (23% reduction of the hydroxyl group resulted in 6 °C higher freezing temperature).<sup>30</sup> Also Fukuta and co-workers showed that the organic molecules with high ice nucleating activity above -5 °C tend to have higher free hydroxyl groups on their surface. Organic molecules such as steroids in the atmosphere also known to have ice nucleating activity,<sup>31-33</sup> and it is predicted that natural soils that were rich in organic molecules were more ice-nucleating active than the soils with less organic molecules.<sup>34</sup>

AgI is known to be the best inorganic ice nucleator (Figure 1-2A).<sup>35, 36</sup> This activity is due to the rigid hexagonal wurtzite structure, which matches to the ice lattice. Patey and co-workers used MD simulation to show that heterogeneous ice nucleation is observed only on the silver exposed surface, and iodine exposed surface did not cause ice nucleation.<sup>25</sup>

Kaolinite<sup>26, 37</sup> (Figure 1-2B) and muscovite<sup>38</sup> are known as the best ice nucleator among minerals. They are both silicate and have low contact angle



between their surface and ice nucleus (from 6° to 12°), whereas for the minerals that have less activity such as quartz and calcite had higher contact angle (from 25° to 27°).<sup>38</sup> Their activity was proposed to be due to the rigid hexagonal hydroxylated (001) surface which can act as a template for the formation of ice structure.<sup>39</sup>

### 1.2.2 Ice nucleating protein

Known INAs include biological origins (insect,<sup>40, 41</sup> pollen,<sup>42-44</sup> bacteria,<sup>45-50</sup> fungal spore<sup>51</sup>, and diatom<sup>52</sup>) and surfaces of cells from many kingdoms of life that is able to initiate ice nucleation at high temperature. The best characterized and most active biological ice nucleator is a bacterial protein of *Pseudomonas syringae* (Figure 1-2D).<sup>45, 53, 54</sup> These bacteria encode the INP gene in their genome and express INP gene product a membrane-bound protein that catalyzes ice formation at subzero temperatures. *P. syringae* is proposed to induce frost damage to access nutrient from plant tissue,<sup>55</sup> and enhance the bacterial pathogenicity.<sup>56</sup> It is also hypothesized that it induces extracellular ice nucleation to increase osmotic concentration on the extracellular water, which results in out flux of intracellular water that decreases the freezing temperature of the cells.<sup>57</sup> The purification of the membrane-associated INPs for the structure elucidation has not been successful due to the tendency of this protein to aggregate.<sup>58, 59</sup>

INP of *P. syringae*, encoded as *inaZ* gene, has molecular weight of 120 kDa, and INPs from different ice nucleating bacteria are homologous.<sup>60</sup> Analysis for

identity of *P. syringae* InaZ protein sequence using BLAST program shows 75.9% identity with protein of *P. fluorescens* InaW, 73.0% with *Xanthomonas campestris* InaX and, 71.8% with *Pa. ananatis* (*Erwinia herbicola*) IceE and all these bacteria show high ice nucleating activities of -2 to -4 °C (Table 1-1). The protein of *P. syringae* is separated into three domains; a central repeating domain that is consisted of 16-residues repeats (AGYGSTXTAXXXSXLX; X is any amino acid), an N-terminal domain, and a C-terminal domain (Figure 1-3).<sup>61, 62</sup> Mutagenesis study of this INP shows that the deletion which disrupted the periodicity of 16 codons in a repetitive region of the INP decreased the threshold temperature of the ice nucleation from -3 °C to -6 °C, which suggest that the repetitive region is responsible for the ice nucleating activity.<sup>63</sup> Current MD study predicted that bacterial INP has  $\beta$ -helical fold<sup>64, 65</sup> that could interact with water through the repetitive TXT motif (X is any amino acid). However, there are neither atomic-resolution structures by experimental studies (X-ray crystallography or NMR) nor structures available for homology modeling exist.<sup>66</sup> It is not clear if any  $\beta$ -helix with that motif would act as ice nucleator. Molinero and co-workers used the MD model of INPs, which predicted that the distance between the hydroxyl groups of the TXT motif match with the basal plane of hexagonal ice structure.<sup>28</sup> Bandyopadhyay and coworkers conducted the MD simulation study of TXT surfaces, which shows that the hydroxyl groups of threonine on peptide surface with TXT motifs match to the arrangement of the basal or prism plane of ice.<sup>67</sup> This

simulation also showed that  $\gamma$ -methyl and  $\gamma$ -hydroxyl groups of Thr are necessary for the ice formation.

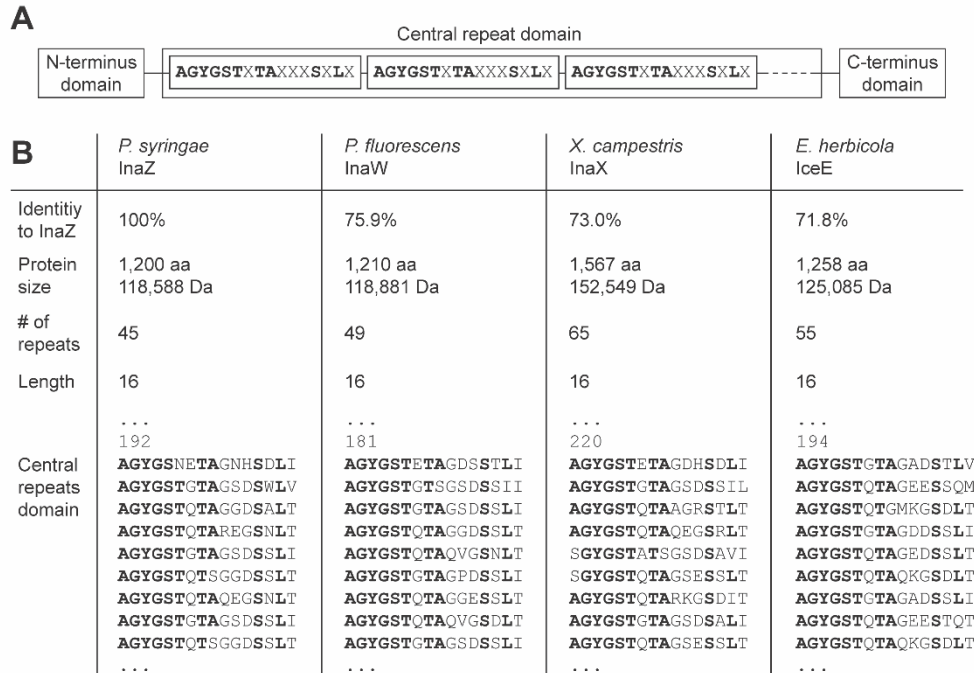


**Figure 1-3.** Consensus repeat of ice nucleating protein from bacteria. (A) Domain structure in ice nucleating protein. (B) Ice nucleating proteins that have highest identity with InaZ from *P. syringae*. The amino acid sequence of central repeat domain (first nine repeats) are shown. Consensus amino acids (AGYGSTXTAXXXSXLX; X is any amino acid) are shown in bold.

Although the role of TXT motif appears to be understood, the reverse experiment providing the necessity and TXT motif (grafting on a non-nucleating protein) has not been performed. It is also known that the large fraction of ice nucleating protein is glycosylated. Arellano and co-workers tested the effect of cleavage of different

glycans by N-glycosidase, O-glycosidase, and  $\beta$ -galactosidase.<sup>58</sup> The result shows that the cleavage of those sugar residues include galactose, glucosamine, and mannose leads to the deletion of most active ice nucleating structure ( $\sim -4.5$  °C). However, the ice-binding protein studies also showed that hydrogen bonds are insufficient in explaining the full ice-binding interaction. The actual binding mechanism might be more complex than only between hydrogen bonding, such as hydrophobic interactions. Therefore, to date the structure-activity relationship of INA that induce nucleation at  $T > -10$  °C is not fully understood. The minimum structural features are difficult to predict and *de novo* design of protein that has nucleation ability is not reported.<sup>68</sup>

**Table 1-1.** The component of the INA and freezing temperature.

	Composition	Freezing temp. (°C)	Technique	Reference
Homogeneous nucleation	-	-38	DFA	Angell <sup>2</sup>
<b>Biological nuclei</b>				
<i>P. syringae</i>	Bacterial protein InaZ	-2	DFA	Caldwell <sup>53</sup>
		-2.7	DFA	Nishikawa <sup>69</sup>
<i>P. fluorescens</i>	Bacterial protein InaW	-2.5	DFA	Nishikawa <sup>69</sup>
<i>P. viridiflava</i>	Bacterial protein InaV	-5.9	DFA	Nishikawa <sup>69</sup>
<i>Pa. ananatis</i> ( <i>Erwinia herbicola</i> )	Bacteria protein IceA	-4.0	DFA	Fall <sup>70</sup>
<i>X. campestris</i> pv. <i>translucens</i>	Bacterial protein InaX	-2.0	DFA	Franc <sup>71</sup>
crane fly <i>Tipula trivittata</i>	Insect protein	-8	Glass capillary	Castellino <sup>40</sup>
Birch pollen	Pollen surface	-18	DFA, DSC	Grothe <sup>42</sup> Koop <sup>43</sup>
Alder pollen	Pollen surface	-20	DSC	Koop <sup>43</sup>
<i>Thalassiosira pseudonana</i>	Diatom surface	-23	DFA	Aller <sup>52</sup>
<b>Inorganic nuclei</b>				
Silver iodide	AgI	-3.5	Bulk freezing	Vonnegut <sup>36</sup>
		-2.5	Bulk freezing	Vonnegut <sup>72</sup>
Silver bromide	AgBr	-8	Bulk freezing	Vonnegut <sup>36</sup>
Copper iodide	CuI	-2.5	Bulk freezing	Vonnegut <sup>72</sup>
Kaolinite	Al <sub>4</sub> Si <sub>4</sub> O <sub>10</sub> (OH) <sub>8</sub>	-15	ZINC	Kanji <sup>26</sup>
		-27	Optical microscope	Bertram <sup>38</sup>
Muscovite	KAl <sub>2</sub> (Si <sub>3</sub> Al)O <sub>10</sub> (OH,F) <sub>2</sub>	-27	Optical microscope	Bertram <sup>38</sup>
<b>Organic nuclei</b>				
PVA	[CH <sub>2</sub> CH(OH)] <sub>n</sub>	-23	DFA	Wang <sup>30</sup>
Long chain alcohol	C <sub>30</sub> OH	-18	MD simulation	Molinero <sup>24</sup>
Naphthalene SOA	C <sub>10</sub> H <sub>8</sub>	-29.5	MD simulation	Koop <sup>31</sup>

### 1.3 Application of Ice-nucleators

The freezing of water impacts the process that determines the Earth's climate. Atmospheric glaciation ability at sub-zero temperature plays an important role in the global hydrological cycle affect precipitation and cloud formation<sup>32, 73, 74</sup> as well as on the radiative forcing.<sup>75</sup> The model simulation from Hoose et al. showed that the nucleation via dust and soot immersion and contact is the dominant nucleator in the atmosphere.<sup>76</sup> On the other hand, Sands and co-workers showed that more than 69% of the ice nucleators active at high temperatures  $> -7$  °C and  $< -4$  °C from the snowfall samples were biological origin.<sup>73</sup> Pöschl and co-workers also confirmed that the rainfall contains more biological particles compared to the aerosol during dry period.<sup>77</sup> Psenner confirmed that the survival of the airborne microorganisms, which suggests that the ice nucleating bacteria or fungi utilize the atmospheric process as transportation.<sup>78, 79</sup>

For the modification of the local climate, INA such as silver iodide is suggested to be used as the cloud seeding.<sup>80</sup> There exist many examples of cloud seedings by silver iodide aerosol or potassium iodide from planes or rockets to promote cloud formation.<sup>81, 82</sup> Blestrud and co-workers showed the experimental evidence that AgI could initiate the cloud formation and induce precipitation on a mountain surface within a specific target region,<sup>83</sup> and avoid precipitation over designated metropolitan areas. However, the effectiveness of the cloud seeding to the larger area precipitation is still under discussion.

The other practical application that emanated from the investigation of ice-nucleating active bacteria is the use of bacteria to prevent frost injuries. Specifically, a wild type ice-nucleating bacteria (*P. syringae*) is known to be plant pathogens and epiphytic<sup>84</sup> and can harm the crops by causing frost on the plants at a higher temperature than usual (~-5 °C).<sup>45</sup> Ice-minus bacteria, which are the genetically engineered *P. syringae* to lack INP expression, can be used to control frost injury by competition between the wild type and the mutant.<sup>85</sup> This is the first genetically modified organism that was released into the environment. The field test was successful, and result showed that the ice-minus bacteria can effectively prevent the frost injury. However the use of recombinant bacteria in the field brought controversy, but also led to the formation of biotechnology policies in the US.<sup>86-88</sup>

For the effective use of ice-nucleating protein from *P. syringae*, the sterilization method is important. The sterilization by heat denature the INP activity, on the other hand, the gamma-ray inactivation of the cell can maintain the ice-nucleating activity and prevents growth of the cells. The sterilized ice nucleating bacteria *P. syringae* has been exploited for the commercialized artificial snow inducer Snomax.<sup>89</sup>

The lyophilization is a common technique to achieve the better preservation of the product, and it is extensively used in academia and in pharmaceutical and food industries.<sup>90</sup> Increase of the freezing temperature of the sample improves the efficiency of the lyophilization and product quality.<sup>91</sup> The addition of INA such as

protein from ice-nucleating active bacteria or AgI promotes lamellar ice crystal content, which attributes to the faster primary drying rate, but there are probably situations where the use of heavy metals (Ag) and poorly understood products of bacterial origin are simply not acceptable as additives.<sup>92</sup> Availability of chemically defined or “organic” additives might find a broader use.

Protein from ice-nucleating active bacteria, AgI, and other nucleators have been suggested to have potential use in the cryopreservation.<sup>93</sup> To achieve better control of the freezing temperature and efficiency of cooling, since they can provide the special control of the ice nucleation and ice crystal growth. The major difficulty is the low biocompatibility or poor characterization of both substances.

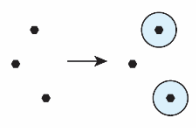
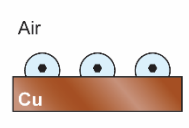
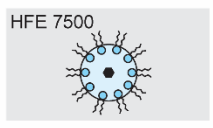
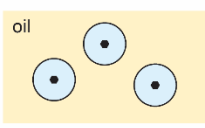
There exists investigations of the use of INAs as the adjuvant of the cryosurgery.<sup>94,95</sup> Cryosurgery is a surgical technique that destroys undesired tissue by causing localized freezing. The proteins that induce ice nucleation at higher temperature or the compounds that promote needlelike shaped ice crystals can enhance destruction of cancerous tumors. Introducing nanoparticles such as MgO into target tissues can increase ice formation and prevent damage in healthy tissues.<sup>96</sup>

These and other the practical applications are limited by the lack of characterization of INAs, and understanding of the relation between nucleation temperature and the structure of the INAs. The control of the ice nucleation, growth



and coarsening involve delicate balance of thermodynamic, kinetic, and rheological factors and the relation between structure need to be further investigated.

## 1.4 Current methods to study ice-nucleators

	Continuous Flow Diffusion Chamber	Droplet Freezing Assay (cryoplate)	Droplet Freezing Assay (microfluidic droplet)	Droplet Freezing Assay (emulsion)
				
Advantage	<ul style="list-style-type: none"> <li>• Computer-controlled system</li> <li>• High-throughput analysis</li> </ul>	<ul style="list-style-type: none"> <li>• Relatively easy setup</li> </ul>	<ul style="list-style-type: none"> <li>• High-throughput</li> <li>• Uniform droplet generation</li> <li>• Automated freezing detection</li> </ul>	<ul style="list-style-type: none"> <li>• Prevent evaporation</li> <li>• Prevent Wegener-Bergeron-Findeisen effect</li> </ul>
Disadvantage	<ul style="list-style-type: none"> <li>• Large chamber size</li> <li>• Expensive machine</li> </ul>	<ul style="list-style-type: none"> <li>• Contact with solid surface</li> <li>• Difficulty in temperature control</li> <li>• Evaporation</li> </ul>	<ul style="list-style-type: none"> <li>• HFE 7500 and surfactant</li> </ul>	<ul style="list-style-type: none"> <li>• Droplet coalescing</li> <li>• Low to medium throughput</li> </ul>
In contact with	<ul style="list-style-type: none"> <li>• No contact</li> </ul>	<ul style="list-style-type: none"> <li>• Cooling plate</li> </ul>	<ul style="list-style-type: none"> <li>• Contact with surfactant</li> </ul>	<ul style="list-style-type: none"> <li>• Silicone / paraffin oil</li> </ul>
Detection	<ul style="list-style-type: none"> <li>• Optical particle counter</li> </ul>	<ul style="list-style-type: none"> <li>• Depolarization of backscattered light</li> </ul>	<ul style="list-style-type: none"> <li>• Depolarization of backscattered light</li> </ul>	<ul style="list-style-type: none"> <li>• Depolarization of backscattered light</li> <li>• DSC</li> </ul>
Separation	<ul style="list-style-type: none"> <li>• Yes (by size)</li> </ul>	<ul style="list-style-type: none"> <li>• No</li> </ul>	<ul style="list-style-type: none"> <li>• Yes / No (Depends on systems)</li> </ul>	<ul style="list-style-type: none"> <li>• No</li> </ul>

**Figure 1-4.** The available technique to study ice nucleators. Ice nucleating activity or INA concentration of sample particles are measured.

### 1.4.1 Microscopic method

For the study of mineral dusts and other environmental INAs, microscopic techniques have been used. The optical microscopy was used to observe the phase transition of the particle immersed in droplets.<sup>97</sup> This system relies on manual

observation, and the setup can achieve the cooling to 170 K. Weinbruch and co-workers used environmental scanning electron microscope (ESEM) to study the condensation and deposition freezing of AgI.<sup>98</sup> The ice nucleation was investigated in the observation chamber with increased vapor pressure. Chemical identification of the ice nuclei is able to be done by ESEM at the same time. Other electron microscopy study of snow crystals and its mineral nuclei showed that there is no relationship between crystal forms and the chemical composition of the nuclei.<sup>99</sup>

#### **1.4.2 Cloud Chambers**

Cloud chambers generate cloud-like conditions and nucleate particles through adiabatic expansion.<sup>100</sup> It measures the ice nucleation efficiency of mineral particles. However, the instruments tend to be large and expensive. They provide ability to adjust many variables in order to obtain comparable measurement.

#### **1.4.3 Continuous Flow Diffusion Chamber**

Continuous Flow Diffusion Chamber (CFDC) was designed by Rogers (1988) to quantify the concentration of the active ice nucleator in the aerosol sample,<sup>101</sup> and it is one of the most commonly used laboratory instrument to investigate the ice nucleators (Figure 1-5).<sup>77, 102</sup> This system uses a temperature gradient to produce supersaturation of vapor to create immersion freezing environment of the sample particles flow through the chamber.<sup>103</sup> The formation of

ice crystals was detected by the depolarization of scattered laser light. There exist several instruments which modified this systems, and one of the most widely used system is Zurich Ice Nucleation Chamber (ZINC).<sup>104</sup>

#### **1.4.4 Droplets freezing assay**

Droplet freezing assay (DFA) have been utilized in the ice nucleation experiments (Figure 1-4). The measurement of the droplets freezing temperature on a copper cold stage covered by oil-coated aluminum sheet system has been commonly used.<sup>105, 106</sup> However, when measuring the droplets freezing temperature, the contact of the droplets with the cooling plate often cause unfavorable ice nucleation which is not due to the sample ice nucleating activity.<sup>107</sup>

Whitesides and co-workers have been developed the microfluidic instruments to investigate the ice nucleation temperature of the aqueous droplets suspended in perfluorinated oil and in contact with perfluoro surfactant.<sup>108</sup> The microfluidic chip contains flow-focusing droplets generator, cooling chamber and the optical detection system of the frozen droplets. The benefit of the microfluidic DFA is that the aqueous sample is encapsulated in the immiscible continuous phase, prevent the contact with the device wall and act as independent sample container. Still each droplet is in an extensive contact with the surfactant and perfluoro oil. Differential scanning calorimetry (DSC) is also used to detect the droplet freezing temperatures that were generated by the microfluidic device.<sup>43, 109</sup> DSC is a

thermoanalytical technique which allows a measurement of the amount of heat flow. The phase transition of the sample can be detected by observing the amount of heat absorbed or released during such transitions.

#### **1.4.5 Molecular dynamics simulation**

Over the past 15 years, molecular dynamics simulations have been used for the homogeneous ice nucleation study<sup>110</sup> and to determine the effect of the INA toward ice formation. Moore and co-workers developed a molecular dynamics simulation to study homogeneous and heterogeneous ice nucleation based on coarse-grained model of water activity, which employs the intermolecular interaction between water molecules, or water and different substances.<sup>111</sup> Molinero and co-workers used this coarse-grained model of water activity to elucidate the effect of different surfaces, for instance water soluble molecules such as polysaccharides of pollen and poly(vinyl alcohol) (PVA)<sup>29</sup> or carbon surfaces<sup>112</sup> on ice crystallization, where both of the substances were found to increase the freezing temperatures. Pereyra and co-workers have used molecular dynamics simulations of water to relate the ice embryo size and the nucleation rate of the heterogeneous nucleation.<sup>113</sup> Michaelides and co-workers used coarse-grained model of water activity to study the hydrophobicity and the morphology of the crystalline surface that promotes ice nucleation, which leads to the conclusion that

the different crystallographic places of the same surface can alter the ice nucleation rate and cause up to different face of water.<sup>114</sup>

Another MD simulation study is conducted to the *P. syringae* protein InaZ combined with the interface-specific sum frequency generation (SFG) spectroscopy to show that hydrogen bonding at the water-INA contact imposes structural ordering on the adjacent water molecules.<sup>115</sup>

MD simulation of ice binding surface is done to observe the hydration enthalpy and entropy, and it is claimed that the enthalpic interactions are as important as pre-ordering the water molecules into ice-like conformation.<sup>116</sup>

## **1.5 Tools for molecular studies of Ice-binders**

The common feature of ice-nucleating and antifreeze proteins is their ability to interact with water molecules to control the kinetics of water crystallization. Structures and ice-binding mechanistic of ice-nucleating and antifreeze proteins have large similarities even though they are opposite in function,<sup>65, 117</sup> and it is often reported that some ice-binding proteins have antifreeze and ice-nucleating property at the same time.<sup>43, 118</sup> Davies and co-workers proposed that distinguishing difference between them might be the size of the molecules<sup>43, 119</sup> and aggregation.<sup>120</sup> Lindow and co-workers hypothesized that the minimum mass of functional ice-nucleating proteins that initiate ice nucleation at -12 to -13 °C is 150 kDa.<sup>121</sup> Šantl-Temkiv and co-workers prepared the truncated version of INP of *P. syringae* and

examined the ice nucleating activity.<sup>122</sup> The result suggests that the short version of the ice nucleating protein does not have efficient ice nucleating activities, even if they contain the ice-binding surface tandem repeat. Tsuda and co-workers also generated a recombinant polypeptide corresponding to a truncated *P. syringae* protein central repeat sequence Tyr176-Gly273.<sup>123</sup> They observed that the truncated INP exhibited antifreeze activity instead, for example hexagonal bipyramid ice crystal shaping, inhibition of ice growth and TH activity. Investigation of the ice-binding molecules has potential to the structural understanding of the heterogeneous ice nucleating mechanism and allow engineering of the new class of ice nucleating molecules.

### **1.5.1 Splat assay**

Splat assay is one of the most accepted methods for assessing ice recrystallization inhibition (IRI) activity since it was developed by DeVries and co-workers in 1987.<sup>124</sup> This method measures the size change of the ice grain size over time. Laybourn-Parry and co-workers proposed a semi-high throughput method of splat assay named high-throughput AFP protocol (HTAP) by incorporating 96 well plate.<sup>125</sup> Using this system, they analyzed 866 isolated bacteria and found 187 to have IRI positive activity.

### 1.5.2 Nanoliter osmometer

Osmometer was originally designed to study the osmolarities of biological sample solutions by measuring the depressions of freezing point. It has been applied for the thermal hysteresis (TH) activity measurement for ice-binding molecule. Drori and co-worker combined nanoliter osmometer and computer-controlled system that was able to achieve highly accurate controlled temperatures and temperature logging to study the TH activity of the molecules.<sup>126, 127</sup>

### 1.5.3 Ice affinity purification

Davies and co-workers invented an affinity based screening method that can identify or purify molecules that interact with ice.<sup>128</sup> When compared to the other ice binding activity methods, which measures qualitative ice recrystallization inhibition (IRI) activities of sample one by one, ice affinity purification offers high-throughput screening of mixture of ice-binding molecules starting from aqueous solution of chemical libraries of potentially any size and complexity. In a complex mixture, affinity purification can separate the molecules that exhibit binding interaction with ice surface from those that do not by inclusion of ice binding in the solid ice. This affinity based selection successfully selected the ice-nucleating bacteria *P. syringae* and IRI active bacteria *Chryseobacterium* sp. C14. *E. coli* without any ice-binding protein was not enriched in the ice fraction.<sup>129</sup> To achieve the higher throughput of this purification method, thin ice-shell inside the round

bottom flask<sup>130</sup> or commercially available ice-making machine<sup>131</sup> has been employed.



## 1.6 Thesis overview

In this thesis, I developed a screening system for the discovery of INAs. In Chapter 1, I described my perspective on the study of ice nucleator studies. I discussed examples of different type of assays that are able to detect molecules that influence ice formation. I compared the different techniques and indicated the challenges in this field.

In Chapter 2, I described Freeze-float selection, that is able to detect the presence of ice-nucleating substances in droplets and separate them. This system employs the difference in density between ice ( $0.916 \text{ cm}^3$ ) and liquid water ( $0.999 \text{ cm}^3$ ) to identify the ice-nucleation events of the aqueous droplets and separate them from others. The system uses simple commercial cooling equipment, and successfully separated the droplets that contained ice nucleator from the droplets that do not. From the further evaluation of its ability to detect ice nucleators, we believe that this system could be upgraded to sort the large number of droplets based on presence of ice-nucleating abilities in these droplets.

In Chapter 3, I improved efficiency and accuracy of the freeze-float selection system. I automated the generation of droplets by a robotic liquid handling system Biomek 2000. To expand the screening scale and accommodate a large number of droplets in one screening experiment, I tested multiple well system in a controlled rate freezer Asymptote. I observed less thermal delay in metal multiwell plate in controlled rate freezer compared to polypropylene 96-well plate in the

commercially available commodity freezer. Those results outline the next steps for the further design of the higher throughput system for screening and detection of ice-nucleators.

In Chapter 4, I described a screening platform of the potential ice-binding glycans that employed ice-shell purification. It incorporated Liquid Glycan Array (LiGA) technology strategy to discover ice-binding glycans. The genetically encoded phage library was screened by the ice affinity purification and enriched glycans were identified by deep sequencing and analysis. The selected glycans were evaluated the selected glycan's effect to the ice formation by the validation test.

Lastly, Chapter 5 summarizes the advances and limitations I encountered in developing the technology described in Chapters 2-4. I outlined future directions to translate my thesis work into a further investigation for INA screening.

## Chapter 2: Freeze-float selection of Ice nucleator

### 2.1 Introduction

Water is one of the most abundant substances on the Earth but many aspects of its behaviour are still poorly understood. It is known that nucleation of ice in water requires the presence of small molecules, nanoparticles, environmental contaminants (pollen, dust), biological macromolecules or whole organisms to induce so-called “heterogeneous” ice nucleation. Homogeneous or spontaneous ice nucleation is rarely observed and is thought to occur only at temperatures around  $-38\text{ }^{\circ}\text{C}$ .<sup>1</sup> It is hypothesized that a significant fraction of ice-nucleating agents (INAs) in the atmosphere are biological origin (i.e., glycoproteins embedded in membranes of bacteria).<sup>59, 73</sup> Interestingly, only a few INAs of well-defined chemical structures are known.<sup>64</sup> The motivation of this chapter is to develop technologies that can accelerate discovery of new INAs of well-defined chemical structures. I believe that discovery of the broader class of INA has the potential to provide insight into ice nucleation mechanisms. In turn, understanding the molecular basis and composition of INAs in environmental samples is critical to our ability to understand changes in climate due to human activity.<sup>132</sup> Chemically-defined INAs will also be useful in many fields including the food industry, atmospheric sciences, production of artificial snow, agriculture, organ preservation, cryobiology and cryosurgery.<sup>133</sup> Here I describe a system that facilitates screening of a large number

of substances and their effect on nucleation of ice to facilitate future unsupervised discovery (i.e., random screening) of INAs.

In this chapter, I developed a screening system that employs the difference in density between liquid water and ice ( $0.9998 \text{ g/cm}^3$  vs.  $0.9168 \text{ g/cm}^3$  at  $0 \text{ }^\circ\text{C}$ ) to identify ice-nucleating agents (INAs) that are encapsulated into droplets of water suspended in silicone oil of intermediate density ( $0.939 \text{ g/cm}^3$ ). Droplets of liquid water stably reside at the interface of the silicone oil and perfluoro oil ( $1.6658 \text{ g/cm}^3$ ); freezing causes the aqueous droplets to float to the top of the silicone oil layer. I demonstrated the feasibility of this screening system by using droplets that contained well-defined ice-nucleator Snomax. The droplets with and without Snomax froze at different temperatures and separated into two groups in our system. I tested the screening system to validate samples that have different ice-nucleating activities. Starting from known ice nucleating active bacteria *P. syringae*, I confirmed that droplets that contain an increasing amount of ice-nucleating bacteria per droplet exhibited a dose-dependent increase in ice nucleation. When droplets containing different amounts of *P. syringae* were separated using a freeze-float setup, I observed that the droplets that floated at higher temperature contained more ice nucleating active bacteria. The outlined system, thus, permits simple power-free separation of droplets that contain effective INA from those that contain weak or no INA. Such setup can be used as a starting point for development of high-throughput approaches for discovery of new INAs.

There exist several approaches to study ice-nucleating activities of INAs in solutions distributed into arrays of droplets spotted onto a surface, or droplets suspended in an immiscible liquid. Ideal unsupervised discovery should permit rapid separation of water droplets that contain INAs from those that do not. The use of droplets that are suspended in liquid or air minimizes the surface induced nucleation that could take place in arrays of droplets on a solid surface. Whitesides and co-workers pioneered the use of microfluidic devices to characterize ice nucleation in monodisperse aqueous droplets suspended in fluorinated oil that flowed through a temperature gradient. The authors observed that droplets could be cooled to the homogeneous nucleation temperature (between -36 and -37.8 °C),<sup>134</sup> and these observations suggested that the effect of the fluorinated oil and fluorosurfactant on nucleation was minimal. Murray and co-workers also developed a microfluidic device to study the atmospheric INAs by encapsulating them into monodisperse droplets and optical recording of droplet freezing on a cold stage.<sup>107</sup> A monodisperse fluoro oil emulsion has subsequently been adopted by Toner and co-workers to test nucleation efficiencies of *P. syringae*-derived substances (Snomax) in D<sub>2</sub>O and H<sub>2</sub>O.<sup>135</sup> These reports set an important precedent for the utility of water/perfluoro oil emulsion for nucleation studies. Unfortunately, as these microfluidic devices are designed for detection of nucleation events and not for separation of droplets that exhibit nucleation, they cannot be implemented directly for selection of new ice-nucleating substances. Development of

microfluidic techniques for separation of droplets that contain “active” vs. “inactive” readout is an intense area of research<sup>136</sup> and a focus of several startup companies.<sup>137</sup> Many strategies for detection and separation of “active” droplet employ complex optical detection of active droplets coupled to electromagnetic or pneumatic actuation of flow to induce separation of desired droplets.<sup>96, 138</sup> Passive methods for separation also exist: these are based on trapping of droplets or their repetitive interaction with pins, walls and other objects in microfluidic channels.<sup>139</sup> For example, Chiu and co-workers developed a microfluidic device which can generate microdroplets, and subsequently trap the frozen droplets in “pockets” in the microfluidic channels with higher selectivity for frozen over non-frozen aqueous droplets.<sup>140</sup>

## **2.2 Experimental Design**

We sought to devise a simple system that separates frozen droplets (i.e., those with substances that induce ice-nucleation) from a large collection of liquid droplets on the basis of the difference in density between water and ice. This screening system should be readily scalable to permit direct separation of ice-nucleating substances from a vast collection of non-nucleators. The design, in principle, requires only one functional component: the buoyant liquid layer with a density intermediate between ice and water that separates ice and water droplets. I developed and implemented the functional prototype that highlights the basic rules

of operation and boundary conditions of buoyancy-based separation based on droplet size, the composition of the surrounding media, cohesion of droplets with one another, and their adhesion to the surrounding surfaces.

We designed our device to satisfy five criteria. i) It should be compatible with approaches that produce droplets of uniform size that can encapsulate tested substances. Such approaches may include flow-focusing microfluidics, droplet-on-demand microfluidic systems or mechanically actuated systems (repeater pipettors). ii) The droplets in the device should be stable during the screening and not merge on contact upon changes in temperature or upon nucleation of ice. iii) The device should be compatible with a large number of droplets in order to obtain statistically significant data, or to screen large number of samples. iv) In early stages of design, I realized the need for an additional layer of density  $> 1.3 \text{ g/cm}^3$  (referred to as “cushion phase” below) to prevent the droplets from contacting the bottom surface of the container; the latter contact causes either ice nucleation, fusion of droplets or adhesion to the container. v) The device should be compatible with many temperature control systems. Ideally, it should work with a generic freezer system. Although cuvettes and a freezer are readily available, a designed bench-top apparatus with controlled electronic cooling inside an insulated container with external viewing would be useful for future work.

## 2.3 Results and discussion

### 2.3.1 Establishment of Freeze-float selection system

The core of the experimental design that I developed, shown in Figure 2-1A, is a separation system which uses the difference in density of ice and liquid

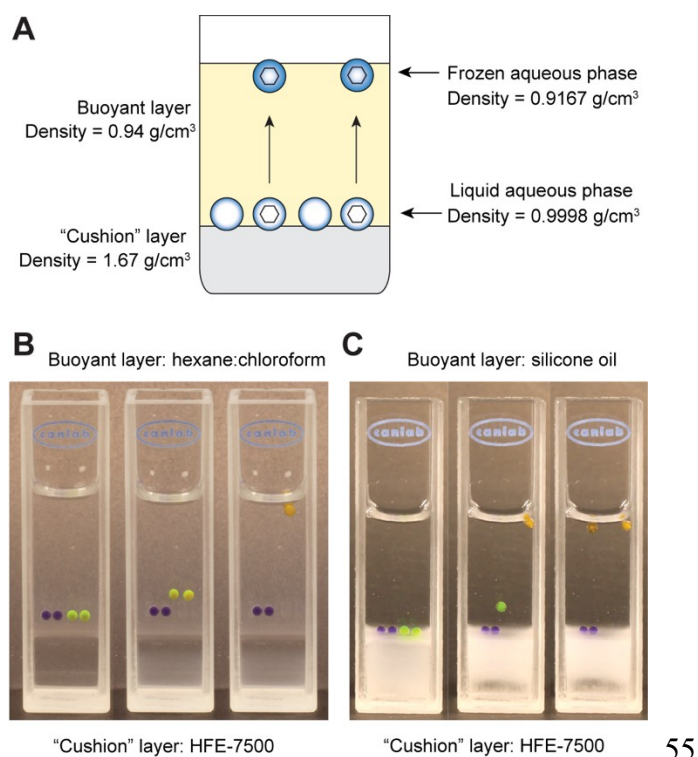


**Figure 2-1.** The design of freeze-float selection system. (A) Scheme of the freeze-float selection system. Droplets that contain liquid water remain at the biphasic interphase between immiscible “cushion layer” and “buoyant layer”. Placing the system in a freezer and lowering the temperature at a rate of  $\sim 0.2 - 1.0$  °C/min leads to freezing of droplets; frozen droplets float to the top of the buoyant layer. (B-C) Images taken during a freeze-float separation experiment employing the buoyant layers composed of hexane chloroform mixture (B) and silicone oil (C). In both systems, droplets contained 1 mg/mL Snomax (yellow droplets) froze and floated at  $-8$  °C, while the droplets that did not contain Snomax (blue droplets) did not freeze and remained at the bottom of the floating layer until the system was cooled below  $-20$  °C.



1A, is a separation system which uses the difference in density of ice and liquid water. By setting the density of the continuous phase to  $\sim 0.95 \text{ g/cm}^3$ , it is possible to make a selection system in which frozen droplets with density of  $\sim 0.91 \text{ g/cm}^3$  float to the top of the oil phase while the non-frozen droplets with density of  $\sim 1.00 \text{ g/cm}^3$  remain at the bottom of the solution. As an “active phase” of the first prototype of the system, I used a mixture of the organic phase (hexane : chloroform, 7 : 3) to achieve the desired density. Although it achieved desired separation (Figure 2-1B), I found that the organic phase has several drawbacks such as instability of the droplets, corrosion of plastic cuvettes, and poor biocompatibility. By thorough iterative testing of several liquids and matching surfactants, I identified silicone fluid DM-Fluid-5cs (Shin-Etsu, Akron, OH) as suitable liquid with density near the temperature of interest ( $0.95 \text{ g/cm}^3$  at  $-3$  to  $-10 \text{ }^\circ\text{C}$ ) optimal for buoyant separation of ice ( $0.9167 \text{ g/cm}^3$ ) from water ( $0.9998 \text{ g/cm}^3$ ) (Figure 2-1C). Guided by the manufacturer’s suggestions and a previous report by Paegel and co-workers,<sup>141</sup> who used a similar silicone oil as the stationary phase for water-oil emulsions, I selected triblockcopolymer silicone emulsifier KF-6017 (Shin-Etsu, Akron, OH) as a surfactant to stabilize the emulsion. As a “cushion phase”, I used hydrofluoroether oil HFE-7500 (3M, St. Paul, MN) that has high density compared to other phases ( $1.6658 \text{ g/cm}^3$ ). A thin, 2-3 mm layer of this liquid sits at the bottom of the system to prevent droplets from adhering to the surface of the container (Appendix A1). HFE-7500 is immiscible with both water and silicone oil (or organic solvents), and

does not interfere with the screening process. As droplets are buoyantly positioned on the interface of two layers, position of the aqueous droplet is calculated based on densities of these liquids (water, silicone oil, HFE-7500) as

$$\rho_{water}(V_1 + V_2) = \rho_{silicone}V_1 + \rho_{HFE}V_2$$

where  $\rho_{water}$  is the density of water,  $\rho_{silicone}$  is the density of the silicone oil,  $\rho_{HFE}$  is the density of HFE-7500,  $V_1$  is the volume of the spherical segment of aqueous droplet that is submerged in silicone oil, and  $V_2$  is the volume of the spherical segment of aqueous droplet that is submerged in HFE-7500. The calculation indicates that 92% of volume of water droplet should protrude into the bottom of silicone oil and 8% submerged into HFE-7500 layer.

To show that the setup is compatible with a low-complexity cooling system, all experiments in this chapter used a commodity chest freezer (Costco #949554) as cooling system. Placing the cuvette in the freezer induced sufficiently slow cooling which promoted temporally-controlled freezing and separation of droplets. The advantage of the freeze-float selection system is the direct comparison of the ice nucleating activities of the multiple different droplets suspended in the same cuvette. Excluding the effect of putative convection of the buoyancy layer, calculated cooling rate of the droplets located in the same cuvette was similar, within little variability due to the thermal gradient across the cuvette. The separation of ice nucleator by the droplets, thus, should only be minimally influenced by the non-linear cooling rate. To measure the freezing temperature,

three identical freeze-float systems that did not contain any droplets were placed in the freezer at the same time. Thermometers placed in the empty systems recorded the temperature during the freeze-float experiment (Figure 2-2 A-B). I note that the setup would work equally well in more sophisticated, temperature controlled freezing system.

Figure 2-1 B-C depicts separation of frozen droplets from water droplets in a freeze-float system made of a 3.5 mL cuvette with 2 mL of “buoyant layer” (organic phase in Figure 2-1B and silicone oil in Figure 2-1C) and 1 mL HFE-7500. Water droplets were pipetted directly into the system and the cuvette was placed on a wet paper to prevent accumulation of static electricity, which was observed to cause destabilization and fusion of the droplets.<sup>142, 143</sup> Two 5  $\mu$ L droplets containing either (i) the ice nucleator Snomax (1 mg/mL Snomax in MilliQ water) marked by fluorescein dye or (ii) no nucleator, marked by Coomassie Brilliant Blue. As the system was cooled, I observed the expected behavior of the droplets: The fluorescent yellow droplets that contained Snomax froze at -8 °C and floated to the top of the organic layer. Conversely, the blue Snomax-free droplets did not freeze at these higher temperatures and remained at the interface of “cushion” and “buoyant” layers even when the system was cooled to -20 °C. Droplets were stable for several hours on the interface between the organic phase and the HFE-7500, but I noticed that prolonged storage of droplets on this interface (>24 hours) led to

increased cohesion between droplets: frozen droplets floated as clusters rather than individual droplets.

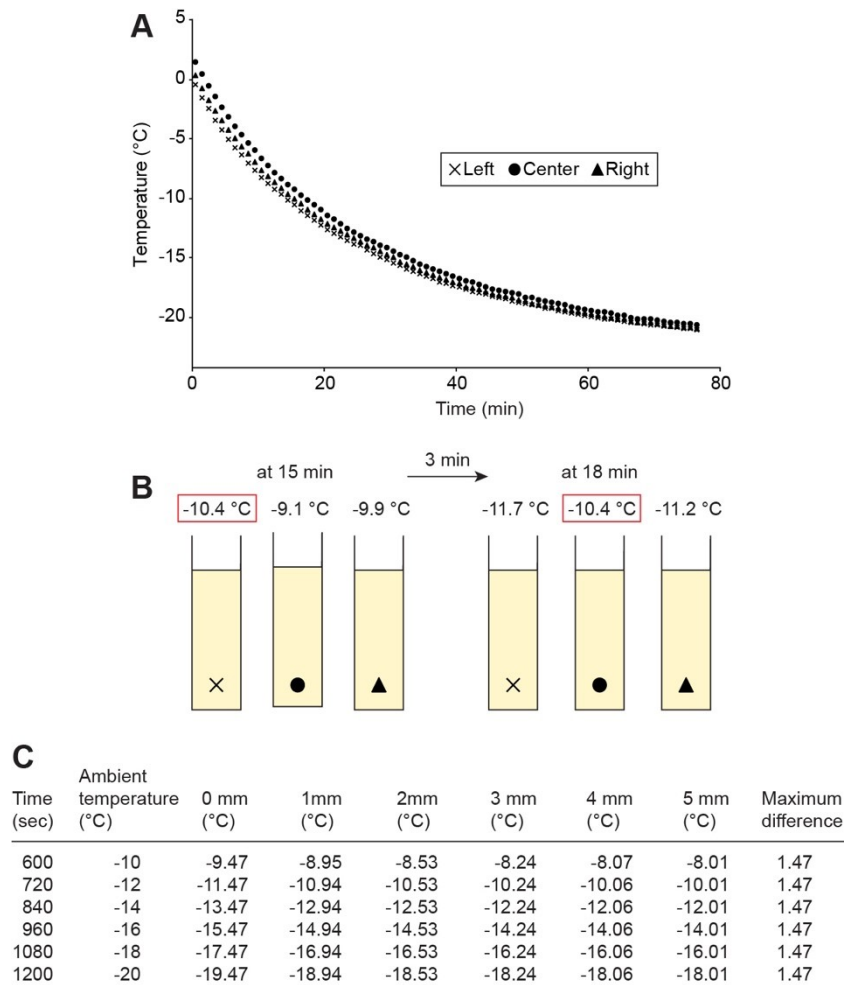


**Figure 2-2.** Thermal gradient of the cuvettes. (A) Inner temperature of three systems over time. The inter system temperature difference due to the nonuniform cooling was between 0.2 to 1.0 °C, and all three systems underwent a similar cooling rate. (B) Illustration of the minor temperature gradient and a temporal delay (here 3 min) required for the different cuvettes or different locations in the same cuvette to reach similar temperatures (here: -10.4 °C). (C) Simulation of temperature diffusion in 1 cm diameter cylindrical vessel with continuous media with thermal conductivity of silicone oil (0.12 W/m·°C) in the absence of convective stirring. The ambient temperature cooling rate was assumed to be -1 °C/min, and the temperature change in the different position in 1 mm thick plastic cuvette filled with silicone fluid DM-F-5cs was calculated. Temperature was calculated at five discrete positions, 0 mm 1 mm, 2 mm, 3 mm, 4 mm, and 5 mm from the edge of the inner cuvette, the latter representing the center of the cuvette.

### 2.3.2. Statistical testing of Freeze-float selection

In a container of 1 cm<sup>2</sup> footprint geometry, the freeze-float separation system can readily accommodate up to 50 1  $\mu$ L droplets at once, for example, 25 droplets with Snomax and 25 without (Figure 2-3). The 50 droplets resided at the interface of silicone oil and HFE-7500 without coalescence. The inner temperature of the system was extrapolated from placing thermometers in two droplet-free cuvettes placed in the vicinity of the test cuvette. Upon cooling, all 25 droplets that

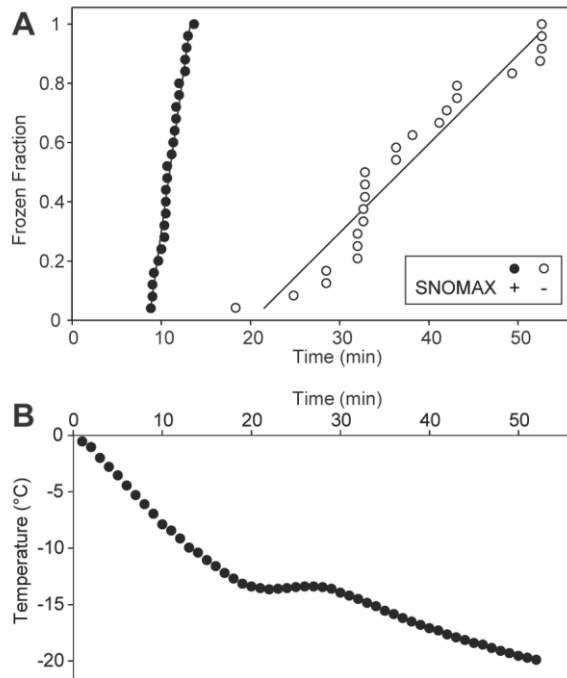


**Figure 2-3.** Validation of freeze-float system with INA positive and negative droplets. (A) Freezing temperature of two groups of droplets, containing either 0.1 mg/mL Snomax in water or water alone. (B) Inner temperature of the freeze-float system measured as a function of the time.

contained nucleator floated to the top of the silicone oil, permitting statistical analysis of nucleation capacity in datasets of modest size (total droplets  $n = 50$ , Figure 2-3A). Characteristic time for droplets to nucleate, freeze and float all the way to the top of the silicone oil layer ( $\sim 3$  cm path) was 20-30 s (Movie S1). I observed two statistically separated groups: all the droplets that contained Snomax floated between 7 and 13 min from the start of the experiment as the temperature of the system decreased from  $-5$  to  $-9$  °C. The droplets without Snomax did not exhibit freezing and floating until the temperature decreased below  $-12$  °C (Figure 2-3B). The effect of the cooling rate was evaluated by comparing the freeze-float selection with higher cooling rate ( $-0.7$  °C/min) and lower cooling rate ( $-0.2$  °C/min). As the cooling rate was lowered, the larger dispersity of the freezing temperature was observed. However similar separation resolution was observed at a both cooling rate (Figure 2-4), which indicated that the effect of the cooling rate was minimum in this separation experiment. The surfactant prevented the 50 droplets from coalescing and aggregating, and provided stability for the emulsion during the freeze-float experiment. The droplets floated individually, confirming no transmission of nucleation events from droplet to droplet. Upon testing of the various container sizes, I concluded that the small footprint of the container of  $1$  cm<sup>2</sup> area was critical for reliable optical monitoring and for maintaining a low temperature gradient across the container. If necessary, 10 or more containers could be set up in parallel to accumulate measurements with up to  $n = 500$  data points,

whereas the use of single container of an equivalent footprint (10 cm<sup>2</sup>) was less optimal due to non-uniform cooling of the bulk liquid.

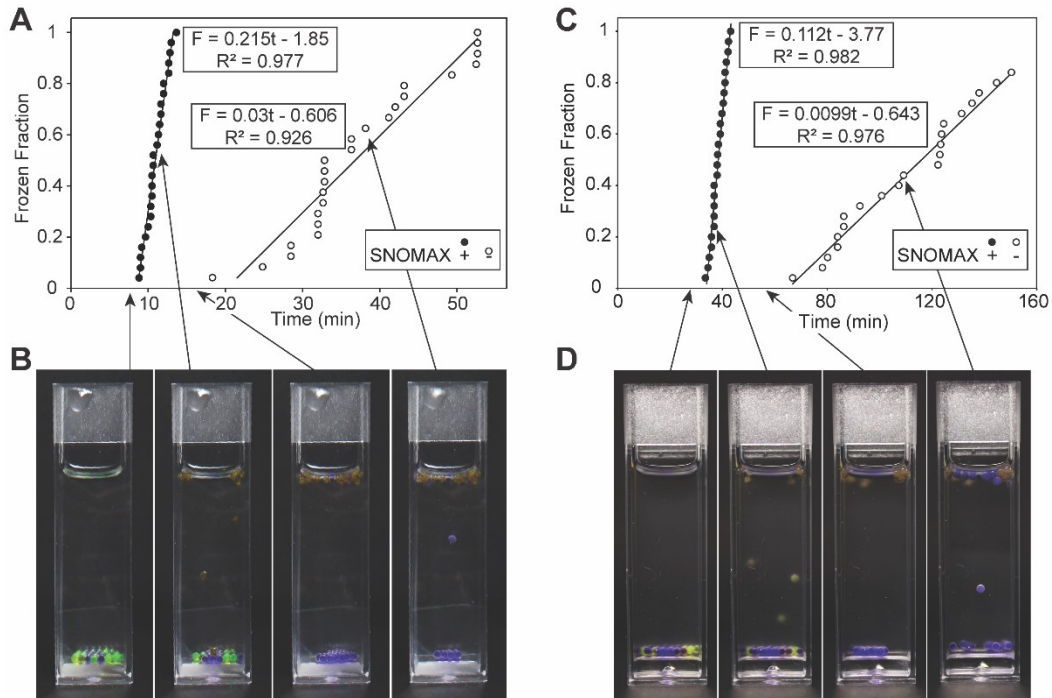


**Figure 2-4.** Optimization of the cooling rate. (A) Freezing temperature of two groups of droplets, containing either 1 mg/mL Snomax in water or water alone cooled at the rate of  $-0.7$  °C/min. (B) Representative images of freeze-float separation experiment. Yellow droplets contained Snomax and fluorescein dye, blue droplets contained aqueous solution of Coomassie Brilliant Blue dye. (C) The same experiment as (A) conducted with the cooling rate of  $-0.2$  °C/min and (D) images of the experiment described in (C). In both cases, the groups of droplets that contained nucleator could be robustly separated from those that did not.



### 2.3.3. Freeze-float selection validation testing

To validate the ability of freeze-float selection system to separate substances that exhibit a continuum of ice-nucleating properties, I used droplets that contained different concentrations of ice-nucleating bacteria, *P. syringae* 31R1 (a generous gift from the Lindow laboratory, University of California, Berkeley). Droplets containing *P. syringae* solutions at four different concentrations (20,000

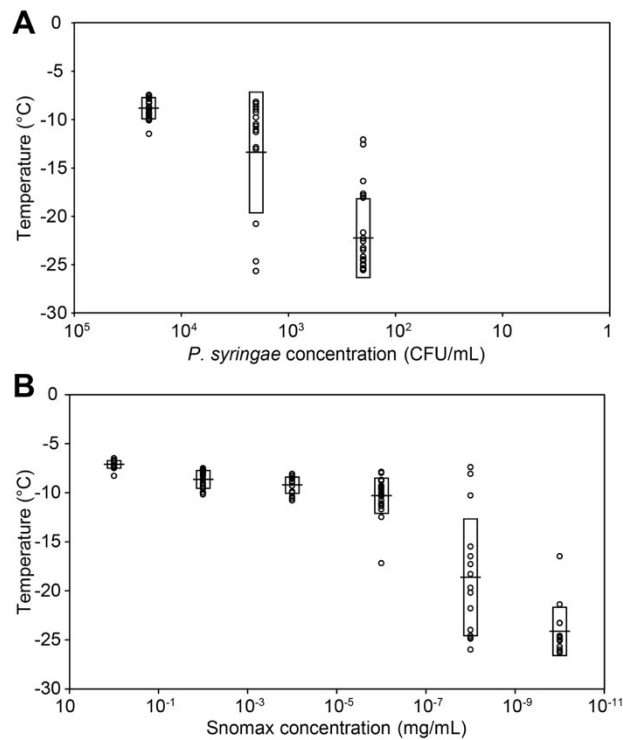


**Figure 2-5.** Ice-nucleating activity and concentration. Freezing temperatures of droplets which contain (A) *P. syringae* and (B) Snomax were measured in  $n = 25$  droplets. The rectangle is centered around population average and its height is  $2 \times$  standard deviation.

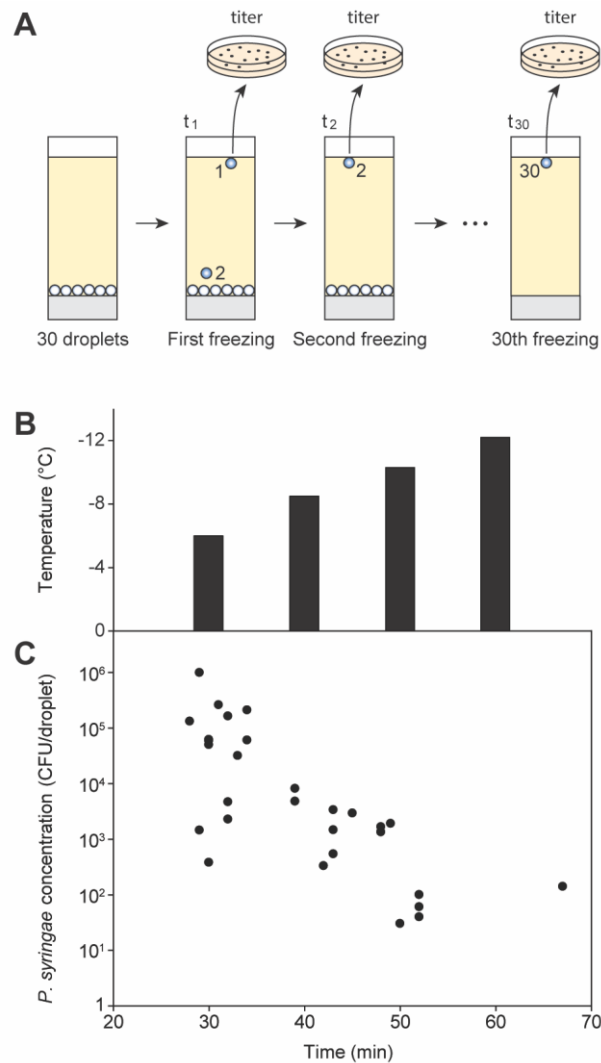


**Figure 2-6.** Validation of freeze-float system with various concentration of INA droplets. (A) The experimental design of the continuous freeze-float separation system. The droplets were picked as they floated to the top of the system and were titered individually. (B) The setup was used to separate 30 droplets containing either 200, 2,000 or 20,000 CFU/droplet of *P. syringae*. (C) *P. syringae* concentration in the droplets as a function of freezing time. With the exception of some outliers, concentrations of INA in recovered droplets exhibited a good correlation with freezing temperatures.

CFU/droplet, 2,000 CFU/droplet, 200 CFU/droplet, 20 CFU/droplet) spotted onto a plastic Petri dish exhibited ice-nucleating activity that was dependent on the concentration of *P. syringae* (Figure 2-5); same observation was previously reported by Lindow and co-workers.<sup>45</sup> Then I tested a new set of droplets containing either 120,000 CFU/droplet, 12,000 CFU/droplet, or 1,200 CFU/droplet in the freeze-float selection screen. The floated droplets were removed from the solution as they froze and thawed in separate containers, to determine the titer of bacteria encapsulated in each droplet (Figure 2-6). The titers indicated that droplets that froze at higher temperatures contained more ice-nucleating bacteria, and those that froze at lower temperatures contained fewer ice-nucleating bacteria (Figure 2-6 B,C). This observation demonstrated the ability of the freeze-float system to distinguish between the substances with differences in their relative ice nucleation capacities. It is intuitively clear that the rate of cooling could influence the selection process. Gradual cooling ( $\sim -0.2$  °C/min) increased the efficiency of the screen when compared to rapid cooling ( $\sim -0.9$  °C/min). Still, even rapid cooling yielded sorting outcome with acceptable fidelity (Figure 2-7). Reduced sorting fidelity at a rapid cooling rate likely originated from the  $\sim 2$  °C temperature gradient across the cuvettes (Figure 2-2), whereas gradual cooling minimized differences in temperature between droplets in different locations of the freeze-float setup.

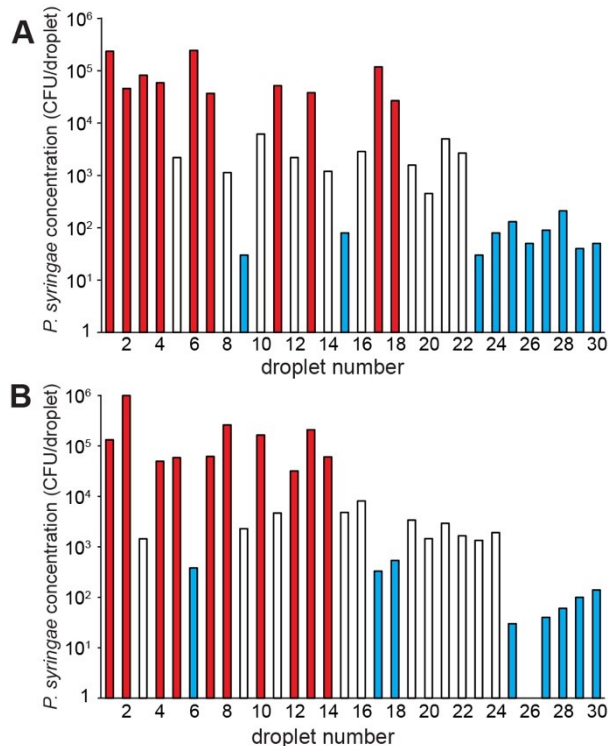


**Figure 2-7.** Optimization of the cooling rate with various concentration of INA droplets. (A) The system was brought from +20 °C to a -20 °C environment and cooled rapidly (-0.92 °C/min). (B) The system was cooled gradually by submerging the setup into ethanol/water bath at the rate of 0.21 °C/min. The ethanol/water bath was continuously stirred during the experiment. Lower cooling rate showed improved fidelity in separating the droplets with 20,000 ice-nucleating bacteria (red) from those with 200 bacteria (blue). Based on data described nucleation temperature as a function of the concentration of bacteria (Figure 2-5), I did not anticipate separating droplets with either 2,000 CFU/droplet from 20,000 or 2,000 CFU/droplet from 200 CFU/droplet populations, because the confidence interval of freezing data for sample with 2,000 CFU/droplet overlapped with both 20,000 and 200 CFU/droplet samples.

## 2.4 Conclusions

A simple suspension of aqueous droplets in a biphasic silicone oil / perfluoro oil layer is a functional, power-free, density-based screening system for

identification of INAs. It separates droplets that contain robust ice-nucleators from substances with a range of nucleatory activity even in a low-cost household chest freezer that does not allow for control of cooling rate of the system with high precision. At a density of 50 droplets/cm<sup>2</sup>, the frozen droplets do not coalesce and it is possible to separate the encapsulated INA substances by simple collection of the buoyant droplets. I am currently upgrading the setup to a high-throughput selection format in 96-well plates. I believe that the freeze-float selection system described in this communication will enable a wide range of experiments for studying ice-nucleating agents. With appropriate external or internal calibration, it also can be used for determination of the freezing temperatures of the solutions of INAs in droplets.

The freeze float selection works effectively with homogeneously pure species; still, I foresee the need for further development of the setup to allow discovery of nucleators from heterogeneous mixtures. Two types of directions will be required for either INAs that can be amplified (bacteria, environmental phage or engineered phage-display or bacteria-display systems) vs. INA that cannot be amplified (inorganic particles). Our reports corroborate the previous finding and indicate that even potent INAs such as *P. syringae* bacteria, have to be present in multiple copies per droplet. I and others previously demonstrated that it is possible to culture bacteria<sup>144, 145</sup> or phage,<sup>142, 143</sup> or phage-displayed libraries<sup>142, 143, 146</sup> in 200-300 micron droplets and achieve up to 1,000 copies of bacteria or up to

1,000,000 copies of clonal phage per droplet providing a sufficient concentration of homogeneous species in each droplet. Thus, if the goal is to isolate ice-nucleating bacteria from a mixed population or identify a phage that displays ice-nucleating proteins, the approach will likely require two-steps: (i) separation of the heterogeneous sample into the droplet-based compartment and culture of these droplets to yield multiple copies of the clonal bacteria or phage in each droplet similarly to previous reports,<sup>142, 143, 146</sup> (ii) separation of the droplets after culture in a freeze-float system in a similar static setup (e.g., a parallel 96-well setup). Efforts towards such two-step separation are ongoing in our laboratory and will be presented in the Chapter 3.

Discovery of INA that cannot be amplified will likely benefit from re-engineering of the geometry of the system to adopt droplets of nanoliter scale. The current report provides the first critical starting point by outlining the composition of the liquids and surfactants. Ideally, a static perfluoro oil/silicone oil bilayer can be replaced by known micro-channel geometries that employ two layers of liquid and two vertically stacked exit ports.<sup>147</sup> I caution that fluid dynamics in such heterogeneous vertically stacked layers is known to be rather complex and lead to complex behaviours such as rotation of the interface that employ viscous and non-newtonian fluids. Development of a setup for nanoliter droplets and a two-layer microfluidic-freeze float separation will be considered in a separate report.

## **2.5 Experimental procedures**

### **2.5.1 Materials and general information**

Fluorescein (#FX325, Matheson Coleman & Bell, Norwood, OH) and Coomassie Brilliant Blue R-250 (#161-0400, BioRad, Hercules, CA) was used for the coloring of the droplets. Milli Q water was used for all the droplet freezing experiments. Snomax was a generous gift from Edmonton Snow Valley Ski Club. Hexane and chloroform were purchased from Sigma Aldrich (#293253 and #319988). HFE-7500 was purchased from 3M (St. Paul, MN). Silicone oil DM-Fluid-5cs and silicone emulsifier KF-6017 were purchased from Shin-Etsu (Akron, OH). 4.5 mL plastic cuvette for the freeze-float system container was purchased from Fisher Scientific (#14-386-20).

### **2.5.2 Freeze-float selection system in organic buoyant layer**

3 mL of mixture of the organic phase (hexane:chloroform, 7:3 (v/v)) was used as the floating layer. To avoid the corrosion of plastic cuvette, I used quartz cuvette for the container. 1 mg/mL Snomax solution marked by fluorescein dye and no nucleator, marked by Coomassie Brilliant Blue was prepared for the positive and negative INA solution. The Freeze-float selection experiment was performed as described in the section 2.5.4 “Freeze-float selection procedure”.

### **2.5.3 Freeze-float selection system in silicone oil buoyant layer**

Silicone oil floating layer was prepared by dissolving 1% (v/v) emulsifier KF-6017 in DM-Fluid-5cs and agitating for 1 hour on a rotator. 200  $\mu$ L of the hydrofluoroether oil and 3 mL of the silicone oil layer was placed in 4.5 mL plastic cuvette. 1 mg/mL Snomax solution marked by fluorescein dye and no nucleator, marked by Coomassie Brilliant Blue was prepared for the positive and negative INA solution. The Freeze-float selection experiment was performed as described in the section 2.5.4 “Freeze-float selection procedure”.

### **2.5.4 Freeze-float selection procedure**

Add 1  $\mu$ L droplets by pipetting of the sample solution into the floating layer with a repeat pipettor (Eppendorf, #022260201). The 3.5 mL cuvette can hold up to 50 droplets without coalescence or adhesion to the walls. Pre-equilibrate a freezer (Costco #949554, DCF038A1WDB, Danby Products LTD., Guelph Ontario, Canada) to 0 °C.

Transfer the cuvette into the freezer and start the freezing experiment by setting the temperature to -20 °C. Record the behavior of the droplets by a digital camera (Canon EOS Rebel T3i #5169B003) placed inside the freezer (Appendix A-3). The lid of the freezer remains closed during the experiment and the illumination of the samples is performed by low-heat LED light sources (Staples, #19639-000) placed in the freezer. The camera was operated remotely by a



controlling software EOS Utility 2 (Canon) and images were recorded every 10 seconds. If necessary, the floated droplets can be transferred to a separate container and used for further analysis.

### **2.5.5 Monitoring of the temperature of freeze-float system**

To record the inner temperature of the freeze-float system and measure the freezing temperature of the droplets without interfering with the system itself, I used a proxy method that measured the temperature of several droplet-free cuvettes placed in the vicinity of the test cuvette during the experiment using digital thermometer (Traceable, #4371). The droplet-free cuvettes were placed 1 cm away from the test cuvettes in which the freeze-float experiment was conducted. The inner temperature of the test cuvette was extrapolated to be within an average and a standard deviation of temperatures in three reference systems. Figure 2-2 A-B shows that the temperatures recorded by these reference systems with a standard deviation of 0.2 - 1.0 °C during a typical cooling cycle.

### **2.5.6 Thermal gradient simulation calculation**

To simulate the inner temperature of the silicone oil freeze-float system (Figure 2-2C), I used one-dimensional non-stationary heat conduction calculation in a cylinder model. According to Fourier's law, the equation of one-dimensional non-stationary heat conduction in cylinder is:

$$\frac{\partial T}{\partial t} = \frac{\alpha}{r} \frac{\partial}{\partial r} \left( r \frac{\partial T}{\partial r} \right)$$

where  $\alpha$  is the thermal diffusivity, and  $r$  is the distance from the center. The thermal diffusivity of DM-F-5cs is  $7.10 \times 10^{-8}$  m<sup>2</sup>/s, and that of polystyrene is  $2.54 \times 10^{-7}$  m<sup>2</sup>/s. Discretizing time as  $t = P\Delta t$ , the distance as  $r = n\Delta r$ , allows estimating the discrete values of  $T_n^P$ , the temperature of the cuvette at a specific time  $p$ , and spatial position  $n$ . The discrete form of the above equation can be represented as:

$$T_n^{P+1} = \Theta_r \left( 1 + \frac{1}{2n} \right) T_{n+1}^P + \Theta_r \left( 1 - \frac{1}{2n} \right) T_{n-1}^P + (1 - 2\Theta_r) T_n^P$$

$$\Theta_r = \frac{\alpha \Delta t}{(\Delta r)^2}$$

The temperatures of silicone oil phase in different positions at the different times were calculated by solving the above equation.

### 2.5.7 Culture of *P. syringae*

*P. syringae* 31R1 was obtained from Lindow laboratory, University of California, Berkeley. The strain was cultured on agar solid media supplemented with 2% glycerol at room temperature. The plates with colonies were maintained at 4 °C up to 1 week. For the individual experiment, one colony was used to inoculate the LB liquid medium with 2% glycerol and cultured in 14 mL Polypropylene Round-Bottom Tube (352059, Falcon, NY) shaken at 200 rpm for 2 days at room temperature.

### **2.5.8 Validation testing of the Freeze-float selection**

As the INA positive solution, varying concentrations (120,000 CFU/droplet, 12,000 CFU/droplet, or 1,200 CFU/droplet) of *P. syringae* solutions were used. The *P. syringae* culture from 2.5.7 was used. This solution was marked by fluorescein dye. The freezing experiments were conducted in the two different conditions; rapid cooling at -20 °C environment and slow linear cooling at 0.21 °C/min. 1 µL 10 droplets from each solution were placed in the Freeze-float selection system, and temperature and droplets freezing behaviour were recorded. System was cooled down and the floated droplets were removed from the solution as they froze and thawed in separate 1.5 mL microcentrifuge tube containing 99 µL LB with 2% glycerol. To determine the titer of bacteria encapsulated in each droplet. The INA concentration was measured by titering the *P. syringae* concentration of the each droplets.

## **Chapter 3: System for achieving enhanced throughput and quality for Freeze-float selection**

### **3.1 Introduction**

In this chapter, I developed the high throughput screening implementation of freeze-float selection platform system I established in Chapter 2. The goal of this chapter is to expand the system to higher throughput and accuracy. In the following sections, I describe the steps for automated droplets generations, adaptation of freeze-float selection using controlled and uniform temperature cooling system, and semi-automated droplets detections program.

Previously in Chapter 2, I reported and published a first proof-of-concept implementation of freeze-float selection system,<sup>148</sup> which was able to identify the ice-nucleation event in droplets that contained ice-nucleating entities. 1 cm<sup>2</sup> geometry cuvette system successfully accommodated up to 50 × 1 μL droplets at once and separated the samples that have ice-nucleating activity from those do not. However, due to the low thermal conductivity of the silicone oil, it was not possible to increase the footprint of the container and accommodate a larger number of droplets without introducing a significant thermal lag (Figure 2-2B). The throughput could be increased by setting up multiple cuvettes in parallel, but setting up more than 5-10 cuvettes in the same freezer system was difficult, and again, resulted in non-uniform results; for example, in setting up 10 cuvettes at the same

time, we observed a difference of a few degrees' between cuvettes. To improve the uniformity of the temperature among multiple cuvettes, the system requires the good heat conductor between cuvettes.

High throughput screening (HTS) in multi-well plates miniaturization and automation of biochemical assays is well-established method to enable a large number of parallel measurements. HTS has been developed originally for drug discovery in the laboratory or pharmaceutical industry to screen the increasing number of potential targets and therapeutic compound libraries.<sup>149-152</sup> The transition from the low-throughput assay to the HTS results in highly efficient and integrated system, which includes the shortened screening time, reduced amount of sample and reagent, and lower costs of the overall process. Miniaturization using 3456-well microtiter plate made it possible to carry out more than 100,000 assays per day and volume of less than 5  $\mu\text{L}$ .<sup>153, 154</sup> Combination of the automated liquid dispensing and plate handling robotics enabled even higher throughput and reproducibility while the increasing number of assays.<sup>155, 156</sup> To process the large data sets associated with the HTS, robust signal detection and statistical analysis systems have also been developed.<sup>157</sup>

Droplets-based assays represent another form of high-throughput assay. It offers the advantage of chemical and physical compartmentalization to avoid cross-contamination of the samples by segmenting the uniform droplets by the immiscible carrier fluid. Successful examples of the droplet microfluidic assays

such as crystallization study<sup>158</sup> or single cell screening of enzyme production<sup>107, 159</sup> reported a million fold reduction of reagent consumption and 300-folds increase in throughput when compared to the HTS-multiwell assays. Droplet-based assays have also been employed to measure tens of thousands ice nucleation events at one experiment.<sup>107, 108</sup> Microfluidic droplet based cell and virion counting techniques are also reported.<sup>160</sup> Droplet based analysis became a commercial success in digital polymerase chain reaction (dPCR)<sup>161</sup> and single-cell genomics.<sup>162, 163</sup> This technology successfully increased the sensitivity of the absolute nucleic acid quantification by compartmentalizing the individual DNA molecule into uniform droplets. When compared to HTS plate-based assays, the drawback of droplet systems is difficult in measuring a large number of droplets of arbitrary compositions.

### **3.2 Experimental Design**

In this chapter, we aimed to improve previously published system to add functional advantages, such as; a) increased efficiency of the screening with fewer manipulation steps; b) increased accuracy of measurement due to the increased sample size; c) increased uniformity of temperature distribution by incorporating the controlled-rate freezer. In the following sections, we describe the steps for automated droplets generations, freeze-float system adaptations using controlled

and uniform temperature cooling system, and semi-automated droplets detection program.

Preparation of polydisperse silicone oil emulsions by simple mixing have been used in biochemical applications.<sup>164</sup> Despite the ease of manufacturing, polydispersity is detrimental in ice-nucleation studies because the freezing temperature is directly proportional to the logarithm of droplets diameter.<sup>6</sup> The polydispersity of the droplets can directly influence the accuracy of the freezing measurement. Swanson and co-worker observed that the droplet diameter and homogeneous freezing temperature can be expressed as

$$y = \ln(x) - 26.8$$

where  $y$  is nucleation temperature and  $x$  is droplet radius.<sup>8</sup> This approximation will lead to 2.3 °C difference of mean freezing temperature between the 1 mm diameter and 0.1 mm diameter droplets. Microfluidics can produce uniform droplets but interfacing of microfluidics and microtiter well plates used in HTS is not obvious and not trivial. Based on this knowledge, we produced uniform size droplets via the commercially available automated pipetting system and confirmed the monodispersity by image analysis.

To obtain the reliable freezing temperature, sample number is also important. Confidence interval of the freezing temperature of droplets was calculated via the formula:

$$n \approx (2k/CI)^2 s^2$$

$n$  is the sample number,  $k$  is the value for desired confidence level (1.96 for 95% confidence),  $CI$  is the confidence interval, and  $s$  is the standard deviation of the outcome of interest. From the obtained value, we concluded that more than 30 droplets sample is sufficient to observe the reliable freezing temperature.

I introduced the robotic liquid transfer system Biomek® 3000 (Beckman Coulter, Indianapolis, IN) to enable the automated parallel generation of droplets in wells of a multi-well plate. Biomek 3000 replaced manual generation of droplets by repeat pipetting employed in our previous report. This robotic system provides liquid handling operations with a spatial positioning ability compatible with many multi-well plate geometries. Simple modification to the Biomek program allowed changing the parameters of droplets generation including droplets number or droplets size.

From the prior study, the droplet freezing is hypothesized to be a random nucleation process which can be accelerated in the presence of ice nucleators. Due to the stochastic freezing behavior, the freezing spectra in droplet freezing assays usually shows inherent distributions, which results in a spread of the freezing temperature among droplets even when all the droplets have identical size and contain the same number of the INA species.<sup>165</sup> This dispersion makes it difficult to determine the ice nucleating temperature from a small number of samples. By expanding the size of the assay vessel from a 1 cm<sup>2</sup> footprint cuvette that contains up to 50 droplets to the 48 cryovials that can contain up to 40 droplets (40 droplets



× 48 vials = 1920 droplets), the throughput can be increased by the factor of 38. The cooling setup employed the metal cooling plate and sample holder to achieve the homogeneous cooling through the vial to vial.

Wills and co-workers have reported that the droplet freezing assays with cooling rates from 0.8 to 10 K/min produced nucleation rates fit in a single line,<sup>166</sup> which suggested that the difference in cooling rate had minimum effect on the nucleation rate coefficients. However linear cooling rate is important for the droplet freezing assay in the stochastic model of heterogeneous nucleation measurement.<sup>166</sup> Based on this report, we conducted the freeze-float experiment incorporating a constant rate freezer Asymptote VIA freezer. This commercially available instrument affords a constant rate cooling with high precision down to -0.5 °C/min. We equipped this bench-top instrument with custom-made glass lid to enable automated image recording by generic digital camera.

### **3.3 Results and Discussion**

#### **3.3.1 Automated droplets generation**

To implement the freeze-float selection at the higher throughput scale, we first tested the 96 deep well plate which is compatible with the robotic liquid handling machine Biomek 3000 (Figure 3-1 A-B). We used the same silicone oil buoyant layer with 1% silicone surfactant system and HFE-7500 cushion layer as we used in the previous publication.

We dispensed  $30 \times 1 \mu\text{L}$  droplets into the silicone oil layer of 96 deep well plate using Biomek 3000. At a standard dispensing rate 1 droplet per 2 seconds, a pipetting arm successfully generated 40 uniform droplets in 96 wells (up to ~3800 droplets at once) in ~15 minutes. The rate can be further accelerated by using a multi-head dispenser.

Uniform volume is the key for quantitative detection of ice-nucleation events. To assess the droplets dispersity, we prepared the 60  $1 \mu\text{L}$  droplets with fluorescein dye by the Biomek 3000 in the silicone oil in the 12 well plate filled with silicone oil and acquired the fluorescent image by ChemiDoc MP (Bio-Rad, CA) (Figure 3-1C). The droplet diameters were measured by using Matlab automated circle detection program Droplet\_Dispersion.m (Appendix B-11). This program detects the circles in image in an automated manner and analyze the diameter of each droplets. The polydispersity of the 60 droplets defined as standard deviation of the radii of the droplets (here  $2.86 \times 10^{-5}$ ) divided by the mean radius (here  $3.10 \times 10^{-4}$  m) was 9.2%, which indicated that the droplets generated by the robotic system have sufficiently uniform volume (Figure 3-1 D-E). Swanson and co-worker observed that the droplet diameter and homogeneous freezing temperature can be expressed as

$$y = \ln(x) - 26.8$$

where  $y$  is nucleation temperature and  $x$  is droplet radius.<sup>8</sup> Based on the standard deviation of the radii of the droplets, we calculated the temperature error from the .<sup>8</sup>

we expected no more than  $\pm 0.09$  °C dispersion in the measurement of the nucleation temperature.

We took several precautions to eliminate droplets coalescence. To avoid contact with the plastic wall which can cause the droplets destabilization, the HFE-7500 was always placed at the bottom of the system as a cushion layer. The static electricity of the Biomek 3000 which could cause coalescence of the droplets was removed by using Auto-set Ion Pump (#19500, Charles Water, MA). This machine is bench-top equipment that discharges static potential accumulation caused by the Biomek 3000 operation. Also when we move the droplet system, wet filter paper was placed below the plastic plate to minimize the accumulation of static electricity.

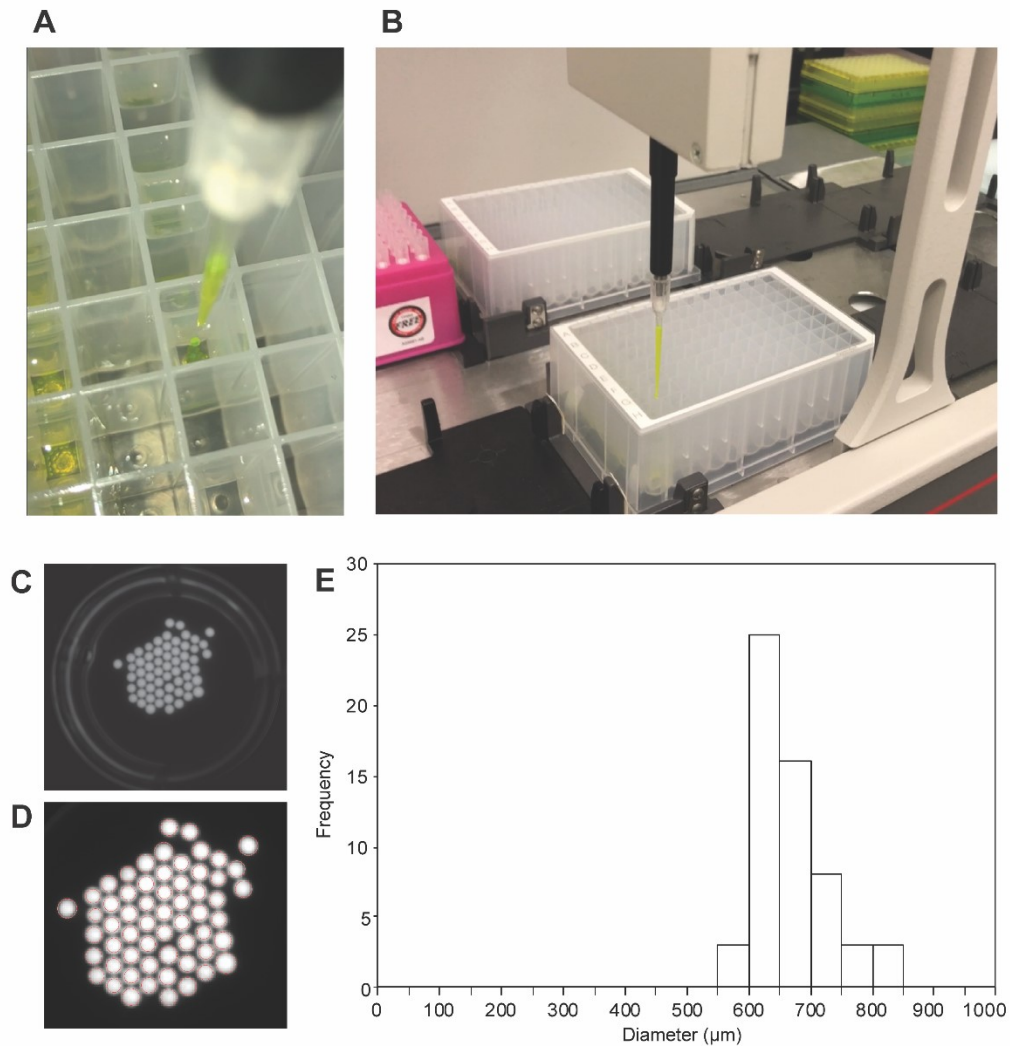


**Figure 3-1.** Automated droplets generation system using Biomek 3000. (A) Digital imaging of the automatic droplet generation. 1  $\mu\text{L}$  droplets were dispensed into the deep wells by the repeat pipetting. (B) Overview of the droplets generation machine. (C) Fluorescent imaging of the droplets. (D) Droplet detection system by Matlab. (E) Histogram of estimated droplets size. The droplets' polydispersity was 9.3%.

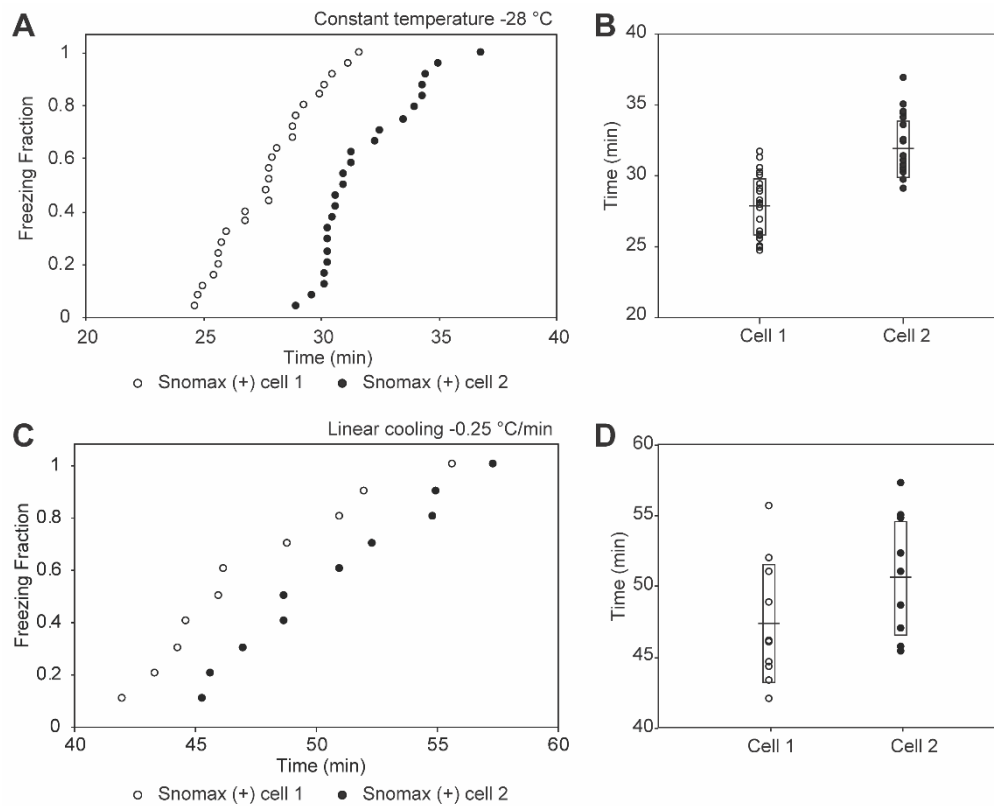


**Figure 3-2.** Thermal gradient in Biomek 3000 deep well system. (A) and (B) show the freezing temperature dispersion on constant temperature cooling at  $-28\text{ }^{\circ}\text{C}$  in different position of the deep well, and (C) and (D) show the linear cooling at  $-0.25\text{ }^{\circ}\text{C}/\text{min}$  in different position of the deep well. Freezing temperatures of 1 mg/mL Snomax droplets were measured over time.

I conducted freeze-float validation experiment of the system implementing Biomek 3000. The Biomek 3000 successfully prepared 30 aqueous droplets with 1 mg/mL Snomax colored with yellow fluorescein dye in a 96 deep well system. I placed this system in the commodity freezer employed in the previous chapter, and recorded the droplets freezing and floating behaviour (Figure 3-2). The INA

droplets showed droplet freezing behaviour with a good agreement with the previous report.

We used Python script KStest.ipynb (Appendix B-13) to compare the freezing temperature distribution of droplets from two different samples. Briefly, this script compares cumulative distributions of the freezing temperature from two samples and calculate the p-value using Kolmogorov-Smirnov test to show if the freezing temperature profile of the two samples are drawn from the same distributions.

To achieve the high throughput screening, it is necessary to establish the multi-well platform that can give uniform cooling through all wells in a plate. However, due to the low thermal conductivity of the silicone oil and geometry of the 96 deep well plate, it was difficult to avoid the cell to cell thermal gradient. The freezing temperature in cells in the same deep well plate showed p-value of  $4.4 \times 10^{-7}$  at constant temperature  $-28\text{ }^{\circ}\text{C}$  generic freezer (Figure 3-3). The thermal gradient was decreased ( $p = 0.31$ ) with linear cooling ( $-0.25\text{ }^{\circ}\text{C}/\text{min}$ ) compared to the constant temperature cooling, however it significantly increased the range of freezing time, and mean freezing time between the cells were different (47.4 and 50.6 min). I concluded that using these 96 deep well plate approaches as the screening platform is not a promising path.

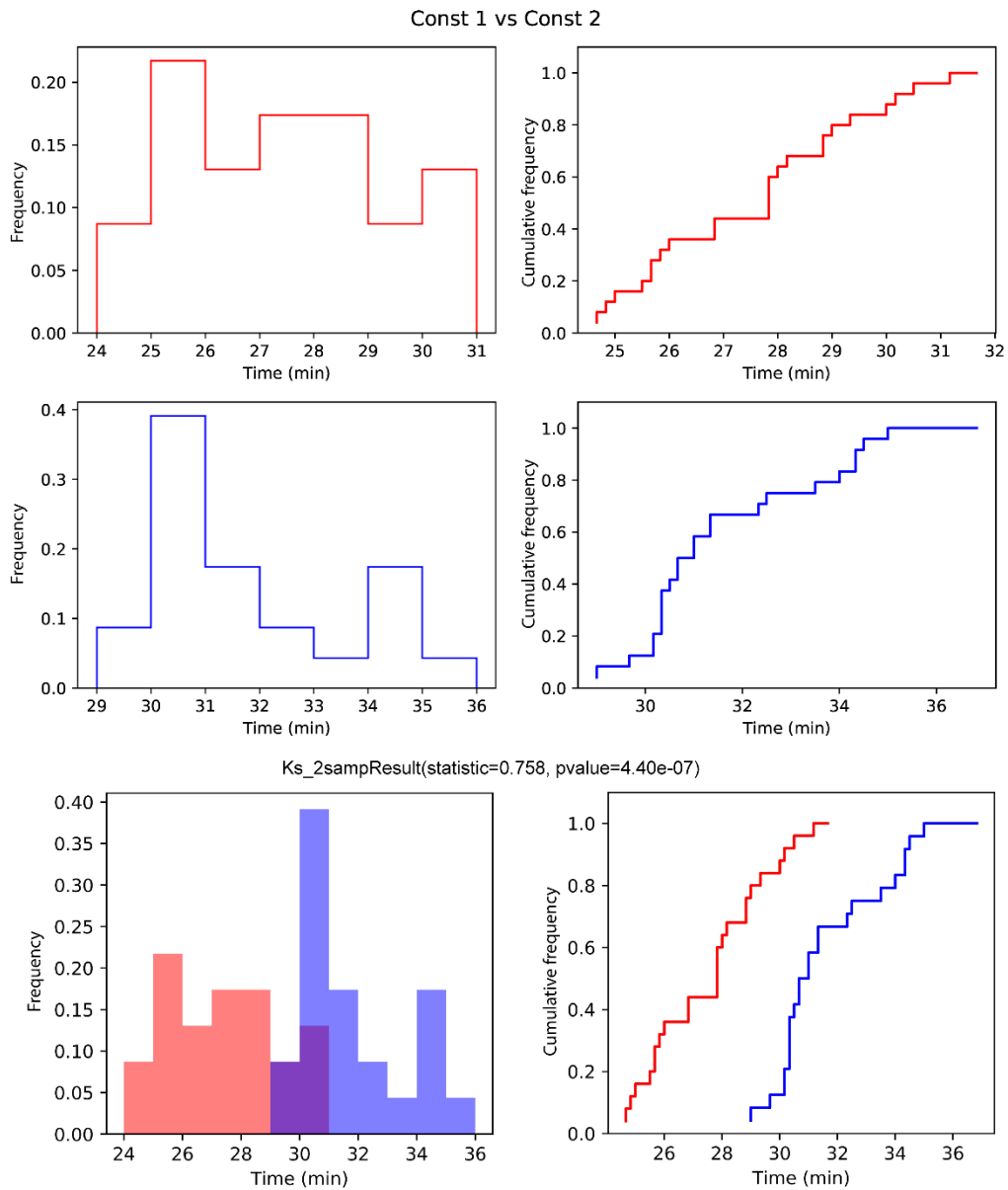


**Figure 3-3. Comparison of droplet freezing temperature dispersions by Kolmogorov-Smirnov test.**

These results show the comparison of the cells in different position. Commodity freezer system with constant temperature (at  $-27\text{ }^{\circ}\text{C}$ ) was used. Both used  $1\text{ mg/mL}$  Snomax droplets.

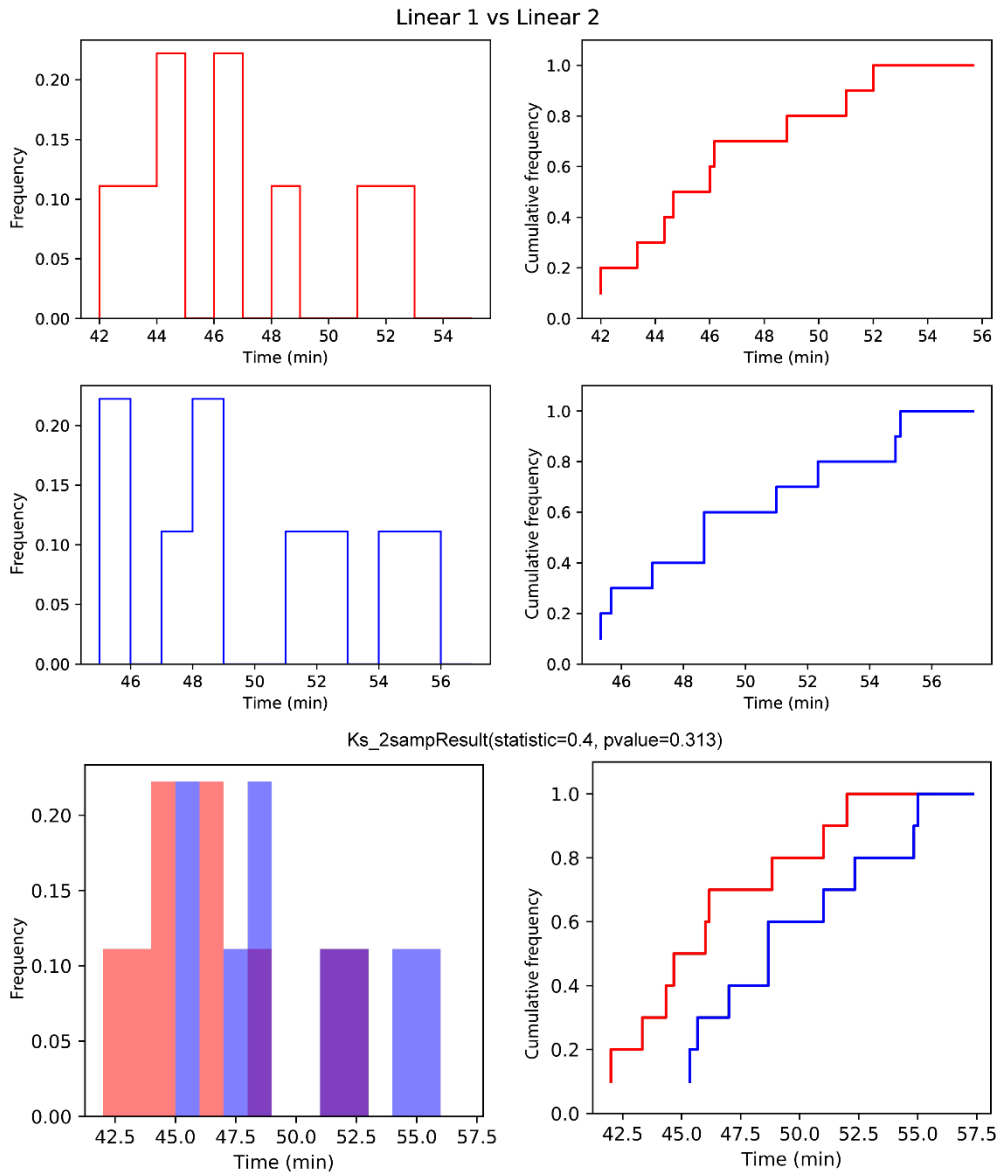


**Figure 3-3. (Cont.)** Comparison of droplet freezing temperature dispersions by Kolmogorov-Smirnov test. These results show the comparison of the cells in different position. Commodity freezer system with linear cooling ( $-0.25\text{ }^{\circ}\text{C}/\text{min}$ ) was used. Both used  $1\text{ mg}/\text{mL}$  Snomax droplets.



### 3.3.2 Asymptote VIA freezer

To achieve the constant rate cooling of the freeze-float system and better uniformity of the cell to cell temperature, I employed VIA Freeze<sup>TM</sup> Research controlled rate freezer (Asymptote, Cambridge, UK). The freezer successfully provided high accuracy control of the cooling temperature and accommodate up to 48×1 mL cryovials in an instrument-specific metal holder.

Each cryovial contained 50  $\mu$ L of HFE-7500 at the bottom of the cryovial as a cushion layer, 1 mL silicone oil with 1% surfactant floating layer, and 20 aqueous droplets with 1 mg/mL Snomax marked with fluorescein, and 20 droplets of INA free milli Q water marked with Coomassie Brilliant Blue dye. Similar to the previous observations, the droplets with INA froze at  $-7.1 \pm 0.59$  °C and droplets without INA did not freeze until the temperature reached to  $-12.3$  °C in the Asymptote freezer (Figure 3-4). This observation suggested that the controlled cooling rate provided better detection of INA compared to the freeze-float selection in a commodity freezer system (mean temperature  $-7.5 \pm 0.97$  °C).

To evaluate the uniformity of the cooling between cells at different positions, we compared the temperature at which 1 g/mL Snomax droplets froze in Asymptote controlled rate freezer system and 96 deep well in generic freezer. We used python script KStest.ipynb (Appendix B-13) to compare the freezing temperature distributions. We observed well to well variability and inter-well dispersion in the freezing time in the 96 deep well system ( $p = 0.31$ , standard deviation 1.6), whereas

the distribution of freezing of droplets in Asymptote freezer (Figure 3-5) showed less difference of well to well freezing temperature ( $p = 0.83$ , standard deviation 0.73) and overall 36% lower dispersion (Figure 3-6).

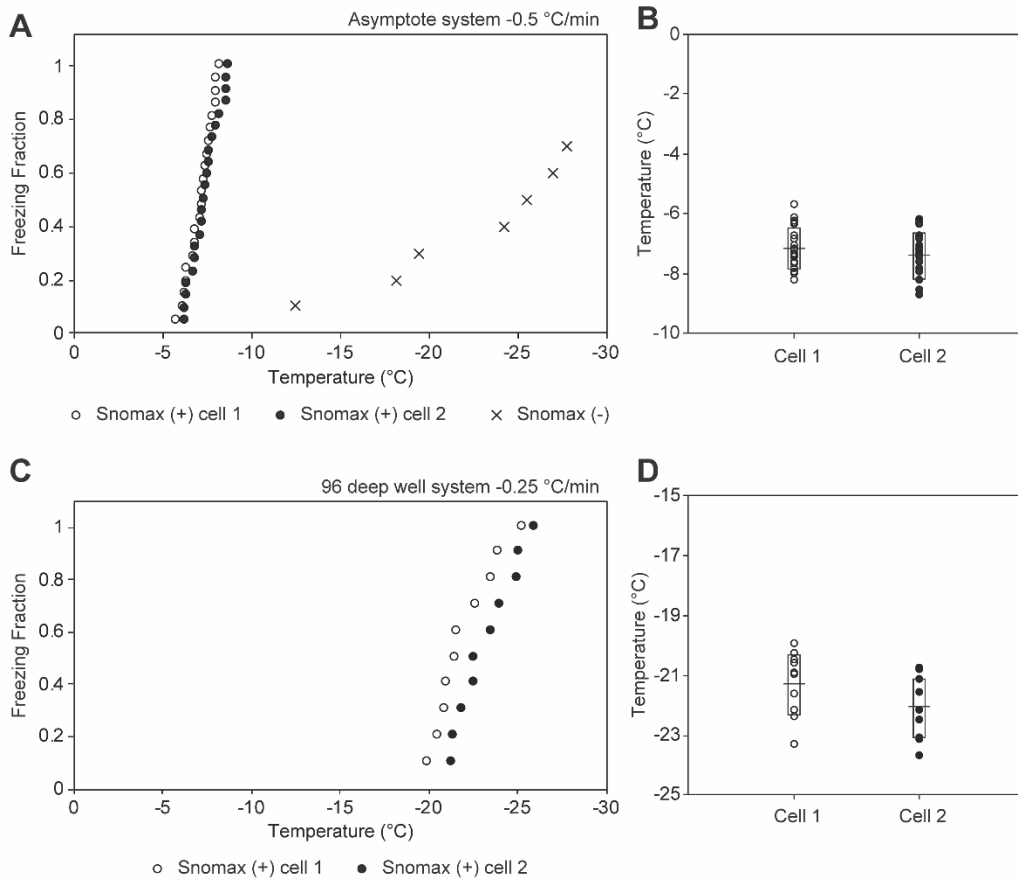


**Figure 3-4.** Thermal gradient in Asymptote system. (A-B) Asymptote constant-rate freezer with cooling rate at  $-0.5\text{ °C/min}$  in different position and (C-D) 96 deep well system with cooling rate at  $-0.25\text{ °C/min}$  in different position as a reference. Freezing temperatures of two groups of droplets, containing either 1 mg/mL Snomax in water or water alone, were measured over time.

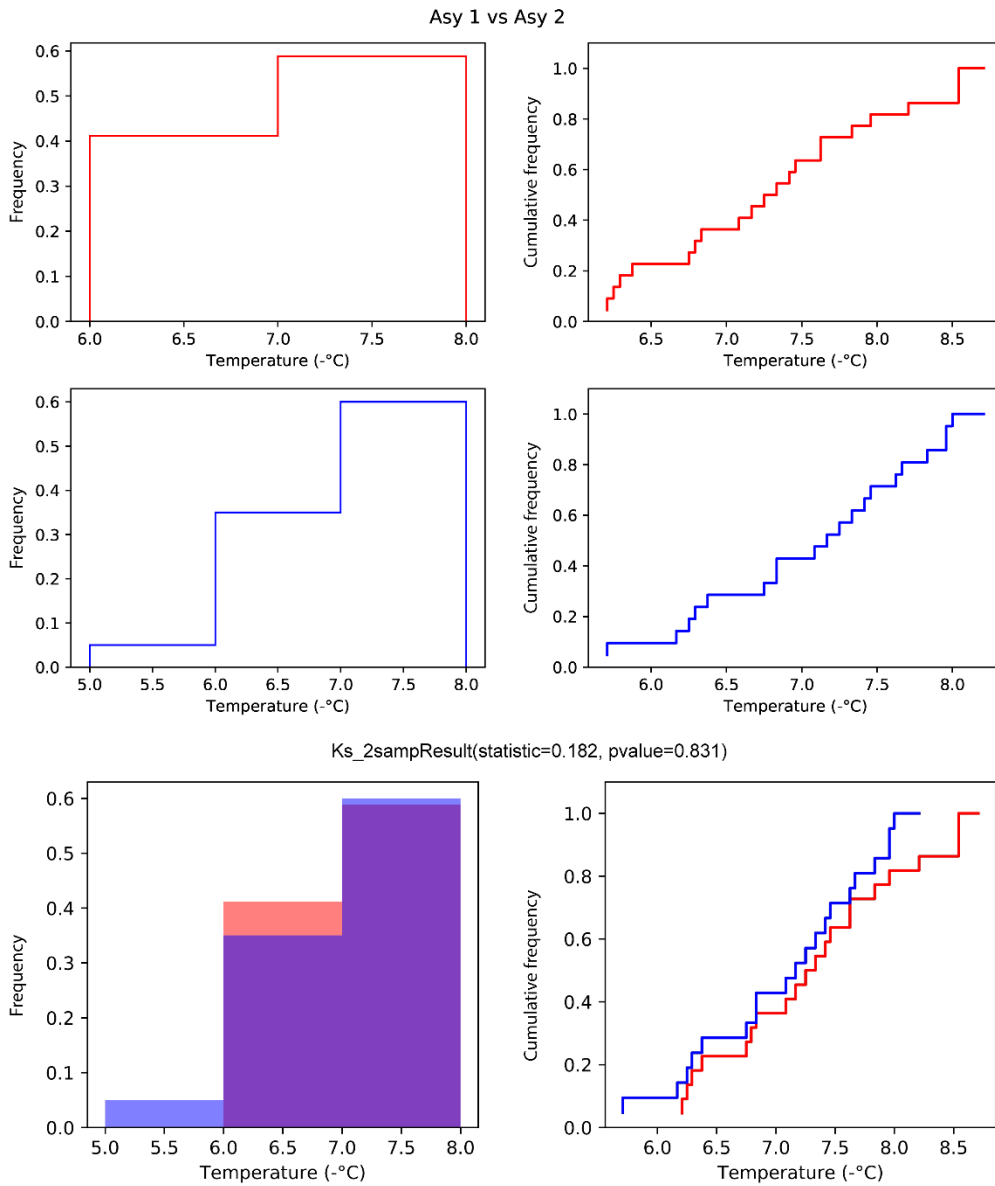


**Figure 3-5.** Comparison of droplet freezing temperature dispersions by Kolmogorov-Smirnov test.

These results show the comparison of the cells in different position cooled with Asymptote freezer (cooling rate  $-0.5\text{ }^{\circ}\text{C}/\text{min}$ ). Both used  $1\text{ mg}/\text{mL}$  Snomax droplets.

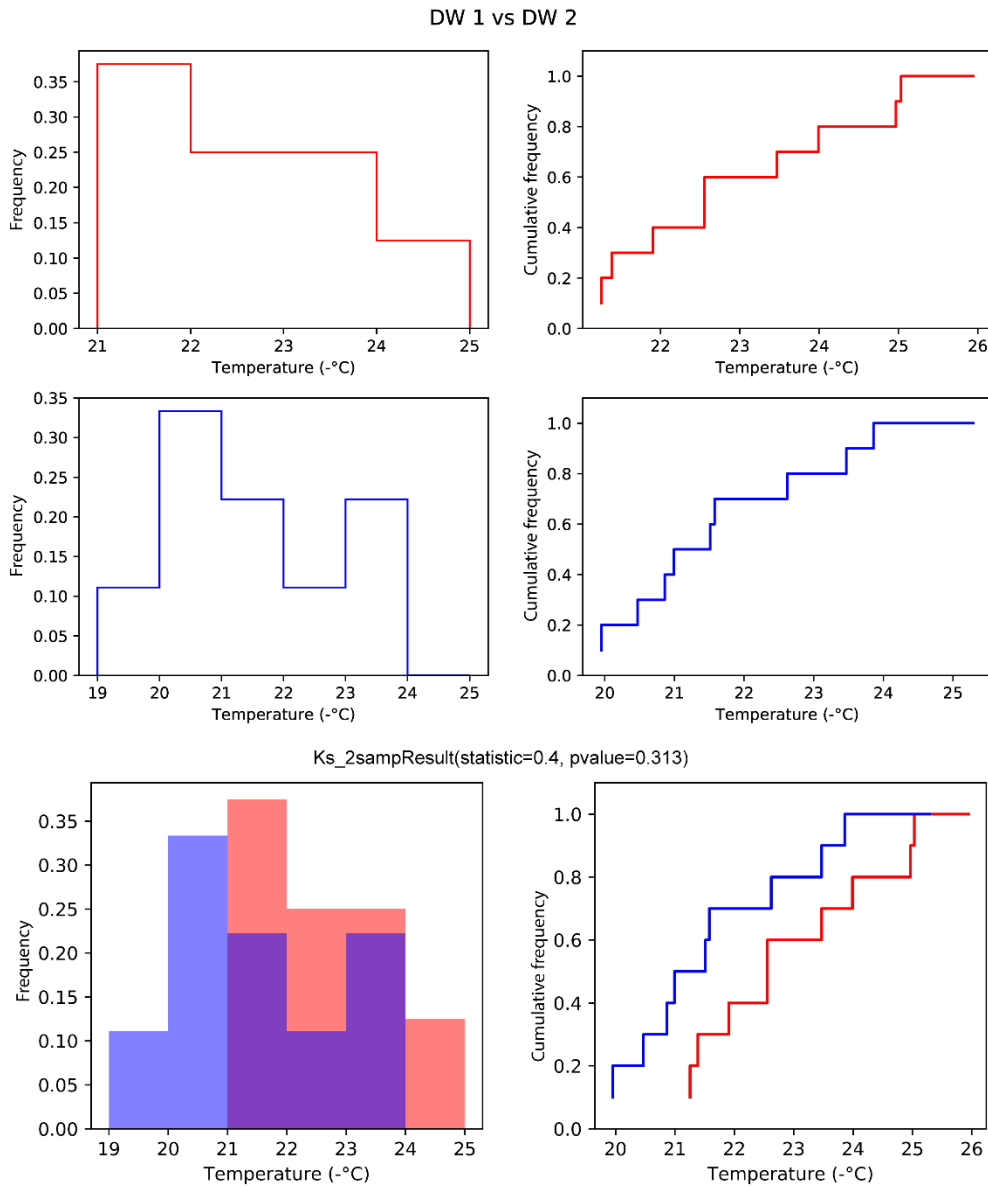


**Figure 3-5. (Cont.)** Comparison of droplet freezing temperature dispersions by Kolmogorov-Smirnov test.

These results show the comparison of the deep well cells in different position cooled with commodity freezer system (linear cooling at  $-0.25\text{ }^{\circ}\text{C}/\text{min}$ ). Both used  $1\text{ mg}/\text{mL}$  Snomax droplets.

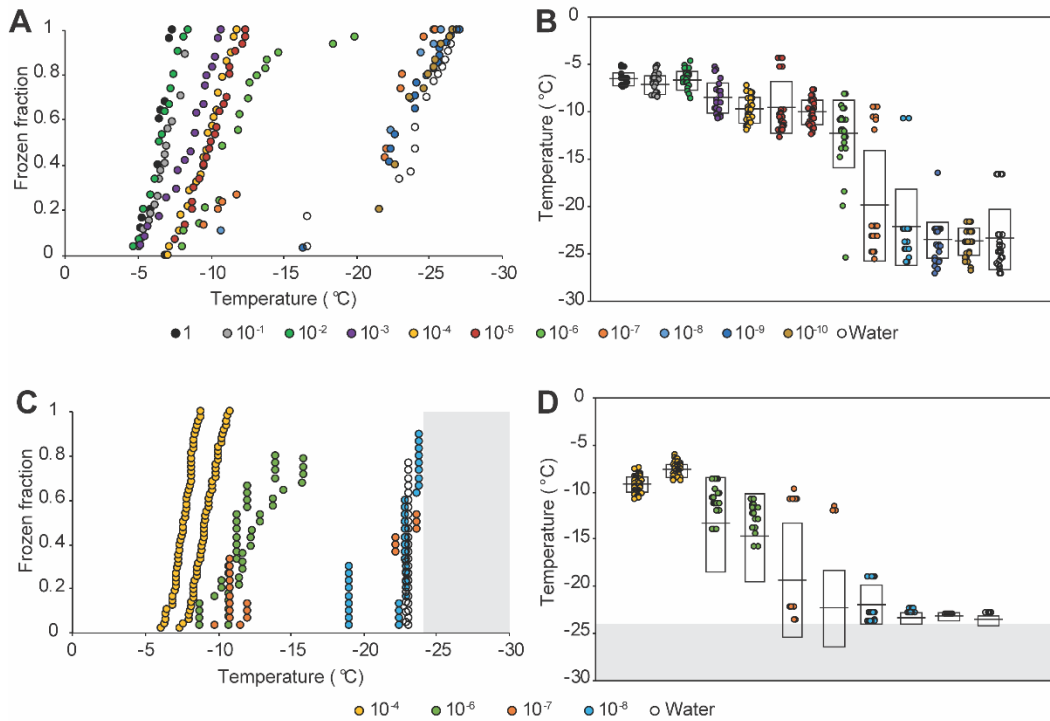


**Figure 3-6.** Droplet freezing temperatures of serial dilution of INA solution. Freeze-float selection system was cooled either (A, B) Asymptote freezing system or (C, D) generic freezer system.

### 3.4 Conclusion

To increase the efficiency and accuracy of the freeze-float system from Chapter 2, we employed the automated droplets dispensing system and controlled rate freezer. By using Biomek 3000 liquid handling system, theoretically generates up to ~3800 uniform 1  $\mu$ L droplets in the 96 well plate freeze-float system. The droplets generated by this system and contained INA showed similar freezing and floating behaviour to the experiment I conducted in the previous chapter, which indicates that this system can be implemented to the high throughput freeze-float

system. However, when the system needs to be transferred certain distance, for example from one laboratory to another, the droplet stability was not sufficient and static electricity caused by frictions caused coalescing. Due to this problem, it was not successful to combine the droplets generation system.

Next, we implemented the controlled-rate Asymptote freezer system to enlarge the capacity of the droplets and improve the accuracy of the system. The cell to cell thermal delay was improved by the constant linear cooling (from  $p = 4.4 \times 10^{-7}$  to  $p = 0.31$ ). To confirm the accuracy of the screening system, the detection threshold of the INA concentration was investigated. At the threshold concentration, controlled-rate cooling system showed better differentiation accuracies ( $p = 4.4 \times 10^{-7}$ ) compared to the commodity freezer ( $p = 0.83$ ).

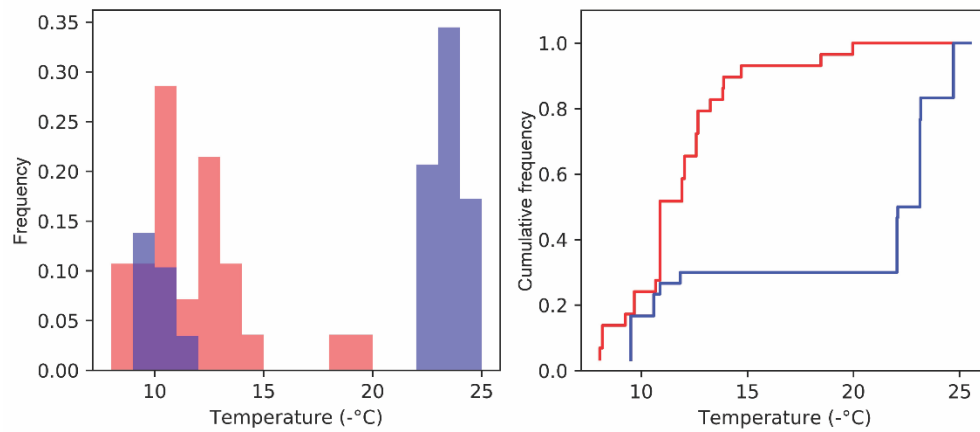
The throughput of the described droplet-based screening enables 50 different samples, measuring 40 droplets each. When combined with automated liquid handling, in principle, this system is suitable for medium throughput, high confidence measurement of 100-1000 unique chemical compositions or concentrations. While the unbiased discovery of INAs from a large chemical library remains a challenge in this setup alone, it can serve as a robust validation step for novel putative INA compositions emanating from large-scale genetically-encoded screens.

**A**

	A 10 <sup>-4</sup>	A 10 <sup>-6</sup>	A 10 <sup>-7</sup>	A 10 <sup>-8</sup>	G 10 <sup>-4</sup>	G 10 <sup>-6</sup>	G 10 <sup>-7</sup>	G 10 <sup>-8</sup>
A 10 <sup>-4</sup>	1.00E+00							
A 10 <sup>-6</sup>	2.18E-04	1.00E+00						
A 10 <sup>-7</sup>	9.91E-08	3.56E-07	1.00E+00					
A 10 <sup>-8</sup>	3.58E-11	1.57E-10	3.01E-02	1.00E+00				
G 10 <sup>-4</sup>	4.01E-02	2.65E-10	2.01E-12	6.36E-17	1.00E+00			
G 10 <sup>-6</sup>	2.94E-03	2.09E-01	3.55E-07	2.27E-10	1.20E-07	1.00E+00		
G 10 <sup>-7</sup>	1.65E-05	1.10E-01	5.95E-02	2.27E-05	1.51E-10	1.02E-01	1.00E+00	
G 10 <sup>-8</sup>	2.39E-13	8.23E-12	2.25E-01	1.09E-01	7.61E-17	2.05E-12	3.56E-04	1.00E+00

**B**

Asymptote freezer 10<sup>-7</sup> mg/mL vs 10<sup>-6</sup> mg/mL



**C**

Generic freezer 10<sup>-7</sup> mg/mL vs 10<sup>-6</sup> mg/mL

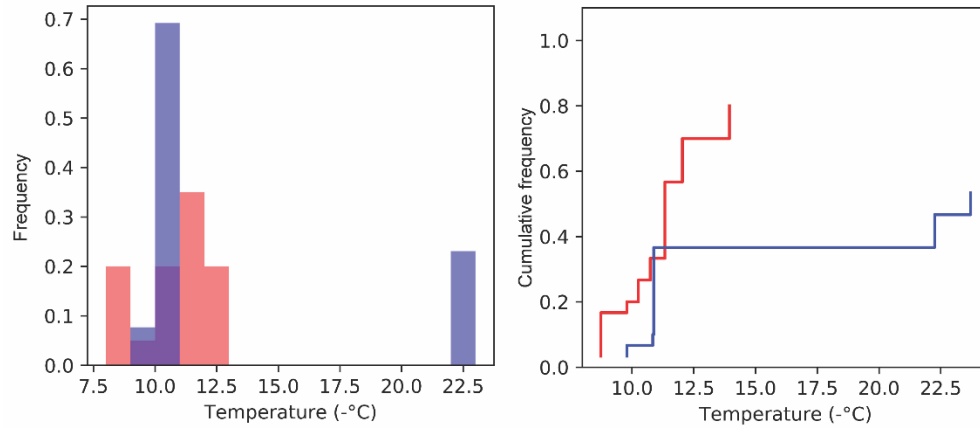


**Figure 3-7.** Comparison of droplet freezing temperature dispersion. (A) P-value from Kolmogorov-Smirnov test. Histogram and cumulative dispersion comparison of 10<sup>-7</sup> mg/mL and 10<sup>-6</sup> mg/mL Snomax droplet freezing temperature of (B) Asymptote and (C) generic freezer experiment.

## **3.5 Experimental Procedures**

### **3.5.1 Materials and general information**

Fluorescein (#FX325, Matheson Coleman & Bell, Norwood, OH) and Coomassie Brilliant Blue R-250 (#161-0400, BioRad, Hercules, CA) was used for the coloring of the droplets. Milli Q water was used for all the droplet freezing experiments. Snomax<sup>TM</sup> was a generous gift from Edmonton Snow Valley Ski Club. HFE-7500 was purchased from 3M (St. Paul, MN). Silicone oil DM-Fluid-5cs and silicone emulsifier KF-6017 were purchased from Shin-Etsu (Akron, OH). 96 deepwell plates were purchased from Eppendorf (#951033405, Germany). Cryovials were purchased from Nalgene (#5000-0012, Rochester, NY).

### **3.5.2 Automated droplets generation and droplet dispersion measurement**

The sample solution of was placed in one of the wells of deep well plate. The silicone oil layer was prepared by dissolving 1% of (v/v) emulsifier KF-6017 in DM-Fluid-5cs (both from Shin-Etsu, Akron, OH). The silicone oil layer was agitated for 1 hour on a rotator.

The droplets generation was carried out by using the Beckman Biomek 3000. The operation program directing the Biomek 3000 was written in Biomek software version 3.3.14. Biomek was programed to suspend 1  $\mu$ L droplets by aspirating 35  $\mu$ L of the sample solution, and dispensing of 1  $\mu$ L was dispensed in the air. The pipette tip was submerged into the silicone oil layer and retracted. As the pipette



tip was removed from the surface, 1  $\mu\text{L}$  droplet was dispensed in the silicone oil. 1  $\mu\text{L}$  of the solution was dispensed again for the next droplets. This procedure was repeated to produce multiple droplets.

To test the droplet dispersity, the experiment was carried out in 12 well cell culture plate (#3513, costar). 100  $\mu\text{g}/\text{mL}$  fluorescein solution was used to generate and image the droplets. 3.8 mL silicone oil with 1% surfactant was placed in the well, and 30 droplets per well were placed in the well plate by the procedure described above. The droplet was imaged via ChemiDoc MP, and droplets size and dispersion were confirmed by the image analysis by custom Matlab script Droplet\_Dispersion.m (Appendix B11). The Matlab script Droplet\_Dispersion.m utilize the circular object detection tool implemented in Matlab to identify droplets in the image. The polydispersity of the droplets generated by Biomek system was calculated from the diameter of the detected droplets.

### **3.5.3 Asymptote VIA Freezer Freeze-float system**

I slowly added 50  $\mu\text{L}$  of the HFE-7500 to the 1 mL cryovials. I added 1 mL of silicone phase to the cuvette. I placed the cryovials in a metal sample holder, and put a wet paper on the metal sample holder to minimize the accumulation of static electricity in the system to prevent coalescence of droplets. I prepared the sample solution of 1 mg/mL Snomax. Add 1  $\mu\text{L}$  droplets by pipetting of the sample solution into the floating layer with a repeat pipettor. The 1 mL cryovial can hold up to 40

droplets without coalescence or adhesion to the walls. I placed the metal sample holder on a cryoplate inside the freezer.

The system was cooled in the Asymptote VIA freezer with a programmed cooling rate. First, the system was cooled to 0 °C in -2 °C/min cooling rate, then the system was held at 0 °C for 10 min to equilibrate the temperature. Then the temperature was cooled by 0.5 °C/min and the program run until the experiment was completed (~ -25 °C). The droplets freezing behaviour was recorded from the top of the freezer through a house-made glass lid by a digital camera (Canon EOS Rebel T3i #5169B003). The camera was operated remotely by a controlling software EOS Utility 2 (Canon) and images were recorded every 5 seconds.

Droplets counting is done with the assistance of the Matlab script available in (Appendix B12). This script utilizes the selection of the region of interest (ROI) and automated circle detection system, and then plot the frozen fraction automatically. This is the interactive program so the final decision making of droplet recognition is done manually so that it could achieve better accuracy.

## Chapter 4: Selection of the Ice-binding Glycans using Genetically Encoded Fragment-based Discovery by Ice Affinity Purification

### 4.1 Introduction

In this chapter, I investigated the feasibility of screening for ice-binding glycans using a combination of “Ice-shell Purification” technology<sup>130</sup> developed by Peter Davies laboratory and “Liquid Glycan Array (LiGA)”, a genetically-encoded glycan library developed in Derda lab.

The ice-shell purification system was shown to be effective in enriching molecules with ice-binding capacity in the ice and excluding non-binders in an unfrozen supernatant. This system, theoretically, can be adopted to screen any type, of molecular mixtures. It can successfully enrich ice-binding proteins from a complex cell lysate,<sup>128, 167-169</sup> and screen the molecules or organisms that display molecules that have ice-affinity.<sup>129</sup> We hypothesized that *in vitro* selection of phage displayed libraries can identify phage clones with affinity towards ice surface and allow the discovery of ice-binding molecules from a large chemical library.

Some proteins<sup>170</sup>, glycoproteins<sup>171-173</sup> and carbohydrates<sup>43</sup> bind to the ice surface and either promote or inhibit ice growth, and the difference in functions might arise from their sizes, which are large in INPs and small in AFPs.<sup>119, 120</sup> To date, a variety of ice-binding biomolecules have been isolated from different organisms (at least seven bacteria)<sup>45-50</sup>. The ice-nucleating protein (INP) of *P. syringae* is known to be mannosylated on asparagine residues via N-glycan bond.

These mannose residues on the glycan are decorated by phosphatidylinositol and the additional glycan residues are attached to INP via O-glycan linkages to serine and threonine.<sup>58</sup> The cleavage of the glycans by N- and O-glycosidase,  $\alpha$ - and  $\beta$ -mannosidase, and  $\beta$ -galactosidase resulted in the deletion of ice-nucleating activities. This observation indicates that the glycans may play a major role in the ability of the INP to bind to the ice surface and induce the ice nucleation process.<sup>174</sup> However, the role of the structure, density presentation of the glycan and the location of its attachment to the INP is not fully understood. To study structure-activity relationship between glycosylation and ice nucleation is not trivial in the context of INP on the surface of *P. syringae* because such SAR requires a toolbox that could precisely control glycosylation in a specific protein of *P. syringae*. To the best of our knowledge, no tools are available to control any glycosyltransferases in this organism. Heterologous expression of INP in *E. coli* is feasible, however cloning of INP in *E. coli* results in protein with no glycosylation and no ice nucleating ability. We reasoned that selection of glycoconjugates with affinity towards ice-surface would not only give rise to new ice-nucleating or antifreeze molecules but also provide new insight into the mechanism of interaction between glycoconjugates and ice.

High-throughput investigation of glycan interaction with glycan binding targets is commonly performed via glycan array technology, however, it is not obvious how the ice-glycan interaction can be investigated by the immobilized

glycan array. As alternative, I employed soluble version of glycan array, “Liquid Glycan Array (LiGA)” composed of chemically glycosylated M13 phage (Figure 4-1 A-B). Both composition and density of the glycan are genetically-encoded in DNA of the phage.<sup>175</sup> Each carbohydrate is attached to phage by reaction between anomeric azidoalkyl linker and dibenzocyclooctyne-modified N-terminus of pVIII protein of M13 phage. Compared to conventional glycan array that is immobilized on a solid support, LiGA can be subjected to affinity capture and pulldown studies to allow investigation of binding between the glycans and glycan binding entities *in vitro* and *in vivo*. The “fluid” composition of LiGA makes it compatible with the investigation of binding toward ice-surface using ice affinity purification and offers potential to provide insight into the recognition of ice by glycans.

## 4.2 Experimental design

Previously, I investigated the ice-nucleator by the direct measurement of ice-nucleating activities. In this chapter, I approached the discovery of the ice-nucleator by screening of the phage-displayed glycans for their affinity towards ice. If such phage displaying glycans are identified, a subset of them may exhibit ice nucleation properties.

To enable identification of ice-binding glycans, we tested a protocol that employs one round selection of LiGA by affinity purification toward ice surface, followed by Illumina sequencing of the phage trapped in ice and remaining in

supernatant (Figure 4-1C). Analysis of the sequencing data identified the top 7 glycans that had high enrichment in the ice phase compared to liquid phase. I further validated this discovery platform by the screening results using reporter phages chemically modified with glycans identified by LiGA screening.

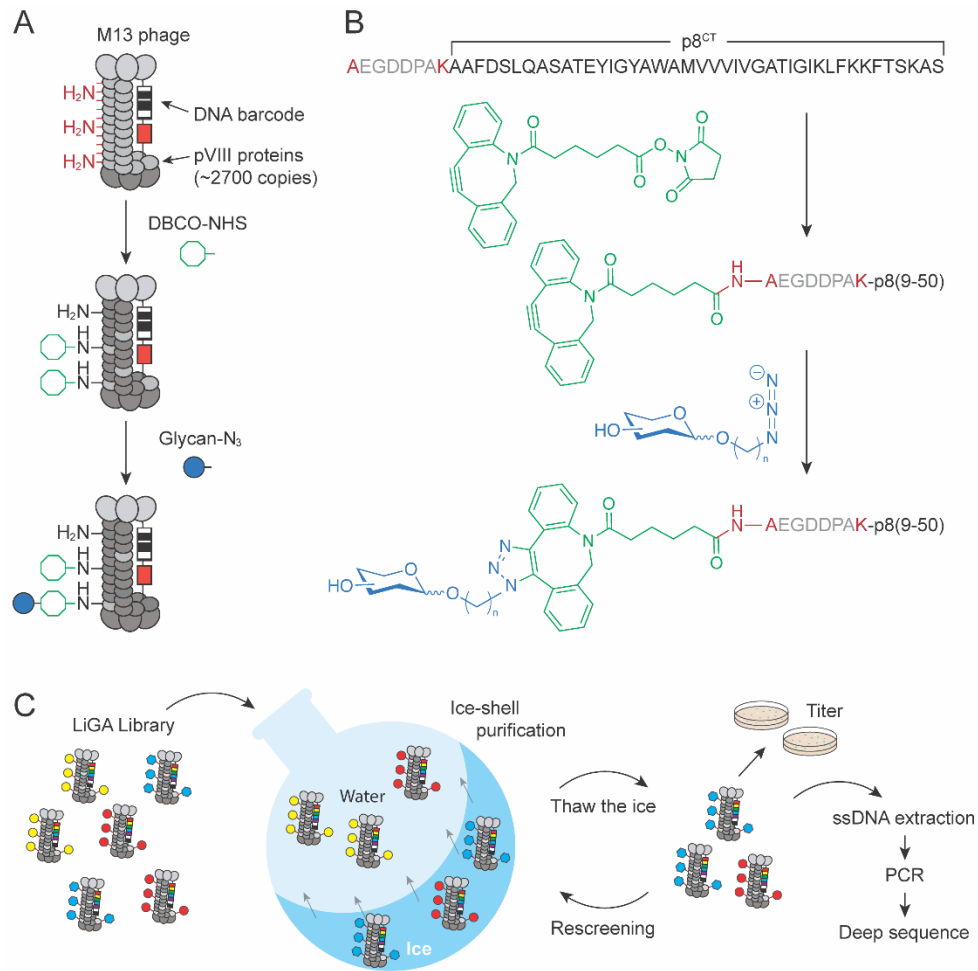


**Figure 4-1.** Ice-shell purification strategy. (A) Chemical modifications of coat protein pVIII of M13 phage. (B) Sequence of pVIII protein and a two-step modification by dibenzocyclooctyne N-hydroxysuccinimide (DBCO-HNS) linker, and ligation of azido glycan. (C) Scheme of ice-shell purification of LiGA. The LiGA sample purified by the ice affinity purification was analyzed by deep sequencing of phage genome to identify the enriched glycans.

## 4.3 Results and Discussion

### 4.3.1 Validation of Ice shell screening

To validate the feasibility of the ice-shell purification as the ice-binder screening system, we used fusion protein of antifreeze protein (eGFP-type III AFP)<sup>176</sup> with confirmed ice-binding activity at a concentration of 29  $\mu\text{g/mL}$  AFP-GFP in the 20 mL of sea salt solution. It is reported that presence of ions from salt solution significantly modify the H-bond properties of ice.<sup>177</sup> We used sea salt solution to maintain the AFP solution environment to be close to the AFP in the nature environment. We coated the round-bottom flask wall with ice formed from  $\sim 1$  mL of Milli Q water. The ice phase and liquid sea salt solution were equilibrated in the ice-water bath at  $-3.5$   $^{\circ}\text{C}$ . At this temperature, the ice grows slowly results in incorporation of 10 mL of solution in the ice phase over 30 min. We purified 20 mL AFP-GFP solution with two round ice-shell purification method and obtained  $\sim 50\%$  ice and  $\sim 50\%$  liquid fractions. The AFP-GFP concentration was obtained from the fluorescein measurement. After the first round, the ice fraction was thawed and used for the second round. Same as the first round, the thawed ice fraction ( $\sim 10$  mL) was added in the round-bottom flask that contains thin ice layer, and separated into the  $\sim 50\%$  ice and  $\sim 50\%$  liquid fractions. The AFP concentrations throughout two rounds of purification were obtained from the fluorescent intensity of the GFP. Normalized intensity (Figure 4-2B) was calculated as the following equation.

$$\text{Normalized intensity} = F \times F_{input} \times V_{input} / (F_{ice}V_{ice} + F_{liq}V_{liq})$$



where  $F$  is the fluorescence intensity of the output,  $F_{input}$  is the fluorescence intensity of the input solution,  $V_{input}$  is the volume of the input solution,  $F_{ice}$  is the fluorescence intensity of the output ice solution,  $V_{ice}$  is the volume of the ice fraction,  $F_{liq}$  is the fluorescence intensity of the output liquid solution,  $V_{liq}$  is the volume of the liquid fraction.

I confirmed that two consecutive purification increased the protein concentrations in the ice phase when compared to the liquid phase by 69% and 90% respectively (Figure 4-2). We noted the decrease of the total GFP fluorescence during experiment indicating either a loss of total protein or loss of active fluorescent form of protein (e.g. due to unfolding of GFP after trapping in and releasing from ice).

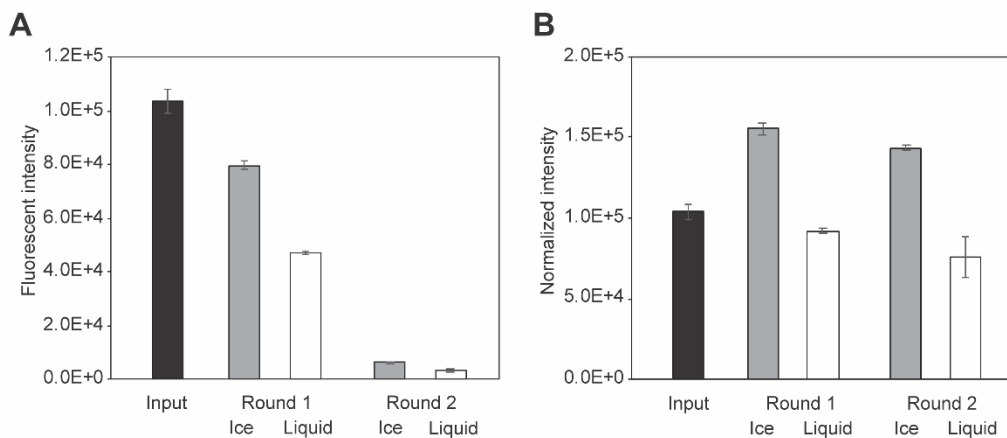


**Figure 4-2.** Ice-shell purification validation test. (A) AFP-GFP concentration in the sample input and ice, liquid fractions of ice-shell screening were assessed by measuring the fluorescence of GFP. (B) Fluorescent intensity after normalization.

### **4.3.2 Screening assay to select ice-binding carbohydrate**

We conducted the affinity purification experiment of LiGA library with 74 different glycan modified phages. The list of glycans is available in Table 4-1. The amount of the phage in input was  $10^9$  PFU in 20 mL of the 40 g/L sea salt water, which gives the total phage amount sufficient for the DNA amplification in the downstream PCR process. The solution was separated into ~10 mL ice and liquid sample.

DNA extraction and PCR of the phage output solution was optimized. Due to the relatively low concentration of phage in a relatively large sample amount of liquid, we employed MiniPrep column purification method. Briefly, after the thawing process of the phage solutions, 1% (v/v)  $\text{CH}_3\text{COOH}$  was added to each solution to precipitate phage. All the phage solutions were loaded onto the column and phage particles were purified by following the MiniPrep purification protocol. The extracted DNA is processed to the amplification by PCR and deep sequencing of the DNA to allow identification of the potential ice-binding glycans.

### **4.3.3 Analysis of Illumina sequencing**

Enrichment of the glycans was determined as the ratio of frequency value of glycans in the fraction of ice sample and liquid sample from the same ice-shell experiment (Figure 4-3). We observed the glycan that had the highest enrichment from the ice fraction compared to liquid fraction was Neu5Ac(a2-8)Neu5Ac(a2-

3)Gal(b1-4)Glc(b1-, that had the highest >3-fold enrichment ( $p < 0.08$ ) (Table 4-3). The glycan with mannose residues, Man(a1-6)[Man(a1-3)]Man(a1-, was predicted to have higher enrichment since INP of *P. syringae* is glycoprotein with mannosylations. However contrary to our prediction, Man(a1-6)[Man(a1-3)]Man(a1- glycan showed the lowest enrichment (0.67) among all glycans. We conclude that the trisaccharide of mannose might not have the ice-binding affinity.

**Table 4-1. SDB id and glycan modifications.**

SDB_id	Modification
1	Galb1-3GlcNacb1-3Galb1-4[Fuca1-3]GlcNac-Sp
2	NeuAca2-3Galb1-3GlcNacb1-3Galb1-4GlcNacb-Sp
6	Neu5Aca2-3Galb1-3GalNacb1-3Gala1-4Galb1-4Glc-Sp
9	Galb1-4Glc-Sp
10	Galb-P4
13	Galb3GalNacb3Gala4Galb4GlcNacb-Sp
15	Neu5Aca2,8Neu5Aca2,8Neu5Aca2,8Neu5Aca2-3Galb1-4Glc-Sp
16	Neu5Aca2,8Neu5Aca2,8Neu5Aca2,8Neu5Aca2-3[GalNacb1-4]Galb1-4Glc-Sp
17	NeuAc(9Ac)a2-3LN-b-sp
21	Neu5Aca2-3[GalNacb1-4]Galb1-4GlcNacb-Sp
22	Fuca1-2Galb1-4[Fuca1-3]GlcNacb1-3Galb1-4[Fuca1-3]GlcNacb-Sp
23	Gala1-3Galb1-4[Fuca1-3]GlcNacb-Sp
24	GalNaca3Galb4[Fuca2]GlcNacb-Sp
26	Gala1-3(Fuca1-2)Galb1-4GlcNacbSp1
29	GalNaca3Galb4[Fuca2]Glc-Sp
34	GalNacb1-4GlcNacb-Sp
35	NeuAca2-6GalNacb1-4GlcNacb-Sp
40	NeuAca2-3[NeuAca2-3Galb1-3GalNacb1-4]Galb1-4Glc-Sp
42	Galb1-3GlcNacb1-3Galb1-4GlcNacb-Sp
45	Neu5Aca2,8Neu5Aca2-3Galb1-4Glc-Sp
47	Galb1-4GlcNacb1-3Galb1-4GlcNacb1-3Galb1-4GlcNacb-Sp
48	Galb1-4[Fuca1-3]GlcNacb1-3Galb1-4[Fuca1-3]GlcNacb-Sp
49	Galb1-4[Fuca1-3]GlcNacb1-3Galb1-4[Fuca1-3]GlcNacb1-3Galb1-4[Fuca1-3]GlcNacb-Sp
51	Neu5Aca2,8Neu5Aca2,8Neu5Aca2-3[GalNacb1-4]Galb1-4Glc-Sp
52	Neu5Aca2-3Galb1-4[Fuca1-3]GlcNacb1-3Galb1-4[Fuca1-3]GlcNacb-Sp1
53	Neu5Aca(2-3)(Galb(1-4))[Fuca(1-3)]GlcNac)3b-Sp
54	GlcNacb1-3Galb1-4Glc-Sp
55	GlcNacb1-3Galb1-4GlcNacb-Sp
56	Galb1-3[Fuca1-4]GlcNacb-Sp
57	Gala1-3Galb1-4Glc-Sp
58	Gala1-4Galb1-4GlcNacb-Sp
59	GlcNacb-Sp
59	Fuca1-2Galb1-3GlcNacb-Sp
66	Galb1-4Glc-Sp
67	Galb1-3GlcNacb-Sp
70	Neu5Aca2-3Galb1-4Glc-Sp
71	Neu5Aca2-3Galb1-4GlcNacb-Sp
73	Neu5Gca2-3Galb1-4GlcNacb-Sp
74	Neu5Gca2-3Galb1-3GlcNacb-Sp
76	Fuca1-2(Galb1-4GlcNacb1-3)3b-Sp
77	Fuca1-2Galb1-4GlcNacb1-3Galb1-4GlcNacb1-3Galb1-4GlcNacb-Sp
79	Neu5Aca(2-6)(Galb(1-4)GlcNacb(1-3))2b-Sp
80	Gala1-3[Fuca1-2]Galb-sp
81	GalNaca1-3[Fuca1-2]Galb-sp
82	Fuca1-2Galb-sp
87	KDNa2-3Galb1-4GlcNacb-Sp
88	Galb1-4GlcNacb1-3Galb1-4Glc-Sp
105	Gala1-3[Fuca1-2]Galb1-3GlcNacb-Sp
106	GalNaca1-3[Fuca1-2]Galb1-3GlcNacb-Sp
107	Neu5Gca2-6Galb1-4GlcNacb-Sp
111	KDNa2-3Galb1-3GlcNacb-Sp
112	Gala1-3Galb1-3GlcNacb-Sp
113	Galb1-4[Fuca1-3]GlcNacb1-3Galb1-3[Fuca1-4]GlcNacb-Sp
114	NeuAca2-3Galb1-4GlcNacb1-3Galb1-3GlcNacb-Sp
115	Neu5Aca2-3Galb1-3GlcNacb1-3Galb1-3GlcNacb-Sp
116	NeuAca2-6-LNb3Le c-bsp
117	NeuAca2-3Le ab3Le a b-sp
118	Gala1-4Galb1-4GlcNacb1-3Galb1-4Glc-Sp
121	Neu5Aca2-3Galb1-3GalNacb1-4Galb1-4Glc-Sp
122	Neu5Aca2-8Neu5Aca2-3[GalNacb1-4]Galb1-4Glc-Sp
124	Neu5Aca2-8Neu5Aca2-8Neu5Aca2-3Galb1-4Glc-Sp
125	Galfb1-5Galfb1-5Galfb1-5Galfb-S8
126	Galfb1-5Galfb1-5Galfb1-5Galfb-S9
127	Mana1-6[Mana1-3]Mana-s6
128	Neu5Aca2-6Galb1-4GlcNacb-Sp
129	Neu5Aca2-3Galb1-4GlcNacb-Sp
132	Galfb1-5Galfb1-5Galfb-S8
149	(Galb1-4GlcNacb1-3)2b-Sp
150	Fuca1-2Galb1-4GlcNacb-Sp
152	Fuca1-2Galb1-4GlcNacb-Sp
153	Fuca1-2Galb1-4Glc-Sp
155	GlcNacb1-3Galb1-3GlcNacb-Sp
160	Neu5Aca2-6Galb1-4GlcNacb-Sp
161	Neu5Gca2-3Galb1-4Glc-Sp

**Table 4-2. Silent barcodes of LiGA library**

SDB_id	SDB clone sequence	Peptide region
1	CTGCTGTTGCGCAATACCACTC	AGTGTGGAGAAGAATGATCAGAAGACTTATCATGCGGGTGGAGGT
2	CTTCTATTGCGCAATCCGCTC	AGTGTGGAGAAGAATGATCAGAAGACTTATCATGCGGGTGGAGGT
6	CTGCTGTTGCGATTCCACTG	AGTGTGGAGAAGAATGATCAGAAGACTTATCATGCGGGTGGAGGT
9	CTPCTTTTTGCAATTCCTCTA	AGTGTGGAGAAGAATGATCAGAAGACTTATCATGCGGGTGGAGGT
10	CTACTGTTTGCATATCCCGCTG	AGTGTGGAGAAGAATGATCAGAAGACTTATCATGCGGGTGGAGGT
13	CTACTTTTTGCAATTCCTCTG	AGTGTGGAGAAGAATGATCAGAAGACTTATCATGCGGGTGGAGGT
15	CTGCTGTTGCGCATACCCCTT	AGTGTGGAGAAGAATGATCAGAAGACTTATCATGCGGGTGGAGGT
16	CTGCTGTTGCGCAATCCCGCTG	AGTGTGGAGAAGAATGATCAGAAGACTTATCATGCGGGTGGAGGT
17	CTACTCTTCGCGATTCGGCTT	AGTGTGGAGAAGAATGATCAGAAGACTTATCATGCGGGTGGAGGT
21	CTACTCTTTGCAATTCGCCCTT	AGTGTGGAGAAGAATGATCAGAAGACTTATCATGCGGGTGGAGGT
22	CTACTGTTTGCATATCCCACTT	AGTGTGGAGAAGAATGATCAGAAGACTTATCATGCGGGTGGAGGT
23	CTGCTCTTTGCAATACCTCTT	AGTGTGGAGAAGAATGATCAGAAGACTTATCATGCGGGTGGAGGT
24	CTACTATTGCGATTCGGCTC	AGTGTGGAGAAGAATGATCAGAAGACTTATCATGCGGGTGGAGGT
26	CTGCTATTGCGATTCGGCTC	AGTGTGGAGAAGAATGATCAGAAGACTTATCATGCGGGTGGAGGT
29	CTGCTATTGCGATTCGGCTC	AGTGTGGAGAAGAATGATCAGAAGACTTATCATGCGGGTGGAGGT
34	CTPCTTTTTGCGATTCGGCTG	AGTGTGGAGAAGAATGATCAGAAGACTTATCATGCGGGTGGAGGT
35	CTGCTGTTTGCATATCCCACTT	AGTGTGGAGAAGAATGATCAGAAGACTTATCATGCGGGTGGAGGT
40	CTPCTGTTGCGATTCGGCTT	AGCGTGGAAAAAGACGATCAAAGACCTTACACGCCGGGGGAGGG
42	CTTCTGTTTGCATACCCCTG	AGCGTGGAGAAGAATGATCAAAGACCTTACACGCCGGGGGAGGG
45	CTGCTGTTTGCATTCCTCTG	AGCGTGGAAAAAATGACCAAAAACCTTACCATGCAGGGGGGGGA
47	TTATTATTCGCAATACCGCTA	AGTGTGAGAGAAGATGACCAGAAGACCTTACACGCCGGGGGGGGG
48	TTATTATTCGCAATTCCTTTA	AGCGTGAAGAAAAACGACCAAGAACCTTACACGCCGGGAGGAGT
49	CTACTGTTGCGATTCGGCTG	AGTGTGGAAAAAATGATCAGAAGACTTACCACGCTGGTGGTGGG
51	CTGCTCTTTGCTATACCCCTA	AGCGTTCGAAAAAATGATCAAAGACCTTACACGCCGGGGGGGGA
52	CTACTGTTTGCATTCGGCTG	AGTGTAGAGAAGAATGACCAAAAACCTTATCATGCGGGGAGGAGT
53	CTGCTGTTTGCATTCGGCTC	AGTGTGGAGAAGAATGACCAAAAACCTTATCATGCTGGAGGGGT
54	TTATTATTCGCAATTCCTTTA	AGTGTGCAAAAAAATGACCAAAAACCTTACACGCCGGGGGGGGG
55	CTGCTCTTTGCAATTCGGCTG	AGTGTGCAAAAAAATGACCAAAAACCTTATCATGCTGGTGGTGA
56	CTACTGTTTGCATACCTCTT	AGCGTTCGAAAAAATGACCAAAAACCTTACCATGCGGGTGGAGGT
57	TTATTATTCGCAATTCCTTTA	AGCGTTCGAGAAGAACGACCAAAAACCTTACACGCCAGTGGCGGG
58	CTACTCTTCGCTATACCCCTC	AGCGTGGAAAAAATGACCAAAAACCTTACCATGCAGTGGTGGC
59	TTATTATTCGCAATTCCTTTA	AGTGTGCAAAAAAATGACCAAAAACCTTATCATGCAGTGGGGGA
66	TTATTATTCGCAATTCCTTTA	AGTGTGCAAAAAAATGACCAAAAACCTTATCATGCAGTGGGGGA
67	CTPCTGTTGCGATACCCCTC	AGCGTGGAGAAGAATGACCAAAAACCTTATCATGCAGTGGGGGA
70	CTACTGTTGCGCAATCCCGCTC	AGTGTTCGAGAAGAACGATCAGAAGACCTACCACGCCGGGGGGGT
71	CTGCTTTTTGCTATTCCTCTG	AGCGTGGAGAAGAATGACCAAAAACCTTATCATGCAGTGGGGGA
73	TTATTATTCGCAATTCCTTTA	AGTGTGCAAAAAAATGACCAAAAACCTTACACGCCGGGGGGGGG
74	CTACTCTTTGCGATTCGGCTG	AGTGTGCAAAAAAATGACCAAAAACCTTATCATGCAGTGGGGGA
76	CTGCTTTTTGCCATACCGCTG	AGTGTGAGAGAAGAATGATCAGAAGACCTACCACGCCGGGAGTGGC
77	CTGCTATTGCGATTCGGCTG	AGCGTTCGAAAAAATGACCAAAAACCTTACCATGCGGGGAGGA
79	CTACTGTTGCGCAATACCTCTC	AGCGTGGAGAAGAATGATCAGAAGACCTTATCATGCTGGTGGTGA
80	CTTCTGTTGCGCATACCCCTA	AGTGTAGAGAAGAATGATCAGAAGACCTTATCATGCGGGGAGGGGT
81	CTACTCTTTGCTATTCGGCTT	AGCGTGGAGAAGAATGATCAGAAGACCTTACCACGCCGGTGGTGGC
82	TTATTATTCGCAATTCCTTTA	AGCGTGGAGAAGAACGACCAAAAACCTTATCATGCAGTGGGGGGG
87	CTACTCTTCGCTATACCCCTC	AGCGTAGAAAAAATGACCAAAAACCTTACCATGCGGGAGTGGG
88	CTGCTGTTGCGCATTCCTCTA	AGTGTAGAGAAGAATGACCAAAAACCTTACCACGCCGGGGGGGGG
105	CTGCTTTTTGCTATTCCTCTT	AGTGTGCAAGAAGAATGATCAAAGACCTTACCACGCCGGTGGTGA
106	CTACTGTTGCGCAATCCCGCTA	AGTGTAGAAAAAATGATCAGAAGACTTACCATGCTGGTGGTGGG
107	TTATTATTCGCAATTCCTTTA	AGTGTGGAGAAGAACGATCAGAAGACCTTACCACGCCAGGAGCGGA
111	CTGCTGTTTGCATTCGGCTA	AGTGTAGAAAAAATGACCAAAAACCTTACCATGCGGGCGTGGG
112	CTACTGTTGCGATTCGGCTG	AGTGTAGAAAAAATGACCAAAAACCTTACCACGCCGGGAGGC
113	CTACTGTTTGCATTCGGCTG	AGTGTGCAAAAAAATGATCAGAAGACTTATCATGCAGGAGGGGGG
114	NTACTGTTTGCATTCGGCTC	AGCGTGGAGAAGAACGACCAAAAACCTTACCACGCCGGGGGAGGG
115	CTACTGTTGCGATTCGGCTG	AGTGTGCAAAAAAATGACCAAAAACCTTATCATGCGGGGGGGGT
116	CTGCTTTTTGCTATACCTCTT	AGCGTGGAGAAGAACGATCAGAAGACCTTATCATGCTGGTGGTGGG
117	TTATTATTCGCAATTCCTTTA	AGCGTTCGAAAAAATGACCAAAAACCTTACCACGCCGGGGGGGGGA
118	CTACTCTTCGCGATACCCCTC	AGTGTGCAAAAAAATGATCAGAAGACTTATCATGCAGTGGTGGT
121	CTGCTGTTTGCATACCCCTT	AGTGTGGAGAAGAACGATCAGAAGACCTTATCATGCTGGGGTGGGA
122	CTGCTTTTTGCTATACCCCTG	AGCGTGGAGAAGAACGATCAAAGACCTTATCATGCAGGGGGGAGGC
124	CTACTGTTTGCATTCGGCTC	AGCGTTCGAAAAAATGATCAAAGACCTTATCATGCGGGAGGCGGG
125	CTGCTATTGCGATTCGGCTG	AGTGTAGAAAAAATGACCAAAAACCTTATCATGCGGGTGGCGGG
126	CTGCTCTTTGCAATTCGGCTG	AGTGTAGAAAAAATGATCAGAAGACCTTACCATGCTGGTGGCGGA
127	CTGCTATTGCGATTCGGCTA	AGTGTGAGAGAAGAATGATCAGAAGACCTTATCATGCAGTGGTGGGA
128	TTATTATTCGCAATTCCTTTA	AGCGTTCGAAAAAATGACCAAAAACCTTACCATGCGGGGAGGG
129	CTPCTGTTGCGATACCGCTG	AGCGTTCGAAAAAATGATCAGAAGACTTATCATGCGGGGGCGGG
132	CTACTGTTGCGCAATACCTCTC	AGCGTAGAAAAAATGATCAAAGACCTTACCACGCCAGTGGCGGA
149	CTACTCTTTGCAATTCGGCTT	AGCGTGGAGAAGAACGACCAAAAACCTTACCACGCCGGTGGTGGG
150	CTGCTCTTTGCTATCCCTCTA	AGTGTTCGAAAAAATGACCAAAAACCTTATCATGCAGTGGTGGG
152	CTGCTTTTTGCTATACCTCTC	AGCGTAGAAAAAATGACCAAAAACCTTACCATGCGGGTGGGGGG
153	CTACTATTGCGATTCCTCTG	AGTGTGCAAAAAAATGATCAAAGACCTTATCATGCGGGTGGGGGT
155	TTATTATTCGCAATTCCTTTA	AGTGTGAGAGAAGAATGATCAAAGACCTTACCATGCAGGCGGAGGT
160	TTATTATTCGCAATTCCTTTA	AGTGTGCAAAAAAATGACCAAAAACCTTACCATGCTGGAGGGGGG
161	CTGCTATTGCGATTCGGCTG	AGTGTGAGAGAAGAATGACCAAAAACCTTACCACGCCGGGGGAGGG
mCherry01	CTPCTATTGCTATTCCTCTA	AGTGTGCAAGAAGAACGACCAAAAACCTTATCATGCGGGGGTGGT
mNeon04	CTACTGTTGCGCAATCCCGCTA	AGTGTGAGAAAAAATGATCAAAGACCTTATCATGCGGGTGGTGGT

SDB\_id

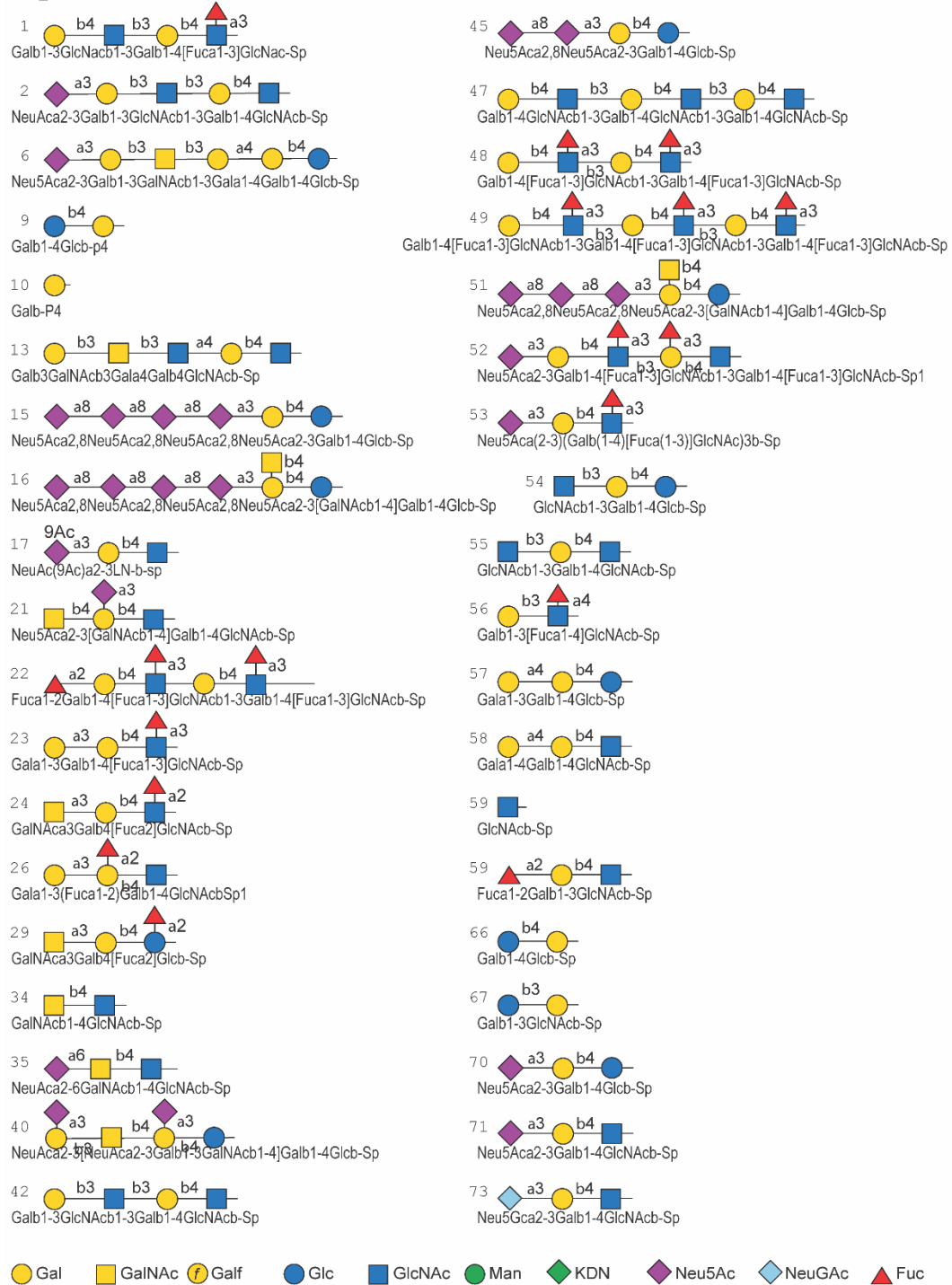


Figure 4-3. Glycan structures of LiGA library.

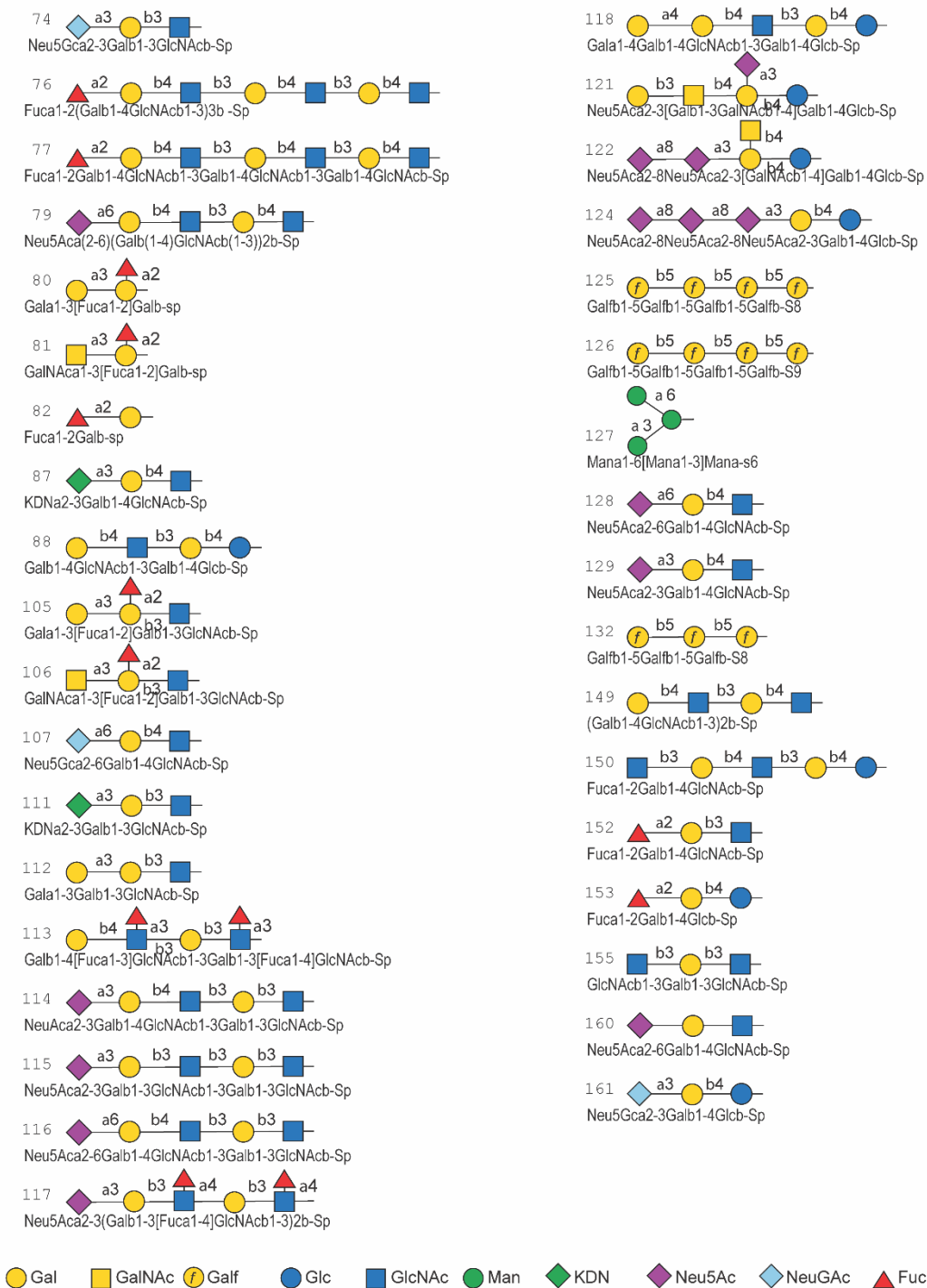


Figure 4-3. Glycan structures of LiGA library (cont.)





**Table 4-3.** Post-selection analysis on LiGA in ice-affinity purification. The glycans that have  $p < 0.1$  and ratio  $> 1.2$  cut off glycans are listed, and arranged in descending order of enrichment.

SDB_id	Glycan												p-value	ice/liquid ratio
45	Neu5Ac(a2-8)Neu5Ac(a2-3)Gal(b1-4)Glc(b1-													
113	Gal(b1-4)[Fuc(a1-3)]GlcNAc(b1-3)Gal(b1-3)[Fuc(a1-4)]GlcNAc(b1-													
149	Gal(b1-4)GlcNAc(b1-3)Gal(b1-4)GlcNAc(b1-													
105	Gal(a1-3)[Fuc(a1-2)]Gal(b1-3)GlcNAc(b1-													
111	KDN(a2-3)Gal(b1-3)GlcNAc(b1-													
161	Neu5Gc(a2-3)Gal(b1-4)Glc(b1-													
152	Fuc(a1-2)Gal(b1-4)GlcNAc(b1-													

SDB_id	input1	input2	input3	ice1	liquid1	ice2	liquid2	ice3	liquid3	ice4	liquid4	p-value	ice/liquid ratio
45	63	60	125	112	23	154	47	56	29	30	4	0.07736	3.417
113	1523	1260	2074	538	254	855	409	538	544	476	119	0.07558	1.815
149	2127	2108	2024	1144	670	875	654	1118	973	1020	353	0.03645	1.569
105	2104	1954	1787	426	323	566	292	611	556	555	209	0.06046	1.564
111	3601	3548	4385	2805	1801	2856	2079	2469	2271	2324	871	0.04329	1.489
161	1274	1336	1462	897	624	1145	771	971	1004	895	493	0.08699	1.351
152	3038	2817	3211	3141	3118	3538	2558	2972	2413	2929	1820	0.06806	1.270

#### 4.3.4 Validation of the potential hit

To validate the ice-binding interaction of glycans on phage, I built a focused array that contains the most enriched glycan Neu5Ac(a2-8)Neu5Ac(a2-3)Gal(b1-4)Glc(b1-, the excluded glycan Gal(a1-4)Gal(b1-4)GlcNAc(b1-3)Gal(b1-4)Glc(b1-, and the phage that does not display any glycan. Glycan Neu5Ac(a2-8)Neu5Ac(a2-3)Gal(b1-4)Glc(b1- was conjugated to the phage clone that expressed lacZ $\alpha$  reporter (Figure 4-5 A-C). The glycan Gal(a1-4)Gal(b1-4)GlcNAc(b1-3)Gal(b1-4)Glc(b1- was conjugated to the tracer phage clone that transduced mCherry reporter into the *E. coli* host. The tracer phage clone that transduced mNeonGreen reporter was used as the non-glycosylated phage

reference. The plaque forming assay of the output samples provided the enrichment information of three types of phage in one ice-binding experiment.

Panning of the potential ice-binding glycan Neu5Ac(a2-8)Neu5Ac(a2-3)Gal(b1-4)Glc(b1- glycosylated phage by ice-affinity purification did not show enrichment compared to Gal(a1-4)Gal(b1-4)GlcNAc(b1-3)Gal(b1-4)Glc(b1- glycosylated phage and non-glycosylated phage, 2.0% and 2.9% increase respectively (Figure 4-5D). However, the incorporation ratio of the glycosylated phage in the ice phase was less compared to the result from section 4.3.3 “Analysis of Illumina sequencing” (3.4 times enrichment), and the enrichment difference between Neu5Ac(a2-8)Neu5Ac(a2-3)Gal(b1-4)Glc(b1- and Gal(a1-4)Gal(b1-4)GlcNAc(b1-3)Gal(b1-4)Glc(b1- was not significant ( $p = 0.343$ ).

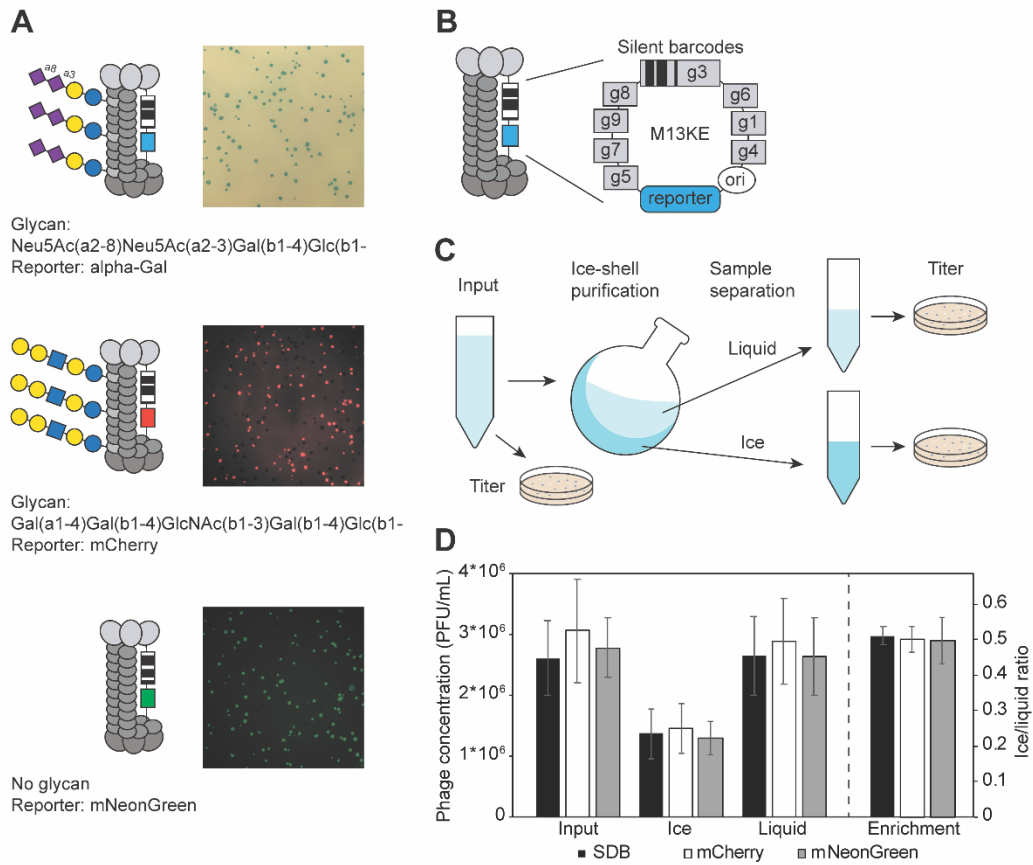


**Figure 4-5.** Validation experiment of glycosylated phage by ice-affinity purification. (A) Reporter phage visualized by plaque forming assays. Phage with LacZ $\alpha$  reporter was conjugated with Neu5Ac(a2-8)Neu5Ac(a2-3)Gal(b1-4)Glc(b1- glycan, phage with mCherry reporter was conjugated with Gal(a1-4)Gal(b1-4)GlcNAc(b1-3)Gal(b1-4)Glc(b1- glycan, and phage with mNeonGreen reporter did not have any glycan conjugation. (B) Location of reporter in the phage genome. (C) Scheme of ice-affinity purification experiment. (D) Phage counts from ice-affinity purification experiments of color-coded glycophasage.

## 4.4 Conclusion

In summary, I tested a methodology to screen the ice-binding glycans that were chemically conjugated to phage. The LiGA array of genetically encoded glycans permitted the screening against immobilized and slowly growing ice surface. We showed the first demonstration of the ice-binding glycan screening result analysis and validation test of the LiGA. However the screening validation results were not reproducible, and hit discovery was inconclusive. Further optimization of the screening platform or library with different glycan modification is needed. Although the result was inconclusive, preliminary screening of ice-binding protein demonstrated the feasibility of affinity-based screening. I believe this platform can be easily adapted for the screening of different modifications, genetically-encoded libraries for further ice-binding molecule discoveries.

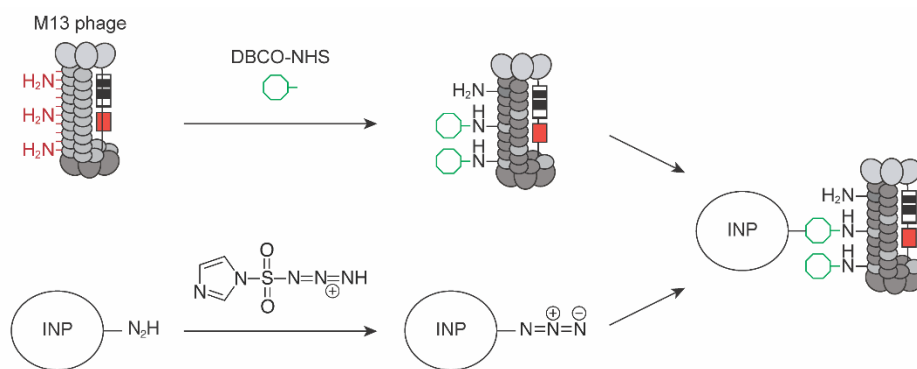


**Figure 4-6.** Phage-IMP conjugation strategy. The ice-nucleating protein can be used as a positive control of the ice-affinity purification, or other INA screening platform.

In future work, this platform may be used to test other chemically modified libraries. It is known that the significant fraction of ice nucleator in nature are relatively long glycoproteins (>120 kDa)<sup>178</sup> and forms multivalent display on bacterial cell membrane. We hypothesize that incorporating a larger size of the glycopeptide libraries will increase the likelihood of identification of ice nucleators.

## **4.5 Experimental procedures**

### **4.5.1 Materials and general information**

PBS 10× (0.1 M) buffer was prepared by mixing NaCl (80 g), KCl (2 g), Na<sub>2</sub>HPO<sub>4</sub> (14.4 g), KH<sub>2</sub>PO<sub>4</sub> (2.4 g) in 1 L of Milli Q water (pH 7.4). Sea salt solution contained 40 g/L sea salt (Sigma-Aldrich, #S9883) in sterilized Milli Q water. Solutions used for ice-shell purification were sterilized by filtration through 0.2 µm PES membrane filter (#566-0020, Thermo Fisher). DBCO-NHS ester (#CP-2033, Conju-Probe) was prepared in dry DMF at the final concentration 50 mM. Zeba™ Spin Desalting Columns (#87767, Thermo Scientific) was used for the desalting and quenching phage and DBCO-NHS mixture.

MS-MALDI-TOF spectra were recorded on AB Sciex Voyager Elite MALDI, mass spectrometer equipped with MALDI-TOF pulsed nitrogen laser (337 nm) (3 ns pulse - up to 300 µJ/pulse) operating in Full Scan MS in either positive or negative ionization modes. Sinapinic Acid is purchased from Sigma (#D7927).

## **4.5.2 Ice-shell purification validation test using AFP-GFP**

### **4.5.2.1 Amplification of AFP-GFP (performed by J. Wickware)**

eGFP-type III AFP was a generous gift from Dr. Peter Davies (Queen's University, CA). The cells were inoculated on 1.5% LB agar plate with 100 µg/mL, and incubated overnight at 37 °C. One colony was picked and cultured in LB media with 100 µg/mL ampicillin until the OD<sub>600</sub> = 0.5. Then the flask was transferred to a 23 °C shaker until the OD<sub>600</sub> = 1.0. To induce the protein expression, isopropyl β-D-1-thiogalactopyranoside (IPTG) was added to a final concentration of 1 mM and incubated in the shaker for overnight at 23 °C.

### **4.5.2.2 Purification of AFP-GFP (performed by J. Wickware)**

The overnight culture was centrifuged at 3500 rpm for 10 min and pellet was resuspended in 25 mL of Binding/Wash Buffer (50 mM Na<sub>3</sub>PO<sub>4</sub> (pH 8.0), 300 mM NaCl, 0.01% Tween 20). Cells were lysed by sonication. The lysate was centrifuged at 16,000 rpm and supernatant was transferred to another tube. Dynabeads His-Tag Isolation and Pulldown (#10103D, Invitrogen) was used to pulldown and purify the AFP-GFP. I followed the instruction of the Dynabeads from Invitrogen. Briefly, I transferred the beads to the conical tube and placed on a magnetic separation rack for more than 2 min, then the supernatant was discarded. The cell sample was added in the tube, and incubated for more than 5 min on a shaker. The tube was placed on a magnetic separation rack for more than 2 min and

supernatant was discarded. The beads were washed with Binding/Wash Buffer for 4 times, and supernatant was discarded. The His-Elution Buffer (300 mM imidazole, 50 mM Na<sub>3</sub>PO<sub>4</sub> (pH 8.0), 300 mM NaCl, 0.01% Tween 20) was added to elute the protein. The solution was incubated for 5 min and placed on a magnetic separation rack for more than 2 min. The eluted protein solution was transferred to another tube.

#### **4.5.2.3 Ice-shell screening procedure**

14 mL Milli Q water was added to 100 mL round bottom flasks and ice shell was formed by submerging the flask into 95% ethanol-dry ice bath (temperature was maintained at -78 °C). Ice shell was formed by manual rotation of the round bottom flask. Once the ice layer of ~1 mm was formed, the remaining water was removed from the flask. The thickness and volume of ice shell were extrapolated from the drained water. We aimed to form a 1 mL ice shell on the surface of the 100 mL flask by this procedure. The flask was dipped in the ethanol bath to freeze the inner water completely, and as the inner water freeze completely, cracks form on the ice shell inside the flask. The flask with ice shell was kept in -20 °C freezer until further experiment.

For selection, a higher temperature cooling bath was prepared with ice-water, salt, and dry ice to control the temperature at -3.5 °C during the purification

process, and dry ice was added manually to maintain the ice bath temperature constant.

The AFP-GFP solution was cooled in the cooling bath for at least 5 min to equilibrate the temperature. The flask with ice shell was attached the rotary evaporator (Buchi R-200 Rotavapor System), the flask was half submerged in the cooling bath and rotated at ~25 rpm. 20 mL of the cooled AFP-GFP solution was added to the ice-shell flask by the serological pipette over 1 min. The flask was rotated in the cooling bath for ~1 h to incorporate ~50% of the sample volume into the ice layer. The flask was removed from the rotary evaporator and the remaining liquid layer was transferred to a 15 mL conical tube. The ice layer was thawed at 4 °C, and solution was transferred to another 15 mL conical tube. The AFP-GFP amounts in ice and liquid fraction were compared by measuring the GFP fluorescence with 395 nm excitation and 509 nm emission wavelengths with a Cytation 5 (BioTek, VT). Output volume difference was taken into account during the calculations of enrichment.

### **4.5.3 LiGA construction**

Description was adapted from the manuscript in preparation Derda et al. “Genetically Encoded, Multivalent Liquid Glycan Arrays”. LiGA library was constructed by Jasmine Maghera in our group. Component of LiGA is shown in Appendix C2. A library of silent double barcode-codons (SDB) in the phage



genome proximal to the pIII cloning site was created by Nicholas Bennett (Derda lab). Briefly, the Gibson Assembly cloning kit (NEB, #E5510) purchased from New England Biolabs was used to introduce the first SDB region into M13KE by NEBuilder HiFi DNA Assembly.

Double stranded DNA from M13KE clone phage containing the stuffer sequence CAGTTTACGTAGCTGCATCAGGGTGGAGGT equating to the peptide QFT\*LHQGGG was used as a template, with \* representing a stop codon. The insert fragment was PCR amplified using the primers P1 and P2 and the vector fragment was PCR amplified using primers P3 and P4:

Name Sequence (5' → 3') :

P1

GAGATTTTCAACGTGAAAAACTNCTNTTYGCNATHCCNCTNGTGGTACCTTTC  
TATTCTCA

P2 TTAAGACTCCTTATTACGCAGTA

P3 TTGCTAACATACTGCGTAATAAG

P4 TTTTTTCACGTTGAAAATCTC

P5

GTGGTACCTTTCTATTCTCACTCGAGYGTNGARAARAAYGAYCARAARACNTAY  
CAYGCNNGNGGNGNTCGGCCGAAACTGTTGAAAG

P6 CGAGTGAGAATAGAAAGGTAC

PCR was performed using 50 ng phage dsDNA with 1 mM dNTPs, 0.5 μM primers, 0.5 μL Phusion High Fidelity DNA polymerase in 1× PCR buffer (NEB #B0518S) in a total volume of 50 μL. The temperature cycling protocol was

performed as follows: a) 98 °C 3 min, b) 98 °C 30 s, c) 60 °C 30 s, d) 72 °C 4 min s, e) repeat b) - d) for 35 cycles, f) 72 °C 10 min, g) 4 °C hold. PCR amplified fragments were treated with restriction enzyme DPN 1 (NEB, #R0176S) and then gel purified. NEBuilder Hifi DNA assembly was then carried out following the manufacturer protocols by mixing 100 ng of vector, 4 ng insert, 10 µL of NEBuilder Hifi DNA assembly master mix, and deionized H<sub>2</sub>O up to a total volume of 20 µL. The resulting ligated DNA was transformed into *E.coli* K12 ER2738 and propagated overnight at 37 °C. The overnight culture was then centrifuged to separate bacteriophage from host cells. The cloning of SVEKNDQKTYHAGGG peptide was conducted as follows. The insert fragment was amplified by PCR following the described protocol using primers P5 and P2. The vector fragment was PCR amplified using primers P4 and P6. PCR fragment were processed using NEBuilder Hifi DNA assembly kit using steps described above. The resulting ligated DNA was transformed into electrocompetent cells *E.coli* SS320 (Lucigen). The resulting overnight culture was centrifuged to remove host cells and incubated with 5% PEG-8000, 0.5 M NaCl for 8 h at 4 °C, followed by 15 min centrifugation at 13000 g to concentrate released phage. PEG precipitated phage was resuspended in PBS-Glycerol 50% and stored at -20 °C. The SDB silent encoding in the SDB region produced a library of chemically identical phage with  $6.1 \times 10^3$  possible sequence combinations, and further cloning in of SVEK sequence results in  $2.1 \times 10^6$  possible sequence combinations. Combined the SDB-SVEK construct  $1.2 \times 10^{10}$

possible sequence combinations. We noted that culture of the mixture of these clones eliminated a few sequences with grow disadvantage.

A 10  $\mu$ L aliquot of phage was diluted and plated at a density of  $\sim$ 100 plaques per plate. Single colonies were manually picked, and individually transferred into 0.5 mL of PBS-Glycerol 50% and incubated at room temperature for 30 min. The tubes were then placed in 55  $^{\circ}$ C heating block for 10 min to inactivate any remaining bacterial cells. After the incubation, 20  $\mu$ L sample of each colony suspension was amplified for 4.5 h in 5 mL of LB supplemented with a 1:100 dilution of log phase *E. coli* K12 ER2738. After amplification the phage clones were collected from the culture supernatant by centrifugation at 4500 g for 10 min. Next, bacterial cell pellet and culture supernatant were processed separately. The supernatant was incubated with 5% PEG-8000, 0.5 M NaCl for 8 h at 4  $^{\circ}$ C, followed by 15 min centrifugation at 13000 g to precipitate the viral particles. The phages were resuspended into 1 mL PBS-Glycerol 50% and stored at -20  $^{\circ}$ C until further use. The bacterial cell pellet was processed for phage-DNA extraction using GeneJET Plasmid Miniprep kit (ThermoFisher, #K0502). For SDB identification, a sample of 400 ng of the phage DNA was submitted for Sanger sequencing at the Molecular Biology Service Unit (University of Alberta). We selected the clones who contained three base pair substitutions from one another (i.e., Hamming distance (H)=3). H=3 permits correction of any point mutations that may have arisen during the analysis by deep sequencing (Appendix C1).

Solution of 150  $\mu\text{L}$  of  $10^{13}$  PFU/mL of phage clone SBD3 in PBS pH 7.4 was distributed by 50  $\mu\text{L}$  aliquots into three. Each sample was reacted with DBCO linker at room temperature for 1 h at 1mM final concentration of linker. The reaction mix was then passed through Zeba Spin column to eliminate unreacted linker. The remaining phages were incubated 8 h at 4 °C with azido-glycan JB-1 (2 mM final concentration). The mix was then filtered through Zeba Spin column.

#### **4.5.4 Ice-shell purification of ice-binding glycans**

For the ice-binding selection, LiGA phage was added to 20 mL to a total of  $1.2 \times 10^9$  PFU in 40 g/L sea salt solution. Ice-shell formation was described in the previous section 4.5.2. ~1 mL ice shell was formed on the inside of 100 mL round-bottom flask. The flask with ice-shell and 20 mL LiGA solution was kept in the -3.5 °C ice-water bath to equilibrate the temperature. LiGA solution was transferred to the flask attached the rotary evaporator by the serological pipette over 1 min. The flask was half submerged in the cooling bath and rotated at ~25 rpm. The flask was cooled in the ice-water bath for ~30 min to incorporate ~50% of the LiGA solution into the ice layer. The flask was removed from the rotary evaporator and the remaining liquid layer was transferred to a 15 mL conical tube. The ice layer was thawed at 4 °C and solution was transferred to another 15 mL conical tube. The ice and liquid phage solutions were subjected to ssDNA extraction and PCR according to the procedure in section 4.6.4.

#### 4.5.5 Preparation for Illumina sequencing

After the ice shell purification, add 100% acetic acid to the phage solutions from ice and liquid fractions (~10 mL each) in 1:100 ratio, and incubate the mixture at room temperature for 2 minutes. Load 0.7 mL of this mixture onto a QIAprep 2.0 Spin Column (#1018398, Qiagen) and centrifuge for 15 seconds at 8,000 rpm, and discard flow-through. Repeat this procedure for ~15 times until all the ~10 mL of solution is loaded onto the column. The remaining procedure follows a standard QIA Miniprep Kits (#27104, Qiagen) steps. Add 700  $\mu$ L of dissociation buffer (#1014966, Qiagen), centrifuge for 15 seconds at 8,000 rpm, and discard the flow-through. Repeat with an additional 700  $\mu$ L of dissociation buffer. Add 700  $\mu$ L of 70% ethanol and centrifuged for 15 seconds at 8,000 rpm, and discard the flow-through. Repeat this procedure two times. Centrifuge for 1 min at 8,000 rpm to dry column. Add 20  $\mu$ L of DNase free water, incubate at 55 °C for 5 min and centrifuge for 15 seconds at 8,000 rpm. Repeat elution with additional 30  $\mu$ L of DNase free water. The extracted phage ssDNA was subjected to PCR according to the procedure described below.

The extracted ssDNA was then converted to Illumina-compatible dsDNA amplicon by PCR. The ssDNA was combined with 1 $\times$  Phusion<sup>®</sup> buffer, 200  $\mu$ M dNTPs (each), 0.5  $\mu$ M forward and reverse primers, and one unit Phusion<sup>®</sup> High-

Fidelity DNA Polymerase in a total volume of 50  $\mu$ L. The temperature cycling protocol was performed as follows: a) 98  $^{\circ}$ C 3 min, b) 98  $^{\circ}$ C 30 s, c) 60  $^{\circ}$ C 30 s, d) 72  $^{\circ}$ C 4 min s, e) repeat b) - d) for 35 cycles, f) 72  $^{\circ}$ C 10 min, g) 4  $^{\circ}$ C hold.

#### **4.5.6 Analysis of the deep-sequencing data**

Sequencing was performed using the Illumina NextSeq platform (Molecular Biology Service Unit, University of Alberta). Data for each experiment was retrieved from the <http://48HD.cloud> server as space-delimited text files containing names of glycans (CFG-codes), DNA (filtered or not), peptide translations and either raw or normalized number of sequencing counts. Experimental replicates are combined in one file. Python script (Appendix C1) consolidated and summed the normalized frequencies of glycans from different sequencing set, calculated the p-value between the ice sample and liquid sample from the same test.

#### **4.5.7 Construction of glycan modified phage**

A solution of 50  $\mu$ L of phage clone ( $1.5 \times 10^{13}$  PFU/mL in PBS) was mixed with 1  $\mu$ L of 50 mM DBCO-NHS ester in dry DMF. The reaction mixture was incubated for 45 min at 4  $^{\circ}$ C and passed through Zeba spin column to eliminate unreacted linker. 20  $\mu$ L of the DBCO-phage was combined with 5  $\mu$ L Neu5Ac(a2-8)Neu5Ac(a2-3)Gal(b1-4)Glc(b1- (10 mM in DMF) and incubated overnight at 4  $^{\circ}$ C. The mix was purified through Zeba spin column. The sample was analyzed

by MALDI-TOF spectrometry (Appendix C4) and plaque forming assay (Figure 4-5D).

#### 4.5.8 Construction of glycan modified mCherry phage

We produced filamentous phage vector that contains the gene for fluorescent protein mCherry and mNeonGreen cloned in place of the lacZ $\alpha$  fragment. Vectors containing mCherry and mNeonGreen genes were generous gifts from Dr. Robert Campbell (University of Alberta). Both constructs were built by HiFi NEB builder ligation of fluorescent protein (FP) fragment and M13 fragment. Vector pBAD-mCherry was used as the source for the mCherry insert, whereas Vector pBAD-mNeonGreen was used as a source for the mNeonGreen insert. FP fragments were PCR amplified using primers P7 and P8, whereas the M13 fragment was PCR amplified from SDB vector using primers P9 and P10.

Name:            Sequence (5' ->3')

P7

GCGGATAACAATTTACACAGGAAACAGCTATGGTGAGCAAGGGCGAG

P8

TTAAATTTTTGTAAATCAGCTCATTTTTTACTTGTACAGCTCGTCCA

P9            AAAATGAGCTGATTTAACAAAAATTTAA

P10          AGCTGTTTCCTGTGTGAAAT

A solution of 50  $\mu$ L of mCherry phage clone ( $10^{13}$  PFU/mL in PBS) was mixed with 1  $\mu$ L of 50 mM DBCO-NHS ester in dry DMF. The reaction mixture was

incubated for 45 min at 4 °C and passed through Zeba spin column to eliminate unreacted linker.

20 µL of the DBCO-phage was combined with 5 µL Gal(a1-4)Gal(b1-4)GlcNAc(b1-3)Gal(b1-4)Glc(b1- (10 mM in DMF) and incubated overnight at 4 °C. The mix was purified through Zeba spin column. The sample was analyzed by MALDI-TOF spectrometry (Appendix C4) and plaque forming assay (Figure 4-5D).

#### 4.5.9 Construction of mNeonGreen phage

We produced filamentous phage vector that contains the gene for fluorescent protein mNeonGreen cloned in place of the lacZα fragment. Vectors containing mNeonGreen genes were generous gifts from Dr. Robert Campbell (University of Alberta). Both constructs were built by HiFi NEB builder ligation of fluorescent protein (FP) fragment and M13 fragment. Vector pBAD-mNeonGreen was used as a source for the mNeonGreen insert. FP fragments were PCR amplified using primers P7 and P8,

Name:            Sequence (5' ->3')

P7

GCGGATAACAATTTACACAGGAAACAGCTATGGTGAGCAAGGGCGAG

P8

TTAAATTTTTGTAAATCAGCTCATTTTTTACTTGTACAGCTCGTCCA

P9            AAAATGAGCTGATTTAACAAAAATTTAA



P10 AGCTGTTTCCTGTGTGAAAT

#### **4.5.10 Analysis of glycosylation of phage by MALDI-TOF MS**

The sinapinic acid matrix was formed by deposition of two layers. Layer1 was prepared as a 10 mg/mL solution of sinapinic acid in acetone-methanol (4:1). Layer2 was prepared as 10 mg/mL solution of sinapinic acid in acetonitrile:water (1:1) with 0.1% TFA. In a typical sample preparation, 2  $\mu$ L of phage solution in what buffer was combined with 4  $\mu$ L of layer2, then a mixture of 1:1 layer1-layer2+phage was deposited on the MALDI inlet plate. To plot the spectrum and estimate the ratio of modified to unmodified pVIII, we fit the data using MatLab script plotONEmaldi.m (Appendix C2).

#### **4.5.11 Validation of the potential hit glycan**

Validation screening test was conducted using the glycosylated and reference phage prepared in section 4.5.7, 8, and 9. Neu5Ac(a2-8)Neu5Ac(a2-3)Gal(b1-4)Glc(b1- modified phage, Gal(a1-4)Gal(b1-4)GlcNAc(b1-3)Gal(b1-4)Glc(b1- modified mCherry phage, and reference mNeonGreen phage were combined in a 1:1:1 ratio based on PFU counts, and  $10^7$  PFU of each phage clone in 20 mL of 40 g/L sea salt solution was used for ice-shell screening in the same procedure as section 4.5.4.

1 mL ice shell was formed on the 100 mL round-bottom flask wall. The flask with ice-shell and 20 mL LiGA solution was kept in the -3.5 °C ice-water bath to equilibrate the temperature. LiGA solution was transferred to the flask attached the rotary evaporator by the serological pipette over 1 min. The flask was half submerged in the cooling bath and rotated at ~25 rpm. The flask was cooled in the ice-water bath for 30 min to incorporate ~50% of the LiGA solution into the ice layer. The flask was removed from the rotary evaporator and the remaining liquid layer was transferred to a 15 mL conical tube. The ice layer was thawed at 4 °C and solution was transferred to another 15 mL conical tube. The phage in the output solution was quantified by plaque forming assay.

## Chapter 5: Conclusion and outlook

### 5.1 Conclusion

This thesis describes the development and validation of platforms for the discovery of molecules which promote ice nucleation. Some biological INAs cause ice nucleation at a significantly higher temperature than other substances do, however the surface chemistry that associate with ice nucleating activities and its mechanism are still not known. Thus, many INA discovery and development mostly rely on the known ice-nucleating substances from natural sources. Development of high-throughput screening platform could accelerate discovery for *de novo* INAs that have higher ice nucleating activities by combining the different chemical library.

First, I demonstrated the detection and separation system of the ice nucleating event for uniform aqueous droplets to identify the stronger ice nucleators in Chapter 2. The density-based selection system was tested using samples with different ice nucleating activities. The system showed correlation of the droplet freezing temperature and the INA concentration of the sample droplets. This system setup pointed out the inability to accommodate a large number of samples (>50 droplets) due to the inability to cool multiple cuvettes at the uniform temperature.

In Chapter 3, to achieve higher throughput, I investigated the introduction of automated droplets generation system and controlled rate cooling system to the

Freeze-float selection. This new setup improved efficiencies (from 50 to theoretically 1920 droplets). Also, we observed better INA concentration differentiation accuracies at threshold concentration (freezing temperature  $p = 4.4 \times 10^{-7}$  to  $p = 0.83$ ), and narrower freezing temperature distribution (standard deviation of freezing temperature 2.0 to 0.73). Higher sensitivity of the system has potential to lead to the discovery of INAs with weak nucleating activity or low concentrations.

In Chapter 4, I describe a screening strategy combining ice-affinity purification technique which is “ice-shell purification” and genetically encoded glycan library “LiGA” to explore the ice-binding glycans. This platform reinforced the advantages of approaches that exploited the “fluid” LiGA screening environment to access the ice binding affinities. The down sized phage-glycan conjugate was used for the validation of screening results. Unfortunately, the glycan that showed enrichment from LiGA screening via the ice-shell purification experiment failed to demonstrate the ice binding interaction in the validation test.

## **5.2 Future directions**

With the characteristic of the INA, nucleating activity, and the binding affinity to the ice surface, the possibility of *de novo* INA discovery and development is vast. The further improvement on the direct ice-nucleating activity

comparison, affinity purification toward ice surface, and investigation of the chemical composition of new INAs will lead to the efficient INA screening strategy.

In Chapter 2 and Chapter 3, I demonstrated the development of the INA screening system by direct ice nucleating activity comparison. The system can combine the automated droplet generation system and higher capacity and temperature controlled system to achieve higher throughput of the INA screening. I envision that this platform could be further expanded to employ custom libraries of different chemicals to select and compare the compounds that have strong ice nucleating activity.

While affinity purification method of ice-binding protein is established, efficient screening of glycans based on their binding affinity towards ice surface and validation test remains challenging. Also correlation between the ice-binding affinity and ice-nucleating activity is not established yet. I envision that the further investigation on the different chemical libraries, especially the larger size or the fragment with high lattice match with the ice confirmation, might be useful for the new INA discoveries.

## Reference

1. Koop, T.; Luo, B. P.; Tsias, A.; Peter, T., Water activity as the determinant for homogeneous ice nucleation in aqueous solutions. *Nature* **2000**, *406* (6796), 611-614.
2. Kanno, H.; Speedy, R. J.; Angell, C. A., Supercooling of Water to -92 {degrees}C Under Pressure. *Science* **1975**, *189* (4206), 880-1.
3. Sosso, G. C.; Chen, J.; Cox, S. J.; Fitzner, M.; Pedevilla, P.; Zen, A.; Michaelides, A., Crystal Nucleation in Liquids: Open Questions and Future Challenges in Molecular Dynamics Simulations. *Chem. Rev.* **2016**, *116* (12), 7078-7116.
4. Tanaka, K. K.; Kimura, Y., Theoretical analysis of crystallization by homogeneous nucleation of water droplets. *Phys. Chem. Chem. Phys.* **2019**, *21* (5), 2410-2418.
5. Liu, X. Y.; Du, N., Zero-sized effect of nano-particles and inverse homogeneous nucleation. Principles of freezing and antifreeze. *J Biol Chem* **2004**, *279* (7), 6124-31.
6. Bigg, E. K., The Supercooling of Water. *Proc. Phys. Soc. Section B* **1953**, *66* (8), 688-694.
7. Duft, D.; Leisner, T., Laboratory evidence for volume-dominated nucleation of ice in supercooled water microdroplets. *Atmos. Chem. Phys.* **2004**, *4* (7), 1997-2000.
8. Kay, J. E.; Tsemekhman, V.; Larson, B.; Baker, M.; Swanson, B., Comment on evidence for surface-initiated homogeneous nucleation. *Atmos. Chem. Phys.* **2003**, *3* (5), 1439-1443.
9. Langham, E. J.; Mason Basil John, N.; Bernal John, D., The heterogeneous and homogeneous nucleation of supercooled water. *Proc. Royal Soc. A* **1958**, *247* (1251), 493-504.
10. Erdemir, D.; Lee, A. Y.; Myerson, A. S., Nucleation of Crystals from Solution: Classical and Two-Step Models. *Acc. Chem. Res.* **2009**, *42* (5), 621-629.
11. Ickes, L.; Welti, A.; Hoose, C.; Lohmann, U., Classical nucleation theory of homogeneous freezing of water: thermodynamic and kinetic parameters. *Phys. Chem. Chem. Phys.* **2015**, *17* (8), 5514-5537.
12. Reinhardt, A.; Doye, J. P. K., Free energy landscapes for homogeneous nucleation of ice for a monatomic water model. *The Journal of Chemical Physics* **2012**, *136* (5), 054501.
13. Sear, R. P., Nucleation: theory and applications to protein solutions and colloidal suspensions. *J. Phys. Condens. Matter* **2007**, *19* (3), 033101.
14. Turnbull, D., Kinetics of heterogeneous nucleation. *J. Chem. Phys.* **1950**, *18* (2), 198-203.

15. Ickes, L.; Welti, A.; Lohmann, U., Classical nucleation theory of immersion freezing: sensitivity of contact angle schemes to thermodynamic and kinetic parameters. *Atmos. Chem. Phys.* **2017**, *17* (3), 1713-1739.
16. Fletcher, N. H., Size Effect in Heterogeneous Nucleation. *J. Chem. Phys.* **1958**, *29* (3), 572-576.
17. Alizadeh, A.; Yamada, M.; Li, R.; Shang, W.; Otta, S.; Zhong, S.; Ge, L.; Dhinojwala, A.; Conway, K. R.; Bahadur, V.; Vinciguerra, A. J.; Stephens, B.; Blohm, M. L., Dynamics of Ice Nucleation on Water Repellent Surfaces. *Langmuir* **2012**, *28* (6), 3180-3186.
18. Chen, J. P.; Hazra, A.; Levin, Z., Parameterizing ice nucleation rates using contact angle and activation energy derived from laboratory data. *Atmos. Chem. Phys.* **2008**, *8* (24), 7431-7449.
19. Reinhardt, A.; Doye, J. P. K., Effects of surface interactions on heterogeneous ice nucleation for a monatomic water model. *J. Chem. Phys.* **2014**, *141* (8), 084501.
20. Lavakumar, A., Solidification. In *Concepts in Physical Metallurgy*, Morgan & Claypool Publishers: 2017; pp 3-1-3-13.
21. Cabriolu, R.; Li, T., Ice nucleation on carbon surface supports the classical theory for heterogeneous nucleation. *Phys. Rev. E* **2015**, *91* (5), 052402.
22. Xu, W.; Lan, Z.; Peng, B. L.; Wen, R. F.; Ma, X. H., Effect of surface free energies on the heterogeneous nucleation of water droplet: A molecular dynamics simulation approach. *J. Chem. Phys.* **2015**, *142* (5), 054701.
23. Winkler, P. M.; McGraw, R. L.; Bauer, P. S.; Rentenberger, C.; Wagner, P. E., Direct determination of three-phase contact line properties on nearly molecular scale. *Sci. Rep.* **2016**, *6*, 26111.
24. Qiu, Y.; Odendahl, N.; Hudait, A.; Mason, R.; Bertram, A. K.; Paesani, F.; DeMott, P. J.; Molinero, V., Ice Nucleation Efficiency of Hydroxylated Organic Surfaces Is Controlled by Their Structural Fluctuations and Mismatch to Ice. *J. Am. Chem. Soc.* **2017**, *139* (8), 3052-3064.
25. Zielke, S. A.; Bertram, A. K.; Patey, G. N., A Molecular Mechanism of Ice Nucleation on Model AgI Surfaces. *J. Phys. Chem. B* **2015**, *119* (29), 9049-9055.
26. Welti, A.; Kanji, Z. A.; Lüönd, F.; Stetzer, O.; Lohmann, U., Exploring the Mechanisms of Ice Nucleation on Kaolinite: From Deposition Nucleation to Condensation Freezing. *J. Atmospheric Sci.* **2013**, *71* (1), 16-36.
27. Ogawa, S.; Koga, M.; Osanai, S., Anomalous ice nucleation behavior in aqueous polyvinyl alcohol solutions. *Chem. Phys. Lett.* **2009**, *480* (1), 86-89.
28. Hudait, A.; Odendahl, N.; Qiu, Y.; Paesani, F.; Molinero, V., Ice-Nucleating and Antifreeze Proteins Recognize Ice through a Diversity of Anchored Clathrate and Ice-like Motifs. *J. Am. Chem. Soc.* **2018**, *140* (14), 4905-4912.

29. Mochizuki, K.; Qiu, Y.; Molinero, V., Promotion of Homogeneous Ice Nucleation by Soluble Molecules. *J. Am. Chem. Soc* **2017**, *139* (47), 17003-17006.
30. Wu, S.; He, Z.; Zang, J.; Jin, S.; Wang, Z.; Wang, J.; Yao, Y.; Wang, J., Heterogeneous ice nucleation correlates with bulk-like interfacial water. *Sci. Adv.* **2019**, *5* (4), eaat9825.
31. Berkemeier, T.; Shiraiwa, M.; Pöschl, U.; Koop, T., Competition between water uptake and ice nucleation by glassy organic aerosol particles. *Atmospheric Chem. Phys.* **2014**, *14* (22), 12513-12531.
32. Koop, T.; Zobrist, B., Parameterizations for ice nucleation in biological and atmospheric systems. *Phys. Chem. Chem. Phys.* **2009**, *11* (46), 10839-10850.
33. Head, R. B., Steroids as Ice Nucleators. *Nature* **1961**, *191* (4793), 1058-1059.
34. Szyrmer, W.; Zawadzki, I., Biogenic and Anthropogenic Sources of Ice-Forming Nuclei: A Review. *Bull. Am. Meteorol. Soc.* **1997**, *78* (2), 209-228.
35. Edwards, G.; Evans, L.; La Mer, V., Ice nucleation by monodisperse silver iodide particles. *J. Colloid Sci.* **1962**, *17* (8), 749-758.
36. Vonnegut, B., The nucleation of ice formation by silver iodide. *J. Appl. Phys.* **1947**, *18* (7), 593-595.
37. Atkinson, J. D.; Murray, B. J.; Woodhouse, M. T.; Whale, T. F.; Baustian, K. J.; Carslaw, K. S.; Dobbie, S.; O'Sullivan, D.; Malkin, T. L., The importance of feldspar for ice nucleation by mineral dust in mixed-phase clouds. *Nature* **2013**, *498*, 355.
38. Eastwood, M. L.; Cremel, S.; Gehrke, C.; Girard, E.; Bertram, A. K., Ice nucleation on mineral dust particles: Onset conditions, nucleation rates and contact angles. *J. Geophys. Res. D* **2008**, *113* (D22).
39. Sosso, G. C.; Tribello, G. A.; Zen, A.; Pedevilla, P.; Michaelides, A., Ice formation on kaolinite: Insights from molecular dynamics simulations. *J. Chem. Phys.* **2016**, *145* (21), 211927.
40. Neven, L. G.; Duman, J. G.; Low, M. G.; Sehl, L. C.; Castellino, F. J., Purification and characterization of an insect hemolymph lipoprotein ice nucleator: evidence for the importance of phosphatidylinositol and apolipoprotein in the ice nucleator activity. *J. Comp. Physiol. B* **1989**, *159* (1), 71-82.
41. Duman, J. G., Antifreeze and Ice Nucleator Proteins in Terrestrial Arthropods. *Annual Review of Physiology* **2001**, *63* (1), 327-357.
42. Pummer, B. G.; Bauer, H.; Bernardi, J.; Bleicher, S.; Grothe, H., Suspendable macromolecules are responsible for ice nucleation activity of birch and conifer pollen. *Atmos. Chem. Phys.* **2012**, *12* (5), 2541-2550.
43. Dreischmeier, K.; Budke, C.; Wiehemeier, L.; Kottke, T.; Koop, T., Boreal pollen contain ice-nucleating as well as ice-binding 'antifreeze' polysaccharides. *Sci. Rep.* **2017**, *7*, 41890.



44. Diehl, K.; Quick, C.; Matthias-Maser, S.; Mitra, S. K.; Jaenicke, R., The ice nucleating ability of pollen: Part I: Laboratory studies in deposition and condensation freezing modes. *Atmospheric Res.* **2001**, *58* (2), 75-87.
45. Lindow, S. E.; Army, D. C.; Upper, C. D., Bacterial ice nucleation - a factor in frost injury to plants. *Plant Physiol.* **1982**, *70* (4), 1084-1089.
46. Varvaro, L.; Fabi, A., THE ROLE OF ICE NUCLEATION ACTIVE PSEUDOMONAS VIRIDIFLAVA IN FROST INJURY TO KIWIFRUIT PLANTS. *Rivista Patol. Veg.* **1992**, *2* (3), 85-90.
47. Corotto, L.; Wolber, P.; Warren, G., Ice nucleation activity of *Pseudomonas fluorescens*: mutagenesis, complementation analysis and identification of a gene product. *The EMBO journal* **1986**, *5* (2), 231-236.
48. Koda, N.; Aoki, M.; Kawahara, H.; Yamade, K.; Obata, H., Characterization and properties of intracellular proteins after cold acclimation of the ice-nucleating bacterium *Pantoea agglomerans* (*Erwinia herbicola*) IFO12686. *Cryobiology* **2000**, *41* (3), 195-203.
49. Kim, H.; Orser, C.; Lindow, S.; Sands, D., *Xanthomonas campestris* pv. *translucens* strains active in ice nucleation. *Plant Dis.* **1987**, *71* (11), 994-997.
50. Wu, Z.; Qin, L.; Walker, V. K., Characterization and recombinant expression of a divergent ice nucleation protein from '*Pseudomonas borealis*'. *Microbiology* **2009**, *155* (4), 1164-1169.
51. Haga, D. I.; Burrows, S. M.; Iannone, R.; Wheeler, M. J.; Mason, R. H.; Chen, J.; Polishchuk, E. A.; Pöschl, U.; Bertram, A. K., Ice nucleation by fungal spores from the classes *Agaricomycetes*, *Ustilaginomycetes*, and *Eurotiomycetes*, and the effect on the atmospheric transport of these spores. *Atmos. Chem. Phys.* **2014**, *14* (16), 8611-8630.
52. Knopf, D.; Alpert, P.; Wang, B.; Aller, J., Stimulation of ice nucleation by marine diatoms. *Nat. Geosci.* **2011**, *4* (2), 88.
53. Maki, L. R.; Galyan, E. L.; Chang-Chien, M.-M.; Caldwell, D. R., Ice Nucleation Induced by *Pseudomonas syringae*. *Applied Microbiology* **1974**, *28* (3), 456.
54. Ruggles, J. A.; Nemecek-Marshall, M.; Fall, R., Kinetics of appearance and disappearance of classes of bacterial ice nuclei support an aggregation model for ice nucleus assembly. *J. Bacteriol.* **1993**, *175* (22), 7216.
55. Bredow, M.; Tomalty, H. E.; Smith, L.; Walker, V. K., Ice and anti-nucleating activities of an ice-binding protein from the annual grass, *Brachypodium distachyon*. *Plant Cell Environ.* **2018**, *41* (5), 983-992.
56. Stile, S.; Seemiiller, E., The Role of Ice Formation in the Infection of Sour Cherry Leaves by *Pseudomonas syringae* pv. *syringae*. **1987**.
57. Duman, J. G., Animal ice-binding (antifreeze) proteins and glycolipids: an overview with emphasis on physiological function. *J. Exp. Biol.* **2015**, *218* (12), 1846.

58. Kozloff, L. M.; Turner, M. A.; Arellano, F., Formation of bacterial membrane ice-nucleating lipoglycoprotein complexes. *J. Bacteriol.* **1991**, *173* (20), 6528.
59. Zachariassen, K. E.; Kristiansen, E., Ice nucleation and antinucleation in nature. *Cryobiology* **2000**, *41* (4), 257-279.
60. Deininger, C. A.; Mueller, G. M.; Wolber, P. K., Immunological characterization of ice nucleation proteins from *Pseudomonas syringae*, *Pseudomonas fluorescens*, and *Erwinia herbicola*. *J. Bacteriol.* **1988**, *170* (2), 669.
61. Wolber, P.; Warren, G., Bacterial ice-nucleation proteins. *Trends Biochem. Sci.* **1989**, *14* (5), 179-182.
62. Green, R. L.; Warren, G. J., Physical and functional repetition in a bacterial ice nucleation gene. *Nature* **1985**, *317* (6038), 645-648.
63. Green, R. L.; Corotto, L. V.; Warren, G. J., Deletion mutagenesis of the ice nucleation gene from *Pseudomonas syringae* S203. *Mol. Gen. Genet.* **1988**, *215* (1), 165-172.
64. Garnham, C. P.; Campbell, R. L.; Walker, V. K.; Davies, P. L., Novel dimeric beta-helical model of an ice nucleation protein with bridged active sites. *BMC Struct. Biol.* **2011**, *11*, 11.
65. Graether, S. P.; Jia, Z., Modeling *Pseudomonas syringae* Ice-Nucleation Protein as  $\alpha$ -Helical Protein. *Biophys. J.* **2001**, *80* (3), 1169-1173.
66. Basu, K.; Campbell, R. L.; Guo, S.; Sun, T.; Davies, P. L., Modeling repetitive, non-globular proteins. *Protein Sci.* **2016**, *25* (5), 946-958.
67. Midya, U. S.; Bandyopadhyay, S., Interfacial Water Arrangement in the Ice-Bound State of an Antifreeze Protein: A Molecular Dynamics Simulation Study. *Langmuir* **2017**, *33* (22), 5499-5510.
68. He, Z.; Liu, K.; Wang, J., Bioinspired Materials for Controlling Ice Nucleation, Growth, and Recrystallization. *Acc. Chem. Res.* **2018**, *51* (5), 1082-1091.
69. Obata, H.; Muryoi, N.; Kawahara, H.; Yamade, K.; Nishikawa, J., Identification of a Novel Ice-Nucleating Bacterium of Antarctic Origin and its Ice Nucleation Properties. *Cryobiology* **1999**, *38* (2), 131-139.
70. Phelps, P.; Giddings, T. H.; Prochoda, M.; Fall, R., Release of cell-free ice nuclei by *Erwinia herbicola*. *J. Bacteriol.* **1986**, *167* (2), 496.
71. Hill, T. C. J.; Moffett, B. F.; Demott, P. J.; Georgakopoulos, D. G.; Stump, W. L.; Franc, G. D., Measurement of ice nucleation-active bacteria on plants and in precipitation by quantitative PCR. *Applied and environmental microbiology* **2014**, *80* (4), 1256-1267.
72. Passarelli, R. E.; Chessin, H.; Vonnegut, B., Ice Nucleation by Solid Solutions of Silver-Copper Iodide. *Science* **1973**, *181* (4099), 549.

73. Christner, B. C.; Morris, C. E.; Foreman, C. M.; Cai, R. M.; Sands, D. C., Ubiquity of biological ice nucleators in snowfall. *Science* **2008**, *319* (5867), 1214-1214.
74. Pratt, K. A.; DeMott, P. J.; French, J. R.; Wang, Z.; Westphal, D. L.; Heymsfield, A. J.; Twohy, C. H.; Prenni, A. J.; Prather, K. A., In situ detection of biological particles in cloud ice-crystals. *Nat. Geosci.* **2009**, *2*, 398.
75. Ramanathan, V.; Cess, R. D.; Harrison, E. F.; Minnis, P.; Barkstrom, B. R.; Ahmad, E.; Hartmann, D., Cloud-radiative forcing and climate: results from the Earth radiation budget experiment. *Science* **1989**, *243* (4887), 57-63.
76. Hoose, C.; Kristjánsson, J. E.; Chen, J.-P.; Hazra, A., A Classical-Theory-Based Parameterization of Heterogeneous Ice Nucleation by Mineral Dust, Soot, and Biological Particles in a Global Climate Model. *J. Atmospheric Sci.* **2010**, *67* (8), 2483-2503.
77. Huffman, J. A.; Prenni, A. J.; DeMott, P. J.; Pöhlker, C.; Mason, R. H.; Robinson, N. H.; Fröhlich-Nowoisky, J.; Tobo, Y.; Després, V. R.; Garcia, E.; Gochis, D. J.; Harris, E.; Müller-Germann, I.; Ruzene, C.; Schmer, B.; Sinha, B.; Day, D. A.; Andreae, M. O.; Jimenez, J. L.; Gallagher, M.; Kreidenweis, S. M.; Bertram, A. K.; Pöschl, U., High concentrations of biological aerosol particles and ice nuclei during and after rain. *Atmos. Chem. Phys.* **2013**, *13* (13), 6151-6164.
78. Morris, C. E.; Sands, D. C.; Bardin, M.; Jaenicke, R.; Vogel, B.; Leyronas, C.; Ariya, P. A.; Psenner, R., Microbiology and atmospheric processes: research challenges concerning the impact of airborne micro-organisms on the atmosphere and climate. *Biogeosciences* **2011**, *8* (1), 17-25.
79. Skirvin, R.; Kohler, E.; Steiner, H.; Ayers, D.; Laughnan, A.; Norton, M.; Warmund, M., The use of genetically engineered bacteria to control frost on strawberries and potatoes. Whatever happened to all of that research? *Sci. Hortic.* **2000**, *84* (1-2), 179-189.
80. Mitchell, D. L.; Finnegan, W., Modification of cirrus clouds to reduce global warming. *Environ. Res. Lett.* **2009**, *4* (4), 045102.
81. Zipori, A.; Rosenfeld, D.; Shpund, J.; Steinberg, D. M.; Erel, Y., Targeting and impacts of AgI cloud seeding based on rain chemical composition and cloud top phase characterization. *Atmospheric Res.* **2012**, *114-115*, 119-130.
82. Simpson, J.; Woodley, W. L.; Friedman, H. A.; Slusher, T. W.; Scheffee, R. S.; Steele, R. L., An Airborne Pyrotechnic Cloud Seeding System and Its Use. *J. Appl. Meteorol.* **1970**, *9* (1), 109-122.
83. French, J. R.; Friedrich, K.; Tessorf, S. A.; Rauber, R. M.; Geerts, B.; Rasmussen, R. M.; Xue, L.; Kunkel, M. L.; Blestrud, D. R., Precipitation formation from orographic cloud seeding. *Proc. Natl. Acad. Sci. U.S.A.* **2018**, *115* (6), 1168.

84. Tegos, G.; Vargas, C.; Perysinakis, A.; Koukkou, A. I.; Christogianni, A.; Nieto, J. J.; Ventosa, A.; Drainas, C., Release of cell-free ice nuclei from *Halomonas elongata* expressing the ice nucleation gene *inaZ* of *Pseudomonas syringae*. *J. Appl. Microbiol.* **2000**, *89* (5), 785-792.
85. Lindemann, J.; Suslow, T. V., Competition between Ice Nucleation-active Wild-type and Ice Nucleation-deficient Deletion Mutant Strains of *Pseudomonas-syringae* and *Pseudomonas-fluorescens* Biovar-1 and Biological-control of Frost Injury on Strawberry Blossoms. *Phytopathology* **1987**, *77* (6), 882-886.
86. Moore, L. W., *Pseudomonas syringae*: disease and ice nucleation activity. *Ornamentals Northwest* **1988**, *12* (2), 3.
87. Drahos, D. J., Field testing of genetically engineered microorganisms. *Biotechnol. Adv.* **1991**, *9* (2), 157-171.
88. Wozniak, C. A.; McClung, G.; Gagliardi, J.; Segal, M.; Matthews, K., Regulation of genetically engineered microorganisms under FIFRA, FFDCA and TSCA. In *Regulation of Agricultural Biotechnology: The United States and Canada*, Springer: 2012; pp 57-94.
89. Cochet, N.; Widehem, P., Ice crystallization by *Pseudomonas syringae*. *Applied Microbiology and Biotechnology* **2000**, *54* (2), 153-161.
90. Wang, W., Lyophilization and development of solid protein pharmaceuticals. *Int. J. Pharm.* **2000**, *203* (1-2), 1-60.
91. Kawasaki, H.; Shimanouchi, T.; Kimura, Y., Recent Development of Optimization of Lyophilization Process. *Journal of Chemistry* **2019**, *2019*, 14.
92. Searles, J. A.; Carpenter, J. F.; Randolph, T. W., The ice nucleation temperature determines the primary drying rate of lyophilization for samples frozen on a temperature-controlled shelf. *J. Pharm. Sci.* **2001**, *90* (7), 860-871.
93. John Morris, G.; Acton, E., Controlled ice nucleation in cryopreservation – A review. *Cryobiology* **2013**, *66* (2), 85-92.
94. Koushafar, H.; Pham, L.; Lee, C.; Rubinsky, B., Chemical adjuvant cryosurgery with antifreeze proteins. *J. Surg. Oncol.* **1997**, *66* (2), 114-121.
95. Rubinsky, B., Cryosurgery. *Annual Review of Biomedical Engineering* **2000**, *2* (1), 157-187.
96. Hou, Y.; Sun, Z.; Rao, W.; Liu, J., Nanoparticle-mediated cryosurgery for tumor therapy. *Nanomedicine* **2018**, *14* (2), 493-506.
97. Koop, T.; Ng, H. P.; Molina, L. T.; Molina, M. J., A New Optical Technique to Study Aerosol Phase Transitions: The Nucleation of Ice from H<sub>2</sub>SO<sub>4</sub> Aerosols. *J. Phys. Chem. A* **1998**, *102* (45), 8924-8931.
98. Zimmermann, F.; Ebert, M.; Worringer, A.; Schütz, L.; Weinbruch, S., Environmental scanning electron microscopy (ESEM) as a new technique to determine the ice nucleation capability of individual atmospheric aerosol particles. *Atmospheric Environment* **2007**, *41* (37), 8219-8227.

99. Kumai, M., SNOW CRYSTALS AND THE IDENTIFICATION OF THE NUCLEI IN THE NORTHERN UNITED STATES OF AMERICA. *J. Meteorol.* **1961**, *18* (2), 139-150.
100. Kanji, Z. A.; Ladino, L. A.; Wex, H.; Boose, Y.; Burkert-Kohn, M.; Cziczo, D. J.; Krämer, M., Overview of ice nucleating particles. *Meteorol. Monogr.* **2017**, *58*, 1.1-1.33.
101. Rogers, D. C., Development of a continuous flow thermal gradient diffusion chamber for ice nucleation studies. *Atmospheric Res.* **1988**, *22* (2), 149-181.
102. Chen, Y.; DeMott, P. J.; Kreidenweis, S. M.; Rogers, D. C.; Sherman, D. E., Ice Formation by Sulfate and Sulfuric Acid Aerosol Particles under Upper-Tropospheric Conditions. *J. Atmospheric Sci.* **2000**, *57* (22), 3752-3766.
103. Rogers, D. C.; DeMott, P. J.; Kreidenweis, S. M.; Chen, Y., A Continuous-Flow Diffusion Chamber for Airborne Measurements of Ice Nuclei. *J. Atmospheric Ocean. Technol.* **2001**, *18* (5), 725-741.
104. Stetzer, O.; Baschek, B.; Luond, F.; Lohmann, U., The Zurich Ice Nucleation Chamber (ZINC) - A new instrument to investigate atmospheric ice formation. *Aerosol Sci Technol* **2008**, *42* (1), 64-74.
105. Niehaus, J.; Bunker, K. W.; China, S.; Kostinski, A.; Mazzoleni, C.; Cantrell, W., A Technique to Measure Ice Nuclei in the Contact Mode. *J. Atmospheric Ocean. Technol.* **2014**, *31* (4), 913-922.
106. Chavan, S.; Park, D.; Singla, N.; Sokalski, P.; Boyina, K.; Miljkovic, N., Effect of Latent Heat Released by Freezing Droplets during Frost Wave Propagation. *Langmuir* **2018**, *34* (22), 6636-6644.
107. Tarn, M. D.; Sikora, S. N. F.; Porter, G. C. E.; O'Sullivan, D.; Adams, M.; Whale, T. F.; Harrison, A. D.; Vergara-Temprado, J.; Wilson, T. W.; Shim, J. U.; Murray, B. J., The study of atmospheric ice-nucleating particles via microfluidically generated droplets. *Microfluid Nanofluidics* **2018**, *22* (5), 25.
108. Stan, C. A.; Schneider, G. F.; Shevkoplyas, S. S.; Hashimoto, M.; Ibanescu, M.; Wiley, B. J.; Whitesides, G. M., A microfluidic apparatus for the study of ice nucleation in supercooled water drops. *Lab Chip* **2009**, *9* (16), 2293-305.
109. Charoenrein, S.; Reid, D. S., The use of DSC to study the kinetics of heterogeneous and homogeneous nucleation of ice in aqueous systems. *Thermochimica Acta* **1989**, *156* (2), 373-381.
110. Matsumoto, M.; Saito, S.; Ohmine, I., Molecular dynamics simulation of the ice nucleation and growth process leading to water freezing. *Nature* **2002**, *416* (6879), 409-413.
111. Molinero, V.; Moore, E. B., Water Modeled As an Intermediate Element between Carbon and Silicon. *J. Phys. Chem. B* **2009**, *113* (13), 4008-4016.

112. Lupi, L.; Hudait, A.; Molinero, V., Heterogeneous Nucleation of Ice on Carbon Surfaces. *J. Am. Chem. Soc* **2014**, *136* (8), 3156-3164.
113. Bermúdez di Lorenzo, A. J.; Carignano, M. A.; Pereyra, R. G., A statistical study of heterogeneous nucleation of ice by molecular dynamics. *Chem. Phys. Lett.* **2015**, *635*, 45-49.
114. Fitzner, M.; Sosso, G. C.; Cox, S. J.; Michaelides, A., The Many Faces of Heterogeneous Ice Nucleation: Interplay Between Surface Morphology and Hydrophobicity. *J. Am. Chem. Soc* **2015**, *137* (42), 13658-13669.
115. Pandey, R.; Usui, K.; Livingstone, R. A.; Fischer, S. A.; Pfaendtner, J.; Backus, E. H. G.; Nagata, Y.; Fröhlich-Nowoisky, J.; Schmäser, L.; Mauri, S.; Scheel, J. F.; Knopf, D. A.; Pöschl, U.; Bonn, M.; Weidner, T., Ice-nucleating bacteria control the order and dynamics of interfacial water. *Sci. Adv.* **2016**, *2* (4), e1501630.
116. Schauerl, M.; Podewitz, M.; Ortner, T. S.; Waibl, F.; Thoeny, A.; Loerting, T.; Liedl, K. R., Balance between hydration enthalpy and entropy is important for ice binding surfaces in Antifreeze Proteins. *Sci. Rep.* **2017**, *7* (1), 11901.
117. Eickhoff, L.; Dreischmeier, K.; Zipori, A.; Sirotinskaya, V.; Adar, C.; Reicher, N.; Braslavsky, I.; Rudich, Y.; Koop, T., Contrasting Behavior of Antifreeze Proteins: Ice Growth Inhibitors and Ice Nucleation Promoters. *J. Phys. Chem. Lett.* **2019**, *10* (5), 966-972.
118. Xu, H.; Griffith, M.; Patten, C. L.; Glick, B. R., Isolation and characterization of an antifreeze protein with ice nucleation activity from the plant growth promoting rhizobacterium *Pseudomonas putida* GR12-2. *Can. J. Microbiol.* **1998**, *44* (1), 64-73.
119. Davies, P. L., Ice-binding proteins: a remarkable diversity of structures for stopping and starting ice growth. *Trends Biochem. Sci.* **2014**, *39* (11), 548-555.
120. Qiu, Y.; Hudait, A.; Molinero, V., How Size and Aggregation of Ice-Binding Proteins Control Their Ice Nucleation Efficiency. *J. Am. Chem. Soc* **2019**, *141* (18), 7439-7452.
121. Govindarajan, A. G.; Lindow, S. E., Size of bacterial ice-nucleation sites measured in situ by radiation inactivation analysis. *Proc. Natl. Acad. Sci. U.S.A.* **1988**, *85* (5), 1334.
122. Ling, M. L.; Wex, H.; Grawe, S.; Jakobsson, J.; Löndahl, J.; Hartmann, S.; Finster, K.; Boesen, T.; Šantl-Temkiv, T., Effects of Ice Nucleation Protein Repeat Number and Oligomerization Level on Ice Nucleation Activity. *J. Geophys. Res. D* **2018**, *123* (3), 1802-1810.
123. Kobashigawa, Y.; Nishimiya, Y.; Miura, K.; Ohgiya, S.; Miura, A.; Tsuda, S., A part of ice nucleation protein exhibits the ice-binding ability. *FEBS Letters* **2005**, *579* (6), 1493-1497.

124. Knight, C. A.; Hallett, J.; DeVries, A. L., Solute effects on ice recrystallization: An assessment technique. *Cryobiology* **1988**, *25* (1), 55-60.
125. Gilbert, J. A.; Hill, P. J.; Dodd, C. E. R.; Laybourn-Parry, J., Demonstration of antifreeze protein activity in Antarctic lake bacteria. *Microbiology* **2004**, *150* (1), 171-180.
126. Au - Braslavsky, I.; Au - Drori, R., LabVIEW-operated Novel Nanoliter Osmometer for Ice Binding Protein Investigations. *JoVE* **2013**, (72), e4189.
127. Drori, R.; Celik, Y.; Davies Peter, L.; Braslavsky, I., Ice-binding proteins that accumulate on different ice crystal planes produce distinct thermal hysteresis dynamics. *J. Royal Soc. Interface* **2014**, *11* (98), 20140526.
128. Kuiper, M. J.; Lankin, C.; Gauthier, S. Y.; Walker, V. K.; Davies, P. L., Purification of antifreeze proteins by adsorption to ice. *Biochem. Biophys. Res. Commun.* **2003**, *300* (3), 645-648.
129. Wilson, S. L.; Kelley, D. L.; Walker, V. K., Ice-active characteristics of soil bacteria selected by ice-affinity. *Environ. Microbiol.* **2006**, *8* (10), 1816-1824.
130. Marshall, C. J.; Basu, K.; Davies, P. L., Ice-shell purification of ice-binding proteins. *Cryobiology* **2016**, *72* (3), 258-63.
131. Adar, C.; Sirotinskaya, V.; Bar Dolev, M.; Friehmann, T.; Braslavsky, I., Falling water ice affinity purification of ice-binding proteins. *Sci. Rep.* **2018**, *8* (1), 11046.
132. DeMott, P. J.; Prenni, A. J.; Liu, X.; Kreidenweis, S. M.; Petters, M. D.; Twohy, C. H.; Richardson, M. S.; Eidhammer, T.; Rogers, D. C., Predicting global atmospheric ice nuclei distributions and their impacts on climate. *Proc. Natl. Acad. Sci. U.S.A.* **2010**, *107* (25), 11217-11222.
133. Teixeira, M.; Buff, S.; Desnos, H.; Loiseau, C.; Bruyere, P.; Joly, T.; Commin, L., Ice nucleating agents allow embryo freezing without manual seeding. *Theriogenology* **2017**, *104*, 173-178.
134. Lüönd, F.; Stetzer, O.; Welti, A.; Lohmann, U., Experimental study on the ice nucleation ability of size-selected kaolinite particles in the immersion mode. *J. Geophys. Res. D* **2010**, *115* (D14).
135. Weng, L. D.; Tessier, S. N.; Smith, K.; Edd, J. F.; Stott, S. L.; Toner, M., Bacterial Ice Nucleation in Monodisperse D<sub>2</sub>O and H<sub>2</sub>O-in-Oil Emulsions. *Langmuir* **2016**, *32* (36), 9229-9236.
136. Baret, J. C.; Miller, O. J.; Taly, V.; Ryckelynck, M.; El-Harrak, A.; Frenz, L.; Rick, C.; Samuels, M. L.; Hutchison, J. B.; Agresti, J. J.; Link, D. R.; Weitz, D. A.; Griffiths, A. D., Fluorescence-activated droplet sorting (FADS): efficient microfluidic cell sorting based on enzymatic activity. *Lab Chip* **2009**, *9* (13), 1850-1858.
137. Volpatti, L. R.; Yetisen, A. K., Commercialization of microfluidic devices. *Trends Biotechnol.* **2014**, *32* (7), 347-350.

138. Tang, S. K. Y.; Li, Z. Y.; Abate, A. R.; Agresti, J. J.; Weitz, D. A.; Psaltis, D.; Whitesides, G. M., A multi-color fast-switching microfluidic droplet dye laser. *Lab Chip* **2009**, *9* (19), 2767-2771.
139. Sesen, M.; Alan, T.; Neild, A., Droplet control technologies for microfluidic high throughput screening (mu HTS). *Lab Chip* **2017**, *17* (14), 2372-2394.
140. Sgro, A. E.; Chiu, D. T., Droplet freezing, docking, and the exchange of immiscible phase and surfactant around frozen droplets. *Lab Chip* **2010**, *10* (14), 1873-1877.
141. Price, A. K.; MacConnell, A. B.; Paegel, B. M., Microfluidic Bead Suspension Hopper. *Anal. Chem.* **2014**, *86* (10), 5039-5044.
142. Derda, R.; Tang, S. K. Y.; Whitesides, G. M., Uniform Amplification of Phage with Different Growth Characteristics in Individual Compartments Consisting of Monodisperse Droplets. *Angew. Chem. Int. Ed. Engl.* **2010**, *49* (31), 5301-5304.
143. Matochko, W. L.; Ng, S.; Jafari, M. R.; Romaniuk, J.; Tang, S. K. Y.; Derda, R., Uniform amplification of phage display libraries in monodisperse emulsions. *Methods* **2012**, *58* (1), 18-27.
144. Guo, M. T.; Rotem, A.; Heyman, J. A.; Weitz, D. A., Droplet microfluidics for high-throughput biological assays. *Lab Chip* **2012**, *12* (12), 2146-55.
145. Boedicker, J. Q.; Li, L.; Kline, T. R.; Ismagilov, R. F., Detecting bacteria and determining their susceptibility to antibiotics by stochastic confinement in nanoliter droplets using plug-based microfluidics. *Lab Chip* **2008**, *8* (8), 1265-72.
146. Matochko, W. L.; Li, S. C.; Tang, S. K. Y.; Derda, R., Prospective identification of parasitic sequences in phage display screens. *Nucleic Acids Res.* **2014**, *42* (3), 1784-1798.
147. Yung, C. W.; Fiering, J.; Mueller, A. J.; Ingber, D. E., Micromagnetic-microfluidic blood cleansing device. *Lab Chip* **2009**, *9* (9), 1171-1177.
148. Kamijo, Y.; Derda, R., Freeze-Float Selection of Ice Nucleators. *Langmuir* **2018**, *35* (2), 359-364.
149. Pereira, D. A.; Williams, J. A., Origin and evolution of high throughput screening. *Br. J. Pharmacol.* **2007**, *152* (1), 53-61.
150. Collins, K. D.; Gensch, T.; Glorius, F., Contemporary screening approaches to reaction discovery and development. *Nat. Chem.* **2014**, *6*, 859.
151. Hughes, J. P.; Rees, S.; Kalindjian, S. B.; Philpott, K. L., Principles of early drug discovery. *Br. J. Pharmacol.* **2011**, *162* (6), 1239-1249.
152. Kansy, M.; Senner, F.; Gubernator, K., Physicochemical High Throughput Screening: Parallel Artificial Membrane Permeation Assay in the Description of Passive Absorption Processes. *J. Med. Chem.* **1998**, *41* (7), 1007-1010.

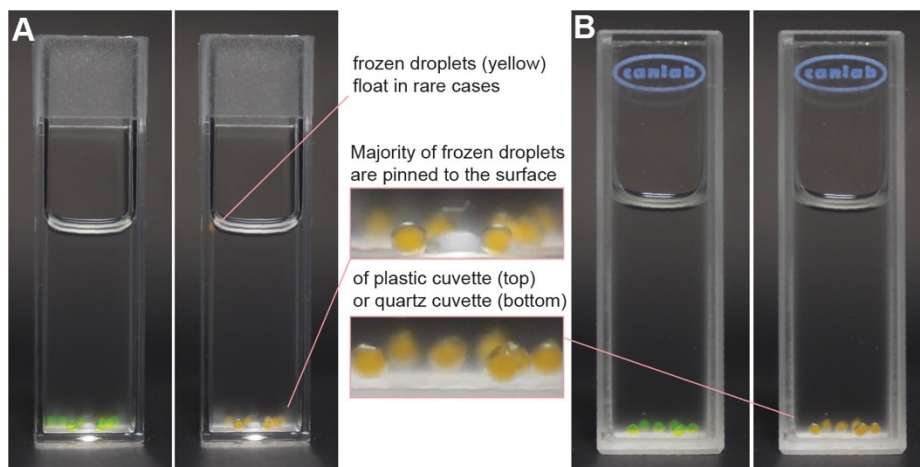


153. Clare, R. H.; Bardelle, C.; Harper, P.; Hong, W. D.; Börjesson, U.; Johnston, K. L.; Collier, M.; Myhill, L.; Cassidy, A.; Plant, D.; Plant, H.; Clark, R.; Cook, D. A. N.; Steven, A.; Archer, J.; McGillan, P.; Charoensutthivarakul, S.; Bibby, J.; Sharma, R.; Nixon, G. L.; Slatko, B. E.; Cantin, L.; Wu, B.; Turner, J.; Ford, L.; Rich, K.; Wigglesworth, M.; Berry, N. G.; O'Neill, P. M.; Taylor, M. J.; Ward, S. A., Industrial scale high-throughput screening delivers multiple fast acting macrofilaricides. *Nat. Commun.* **2019**, *10* (1), 11.
154. Wölcke, J.; Ullmann, D., Miniaturized HTS technologies – uHTS. *Drug Discov. Today* **2001**, *6* (12), 637-646.
155. Burbaum, J. J.; Sigal, N. H., New technologies for high-throughput screening. *Curr. Opin. Chem. Biol.* **1997**, *1* (1), 72-78.
156. Major, J., Challenges and Opportunities in High Throughput Screening: Implications for New Technologies. *J Biomol Screen* **1998**, *3* (1), 13-17.
157. Keserü, G. M.; Makara, G. M., The influence of lead discovery strategies on the properties of drug candidates. *Nat. Rev. Drug Discov.* **2009**, *8*, 203.
158. Zheng, B.; Roach, L. S.; Ismagilov, R. F., Screening of Protein Crystallization Conditions on a Microfluidic Chip Using Nanoliter-Size Droplets. *J. Am. Chem. Soc* **2003**, *125* (37), 11170-11171.
159. Sjostrom, S. L.; Bai, Y.; Huang, M.; Liu, Z.; Nielsen, J.; Joensson, H. N.; Andersson Svahn, H., High-throughput screening for industrial enzyme production hosts by droplet microfluidics. *Lab Chip* **2014**, *14* (4), 806-813.
160. Tjhung, K. F.; Burnham, S.; Anany, H.; Griffiths, M. W.; Derda, R., Rapid Enumeration of Phage in Monodisperse Emulsions. *Anal. Chem.* **2014**, *86* (12), 5642-5648.
161. Vogelstein, B.; Kinzler, K. W., Digital PCR. *Proc. Natl. Acad. Sci. U.S.A.* **1999**, *96* (16), 9236-9241.
162. Kang, H. M.; Subramaniam, M.; Targ, S.; Nguyen, M.; Maliskova, L.; McCarthy, E.; Wan, E.; Wong, S.; Byrnes, L.; Lanata, C. M.; Gate, R. E.; Mostafavi, S.; Marson, A.; Zaitlen, N.; Criswell, L. A.; Ye, C. J., Multiplexed droplet single-cell RNA-sequencing using natural genetic variation. *Nat. Biotechnol.* **2017**, *36*, 89.
163. Macosko, Evan Z.; Basu, A.; Satija, R.; Nemes, J.; Shekhar, K.; Goldman, M.; Tirosh, I.; Bialas, Allison R.; Kamitaki, N.; Martersteck, Emily M.; Trombetta, John J.; Weitz, David A.; Sanes, Joshua R.; Shalek, Alex K.; Regev, A.; McCarroll, Steven A., Highly Parallel Genome-wide Expression Profiling of Individual Cells Using Nanoliter Droplets. *Cell* **2015**, *161* (5), 1202-1214.
164. Kawaguchi, M., Silicone oil emulsions stabilized by polymers and solid particles. *Adv Colloid Interface Sci* **2016**, *233*, 186-199.

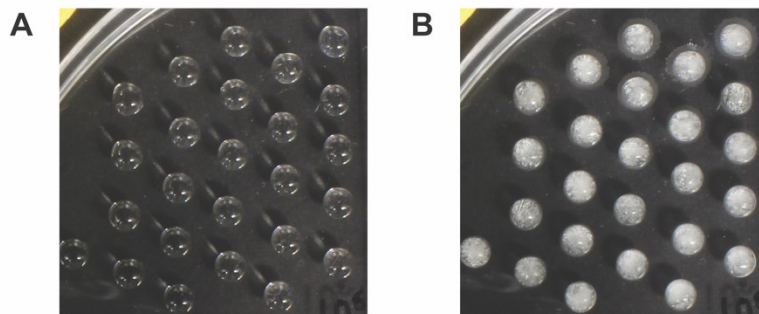
165. Niedermeier, D.; Shaw, R. A.; Hartmann, S.; Wex, H.; Clauss, T.; Voigtländer, J.; Stratmann, F., Heterogeneous ice nucleation: exploring the transition from stochastic to singular freezing behavior. *Atmos. Chem. Phys.* **2011**, *11* (16), 8767-8775.
166. Murray, B. J.; Broadley, S.; Wilson, T.; Atkinson, J.; Wills, R., Heterogeneous freezing of water droplets containing kaolinite particles. *Atmospheric Chem. Phys.* **2011**, *11* (9), 4191-4207.
167. Stevens, C. A.; Semrau, J.; Chiriac, D.; Litschko, M.; Campbell, R. L.; Langelaan, D. N.; Smith, S. P.; Davies, P. L.; Allingham, J. S., Peptide backbone circularization enhances antifreeze protein thermostability. *Protein Sci.* **2017**, *26* (10), 1932-1941.
168. Graham, L. A.; Davies, P. L., Glycine-Rich Antifreeze Proteins from Snow Fleas. *Science* **2005**, *310* (5747), 461.
169. Basu, K.; Wasserman, S. S.; Jeronimo, P. S.; Graham, L. A.; Davies, P. L., Intermediate activity of midge antifreeze protein is due to a tyrosine-rich ice-binding site and atypical ice plane affinity. *The FEBS Journal* **2016**, *283* (8), 1504-1515.
170. Vance, T. D. R.; Graham, L. A.; Davies, P. L., An ice-binding and tandem beta-sandwich domain-containing protein in *Shewanella frigidimarina* is a potential new type of ice adhesin. *The FEBS Journal* **2018**, *285* (8), 1511-1527.
171. Worrall, D.; Elias, L.; Ashford, D.; Smallwood, M.; Sidebottom, C.; Lillford, P.; Telford, J.; Holt, C.; Bowles, D., A Carrot Leucine-Rich-Repeat Protein That Inhibits Ice Recrystallization. *Science* **1998**, *282* (5386), 115.
172. Park, K. S.; Do, H.; Lee, J. H.; Park, S. I.; Kim, E. j.; Kim, S.-J.; Kang, S.-H.; Kim, H. J., Characterization of the ice-binding protein from Arctic yeast *Leucosporidium* sp. AY30. *Cryobiology* **2012**, *64* (3), 286-296.
173. Xiao, N.; Suzuki, K.; Nishimiya, Y.; Kondo, H.; Miura, A.; Tsuda, S.; Hoshino, T., Comparison of functional properties of two fungal antifreeze proteins from *Antarctomyces psychrotrophicus* and *Typhula ishikariensis*. *The FEBS Journal* **2010**, *277* (2), 394-403.
174. Tachibana, Y.; Fletcher, G. L.; Fujitani, N.; Tsuda, S.; Monde, K.; Nishimura, S.-I., Antifreeze Glycoproteins: Elucidation of the Structural Motifs That Are Essential for Antifreeze Activity. *Angew. Chem. Int. Ed. Engl.* **2004**, *43* (7), 856-862.
175. Tjhung, K. F.; Kitov, P. I.; Ng, S.; Kitova, E. N.; Deng, L.; Klassen, J. S.; Derda, R., Silent Encoding of Chemical Post-Translational Modifications in Phage-Displayed Libraries. *J. Am. Chem. Soc.* **2016**, *138* (1), 32-35.
176. Garnham, C. P.; Natarajan, A.; Middleton, A. J.; Kuiper, M. J.; Braslavsky, I.; Davies, P. L., Compound Ice-Binding Site of an Antifreeze Protein Revealed by Mutagenesis and Fluorescent Tagging. *Biochemistry* **2010**, *49* (42), 9063-9071.

177. Bove, L. E.; Gaal, R.; Raza, Z.; Ludl, A.-A.; Klotz, S.; Saitta, A. M.; Goncharov, A. F.; Gillet, P., Effect of salt on the H-bond symmetrization in ice. *Proc. Natl. Acad. Sci. U.S.A.* **2015**, *112* (27), 8216.
178. Novikova, I. V.; China, S.; Evans, J. E., Cell-free production of full-length ice nucleating protein InaZ. *bioRxiv* **2018**, 334987.

## Appendix A: Supporting information for Chapter 2

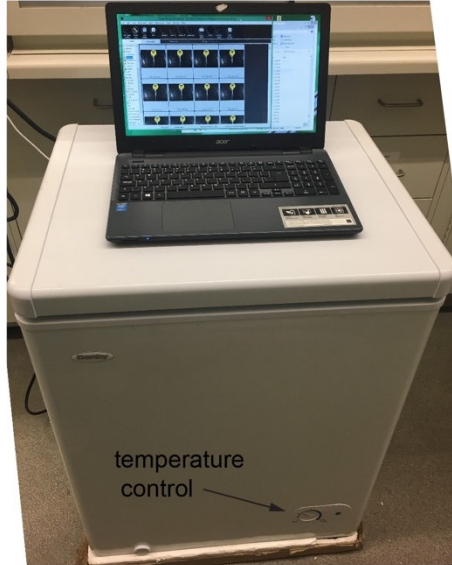


**Appendix A-1.** Digital imaging of the droplets in a freeze-float system without the “cushion” layer before and after freezing of droplets. I have tested a freeze-float system that contained only one layer of silicone oil with 2% surfactant either in (A) polystyrene or (B) quartz cuvettes. 1  $\mu\text{L}$  droplets that contained fluorescein dye were light green in the liquid state, and became orange-yellow in color upon freezing. Floating of the droplets in a system that contains only one layer of liquid and no second “cushion layer” was neither successful nor robust. The use of floating layer with density around 0.95 g/mL allowed separation of some ice droplets from liquid droplets, however, most of the liquid droplets that sedimented to the bottom had aggregated and adhered to the surface of the container. Even when droplets froze, floating was not observed. To avoid this adhesion, incorporating the second layer of liquid immiscible with water and silicone oil and density  $>1.3 \text{ g/cm}^3$  (“cushion layer”) was necessary to prevent the droplets from touching the surface of the container.



**Appendix A-2.** Droplets freezing assay of 1  $\mu\text{L}$  droplets. (A) is unfrozen droplets and (B) is frozen droplets. Polarization-lidar technique was used to determine the droplet freezing.

chest freezer and laptop for remote control of camera



Lid closed during the experiment.  
Illumination inside is maintained by the low-heat  
LED lamps placed inside the chest freezer.

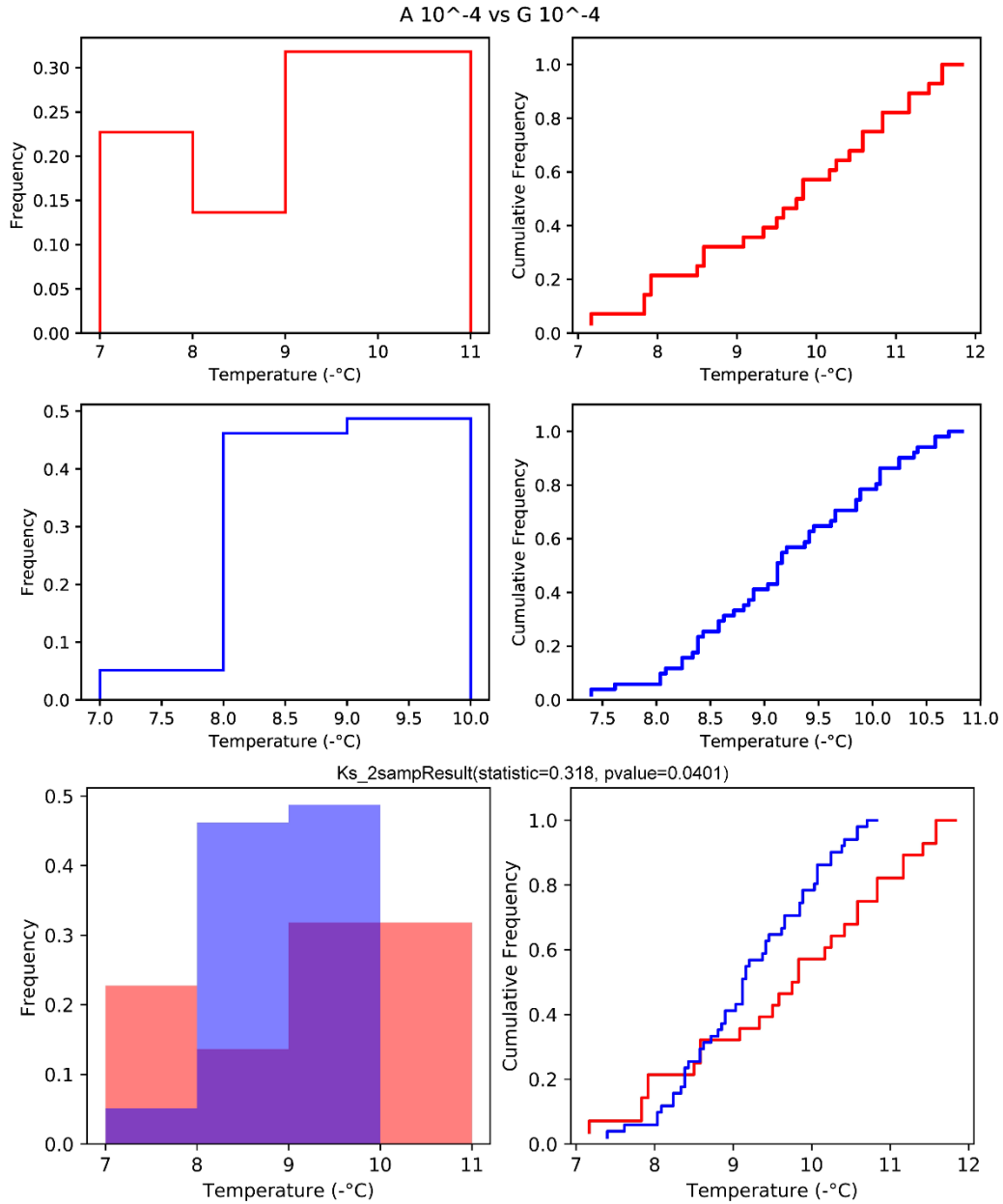
inside the freezer: lights, camera, and cuvette



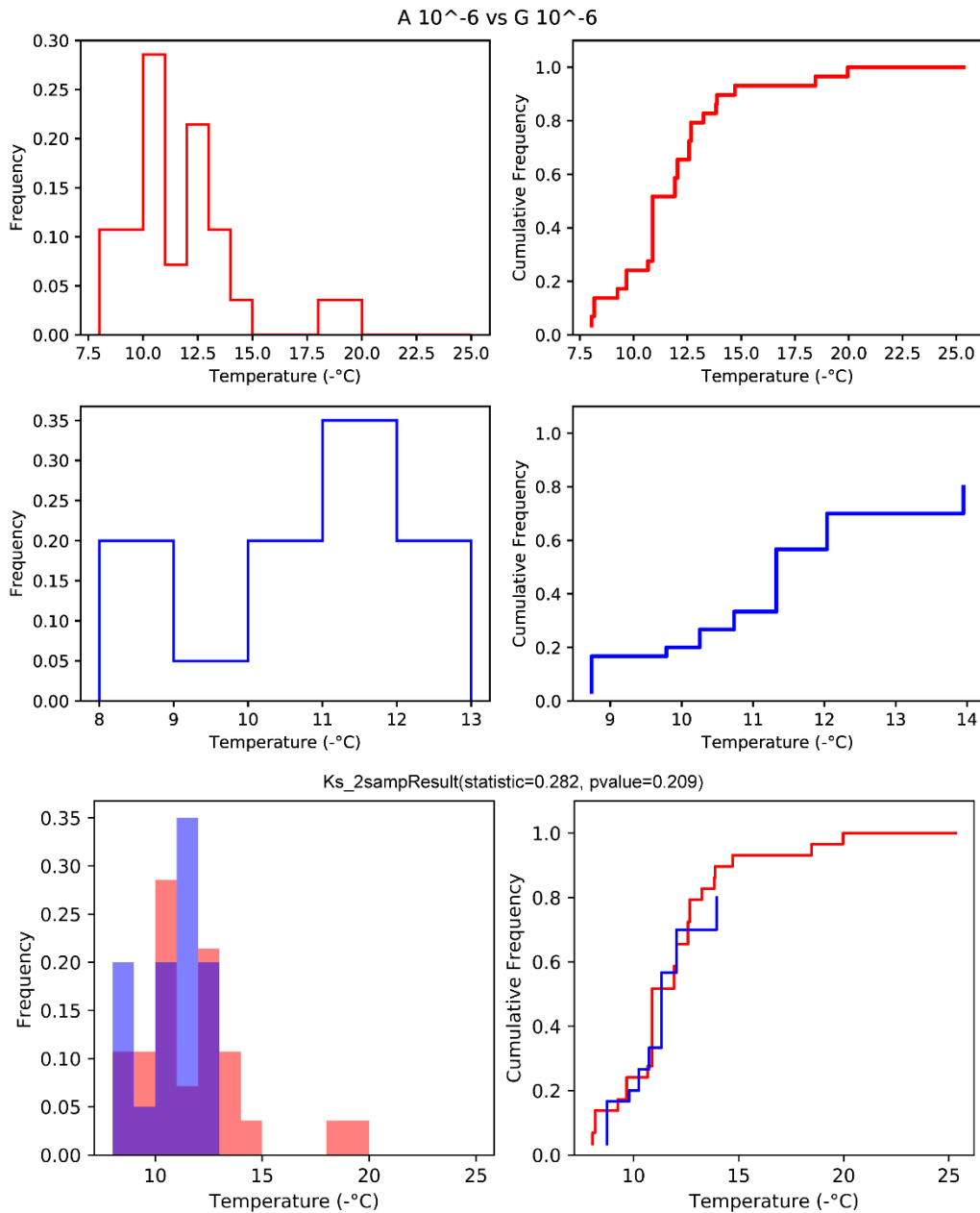
remote control cable for camera

**Appendix A-3.** Setup of the freeze-float selection using a generic freezer. The selection platform sits inside the freezer, and the droplets freezing in the cuvette was illuminated by low-heat LED lamps and recorded by the camera which was placed in the freezer. The camera was controlled by the software on the computer next to the freezer.

## Appendix B: Supporting information for Chapter 3

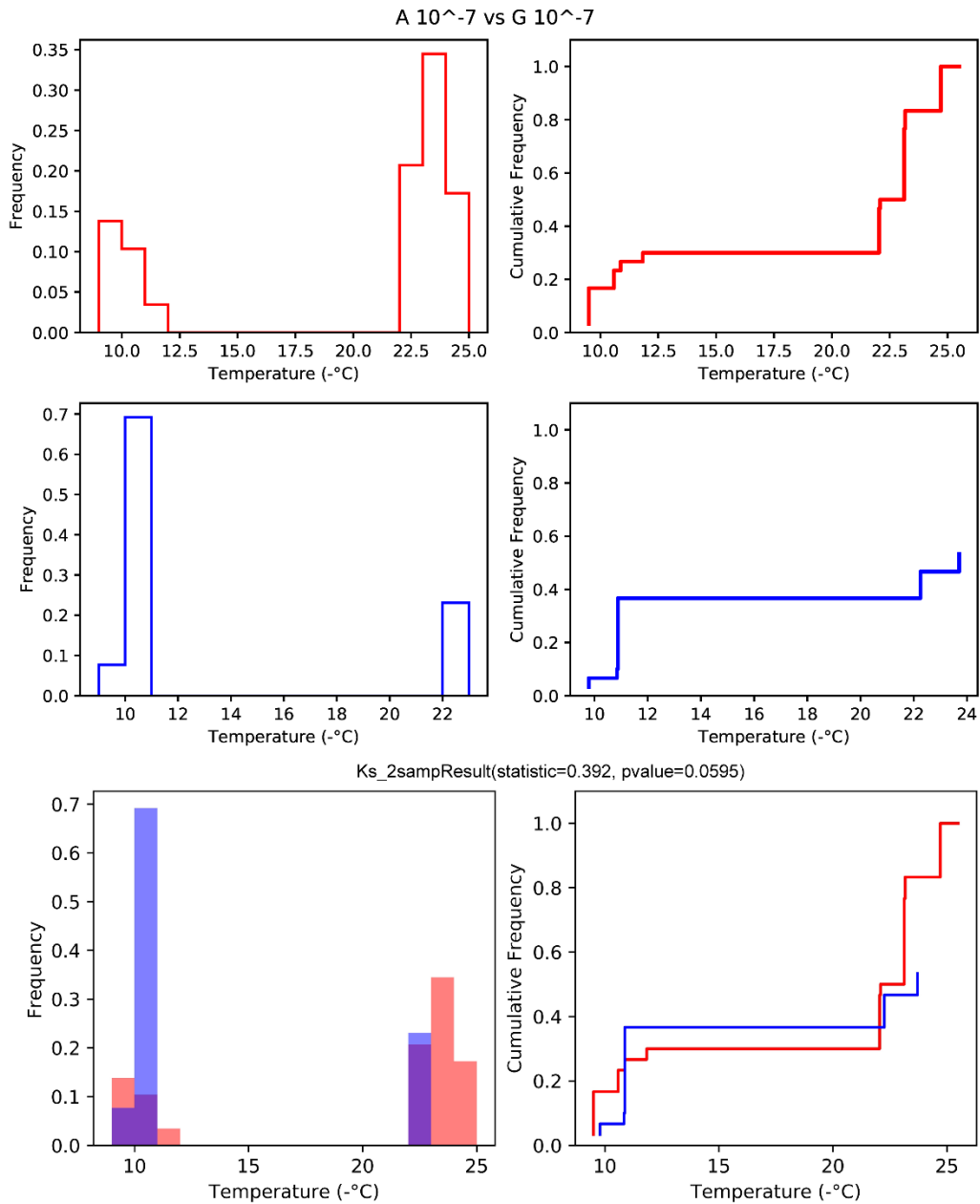


**Appendix B-1.** Comparison of droplet freezing temperature dispersion by Kolmogorov-Smirnov test. These results show the comparison between Asymptote freezer system and commodity freezer system. Both used  $10^{-4}$  mg/mL Snomax droplets.

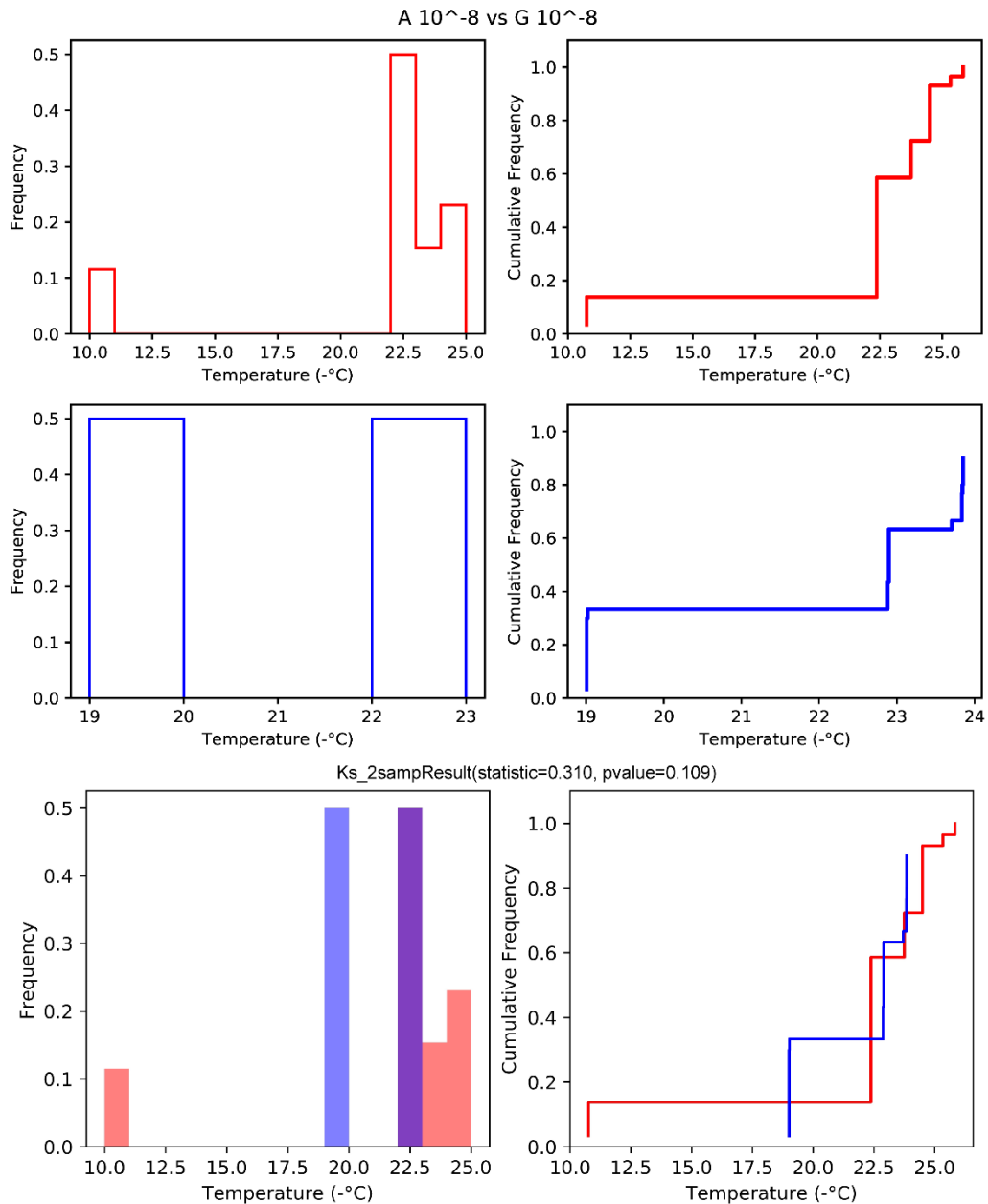


**Appendix B-2.** Comparison of droplet freezing temperature dispersion by Kolmogorov-Smirnov test. These results show the comparison between Asymptote freezer system and commodity freezer system. Both used  $10^{-6}$  mg/mL Snomax droplets.

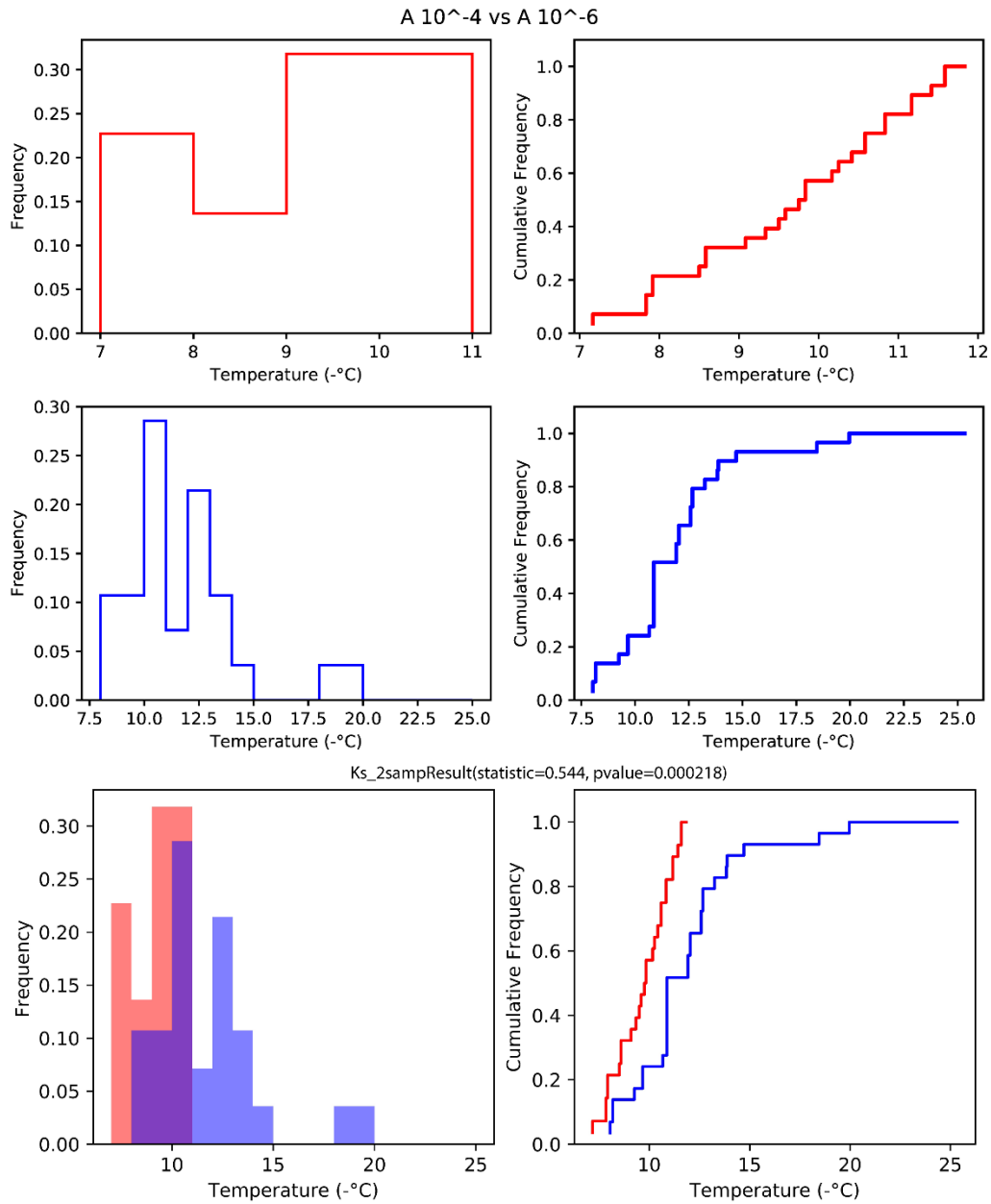




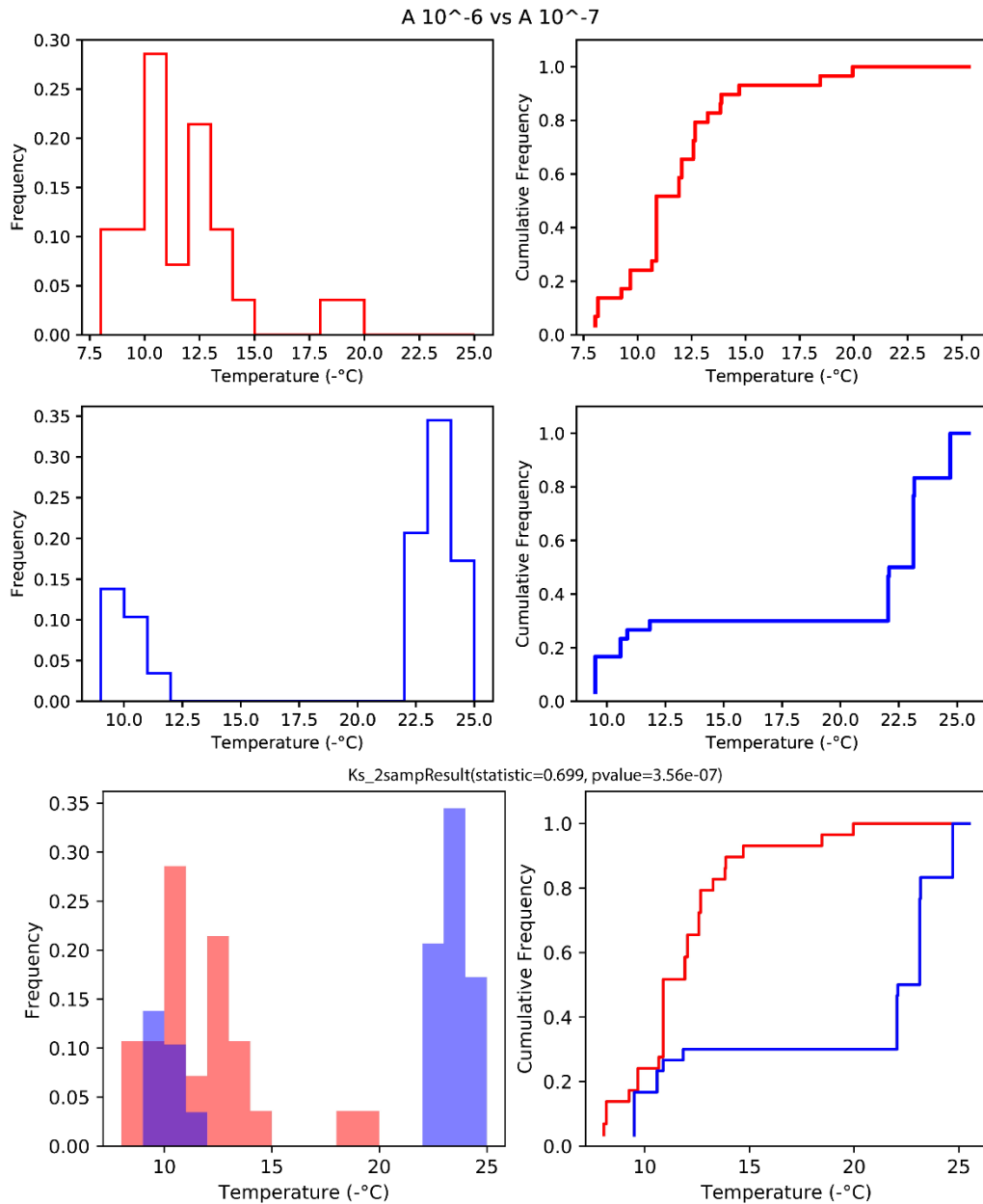
**Appendix B-3.** Comparison of droplet freezing temperature dispersion by Kolmogorov-Smirnov test. These results show the comparison between Asymptote freezer system and commodity freezer system. Both used  $10^{-7}$  mg/mL Snomax droplets.



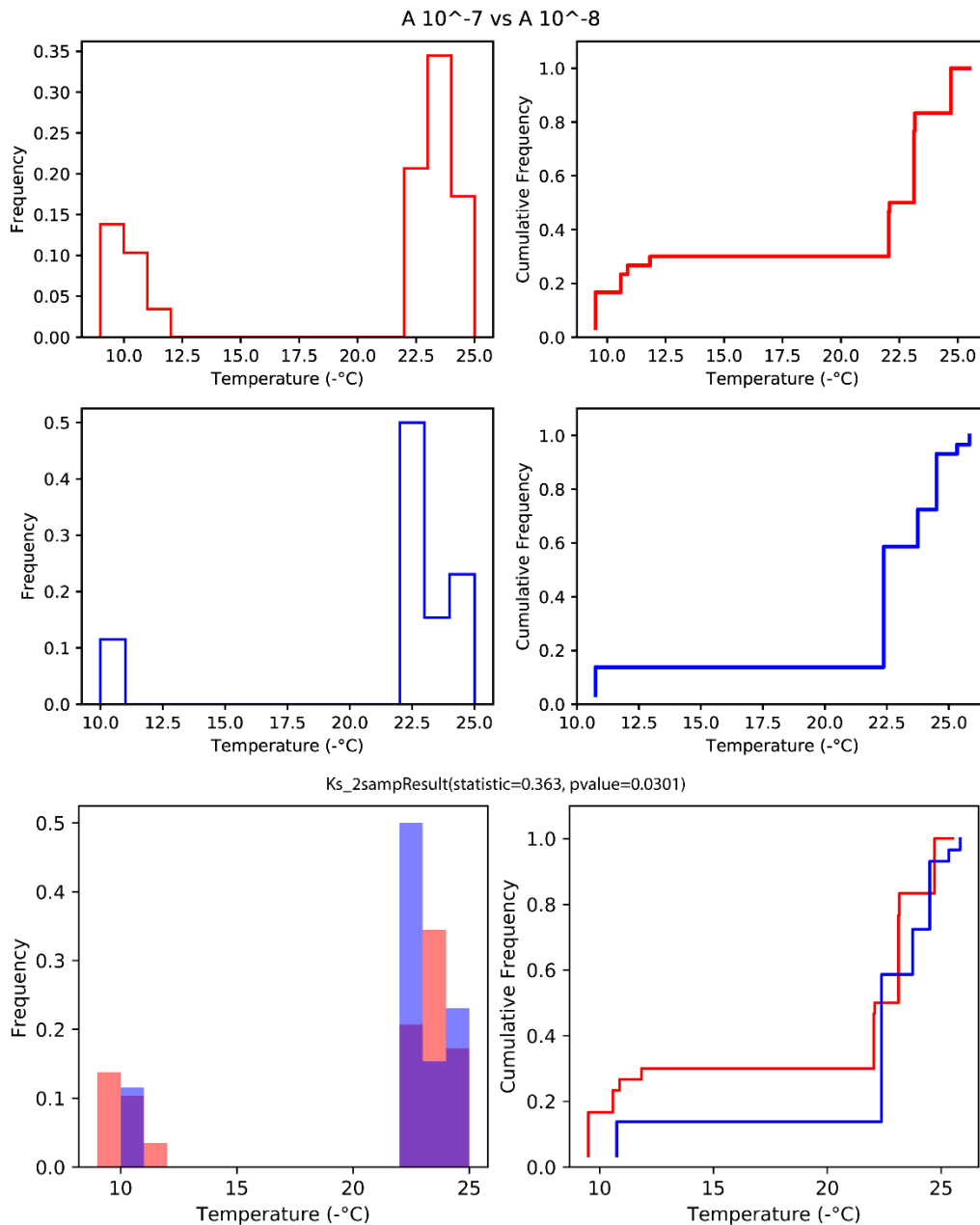
**Appendix B-4.** Comparison of droplet freezing temperature dispersion by Kolmogorov-Smirnov test. These results show the comparison between Asymptote freezer system and commodity freezer system. Both used  $10^{-8}$  mg/mL Snomax droplets.



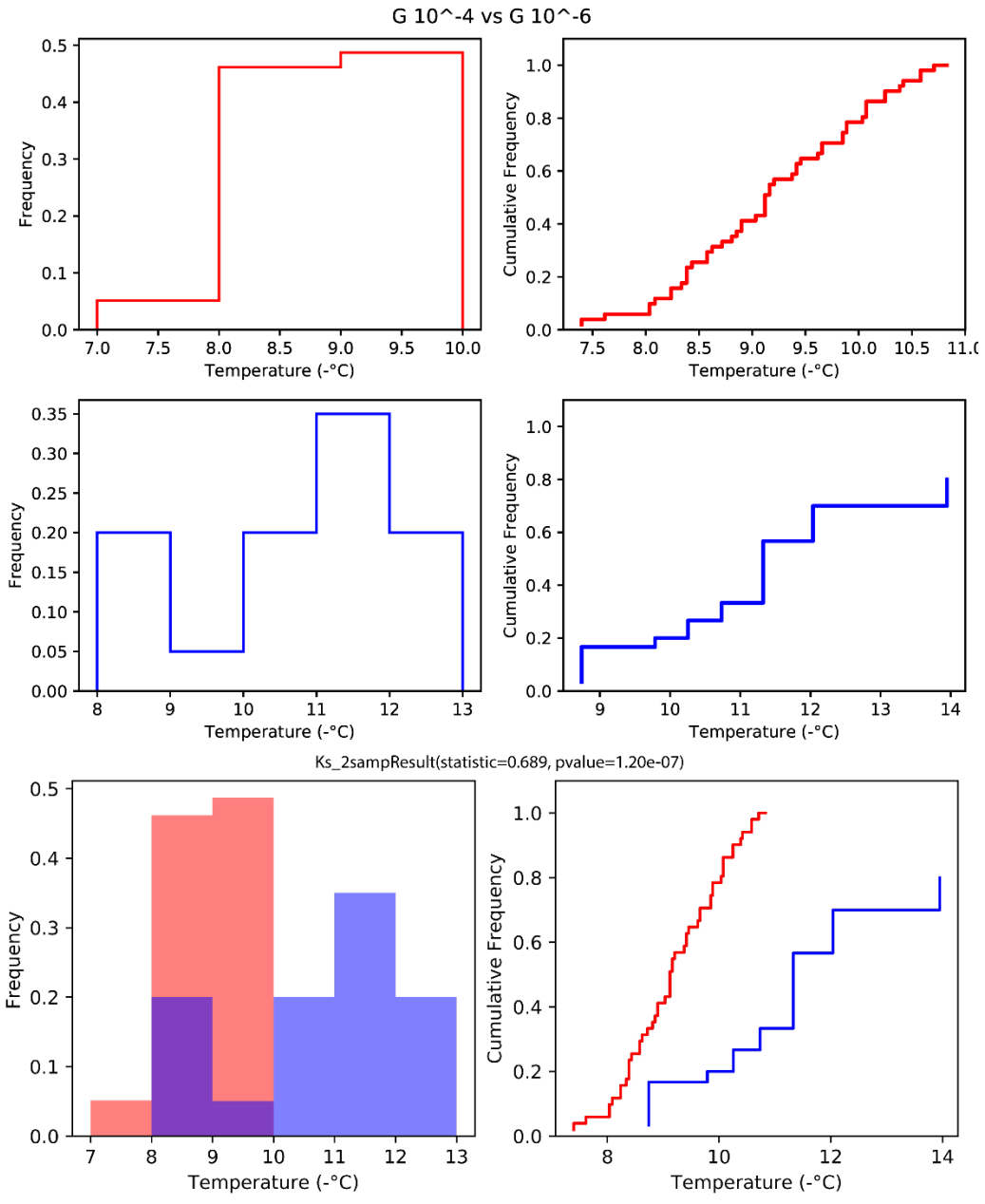
**Appendix B-5.** Comparison of droplet freezing temperature dispersion by Kolmogorov-Smirnov test. These results show the comparison between  $10^{-4}$  and  $10^{-6}$  mg/mL Snomax solution droplets in Asymptote freezer system.



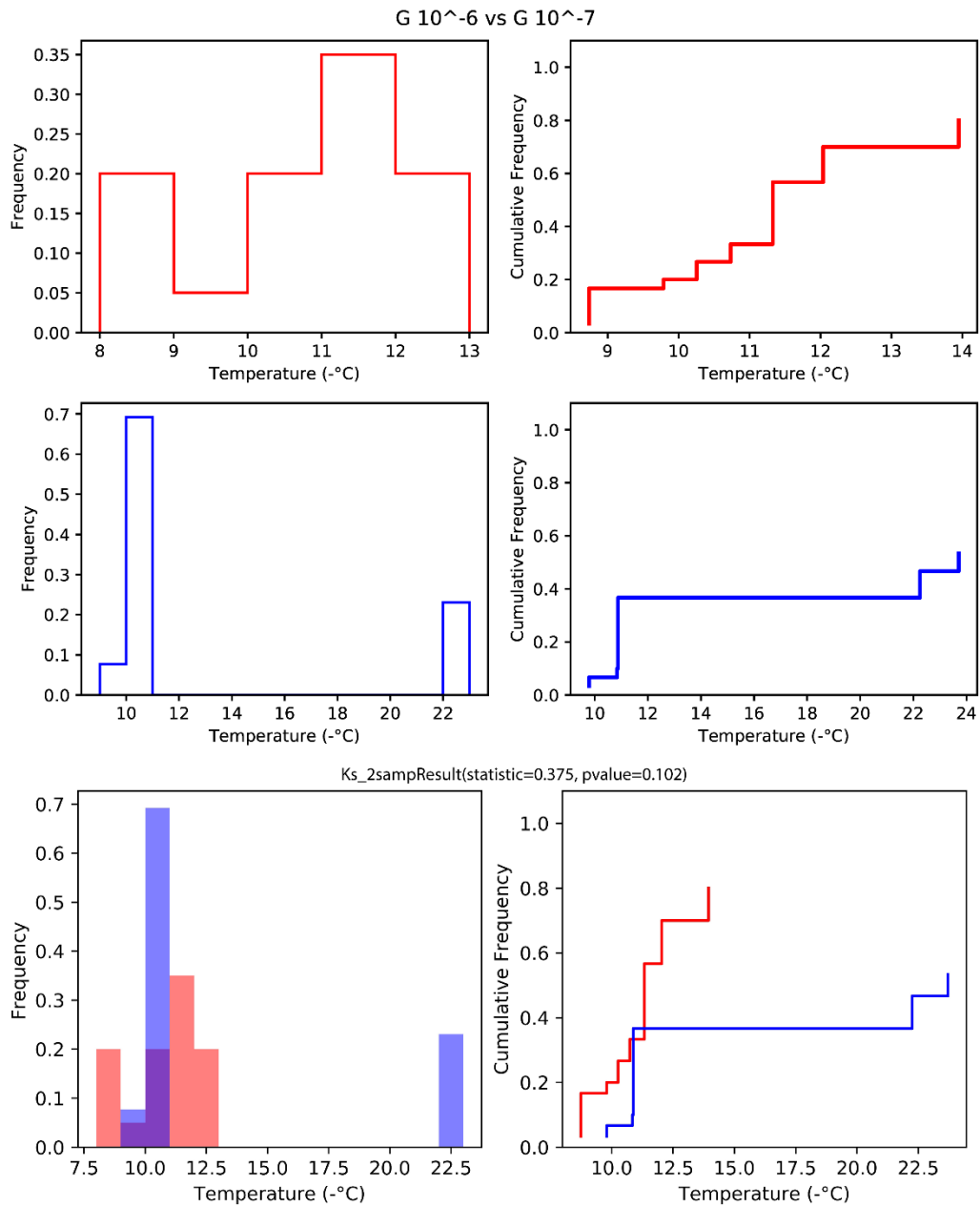
**Appendix B-6.** Comparison of droplet freezing temperature dispersion by Kolmogorov-Smirnov test. These results show the comparison between  $10^{-6}$  and  $10^{-7}$  mg/mL Snomax solution droplets in Asymptote freezer system.



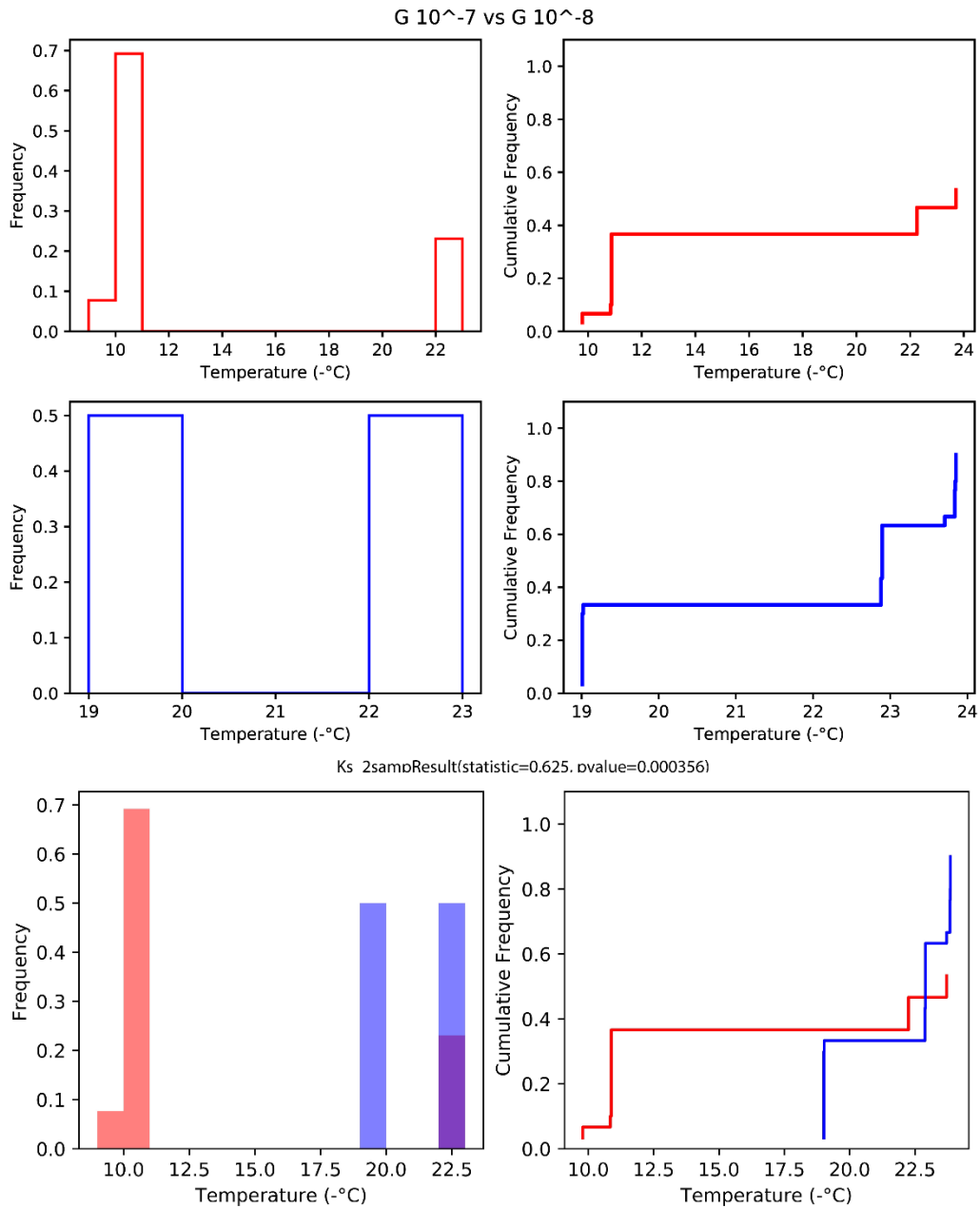
**Appendix B-7.** Comparison of droplet freezing temperature dispersion by Kolmogorov-Smirnov test. These results show the comparison between  $10^{-7}$  and  $10^{-8}$  mg/mL Snomax solution droplets in Asymptote freezer system.



**Appendix B-8.** Comparison of droplet freezing temperature dispersion by Kolmogorov-Smirnov test. These results show the comparison between  $10^{-4}$  and  $10^{-6}$  mg/mL Snomax solution droplets in commodity freezer system.



**Appendix B-9.** Comparison of droplet freezing temperature dispersion by Kolmogorov-Smirnov test. These results show the comparison between 10<sup>-6</sup> and 10<sup>-7</sup> mg/mL Snomax solution droplets in commodity freezer system.



**Appendix B-10.** Comparison of droplet freezing temperature dispersion by Kolmogorov-Smirnov test. These results show the comparison between 10<sup>-7</sup> and 10<sup>-8</sup> mg/mL Snomax solution droplets in commodity freezer system.



## Appendix B-11. Source Code for Matlab script Droplet\_Dispersion.m

Y. Kamijo, Droplet\_HT, (2019), GitHub repository,

[https://github.com/YukiK1201/Droplet\\_HT/blob/master/Droplet\\_Dispersion.m](https://github.com/YukiK1201/Droplet_HT/blob/master/Droplet_Dispersion.m)

```
close all;
clear all;

% select the droplet picture

i = 'Troy 2019-07-04 12h10m30s(Fluorescein).jpg'
img = imread(i);

rgb = imshow(img);
title('Draw circle to define ROI');
d = imdistline(gca,[100 100],[100 200]);

e = drawcircle('Color','k','Label','My Circle');
e.Deletable = false;

BW = createMask(e,img);
BW(:, :, 2) = BW;
BW(:, :, 3) = BW(:, :, 1);
ROI = img;
ROI(BW == 0) = 0;
figure, imshow(ROI);

% Change the circle diameter depends on the droplet size

[centers,radii] = imfindcircles(ROI,[4
9], 'ObjectPolarity','bright', ...
    'Sensitivity',0.93);

a = length(centers)
r = radii

imshow(ROI)
h = viscircles(centers,radii)

histogram(r)

% Write to csv file
```

```
T = table([r])  
writetable(T, 'DropDisperse.csv')
```

## Appendix B-12. Source Code for Matlab script Droplet\_plot.m

Y. Kamijo, Droplet\_HT, (2019), GitHub repository,

[https://github.com/YukiK1201/Droplet\\_HT/blob/master/Droplet\\_plot.m](https://github.com/YukiK1201/Droplet_HT/blob/master/Droplet_plot.m)

```
clear all;
close all;
disp('start')

% define your image
[files,dir,~] = uigetfile('*.JPG','Select multiple images',...
                        'MultiSelect','on');

repeating=1;
a = length(files)

% load the first file
img = imread(fullfile(dir,files{1}));

h_im = imshow(img);
title('Draw circle to define ROI');
d = imdistline(gca,[100 100],[100 200]);

% Draw circle to define ROI circle
e = drawcircle('Color','k','Label','My Circle');
e.Deletable = false;

for i = 1: a
    file = imread(fullfile(dir,files{i}));

    BW = createMask(e,file);
    BW(:,:,2) = BW;
    BW(:,:,3) = BW(:,:,1);
    ROI = file;
    ROI(BW == 0) = 0;
    figure, imshow(ROI);

    % Change the circle diameter depends on the droplet size, and
    % sensitivity to optimize the droplet detection
    [centers,radii] = imfindcircles(ROI,[15
    20],'ObjectPolarity','dark', ...
    'Sensitivity',0.95);

y = length(centers)
```

```

yC = num2str(y)

imshow(ROI)
h = viscircles(centers,radii);

prompt = {'Droplet number:'};
title = 'Input';
dims = [1 36];
definput = 136;
answer(i) = inputdlg(prompt,title,dims,definput)
end

prompt1 = {'Time(sec):','Max # of the droplets:'};
title1 = 'Time intervals';
dims1 = [1 36];
definput1 = {'10','30'};
sec = inputdlg(prompt1,title1,dims1,definput1)
s = cell2mat(sec)
s2 = str2num(s)
s3 = s2(1,1)

dmax = s2(2,1)

y2 = str2double(answer)
y3 = y2./dmax

x1 = 1:a
x2 = 1/60*s3
x = x1.*x2

scatter(x,y3)

xlabel('Time (min)');
ylabel('Frozen fraction');
ylim([0 1])

Time = x.';
FF = y3.';
T = table([Time],[FF])

writetable(T,'FF.csv')

```

### Appendix B-13. Source code for Python script KStest.ipynb

Y. Kamijo, Droplet\_HT, (2019), GitHub repository,

[https://github.com/YukiK1201/Droplet\\_HT/blob/master/KStest.ipynb](https://github.com/YukiK1201/Droplet_HT/blob/master/KStest.ipynb)

```
from scipy import stats
import numpy as np
from matplotlib import pyplot as plt
```

```
import pandas as pd
from pandas import DataFrame
```

```
# read input data file
df = pd.read_excel('KStest.xlsx')
df
```

```
list(df.columns.values)
```

```
#select the comparison data
asy = 'A 10-7'
gen = 'A 10-8'
```

```
title = asy + ' vs ' + gen
asyFF = asy + ' FF'
genFF = gen + ' FF'
print(title)
```

```
a = df[asy]
b = a.dropna()
c=b * -1
```

```
d = df[asyFF]
e = d.dropna()
```

```

o = df[gen]
p = o.dropna()
q = p * -1

r = df[genFF]
s = r.dropna()

stats.ks_2samp(c, q)

plt.figure(figsize=(8.5, 6.5), dpi=100)
plt.suptitle(title, fontsize=12)

plt.subplot(2,2,1)

bins = np.arange(np.floor(c.min()), np.ceil(c.max()))
plt.hist(c, bins=bins, density=True, histtype="step", color='red')
plt.xlabel('Temperature (-°C)')
# plt.ylabel('ylabel')

plt.subplot(2,2,2)
plt.step(c, e, color='red')
plt.xlabel('Temperature (-°C)')
plt.ylim((0, 1.1))
# plt.ylabel('ylabel')

plt.subplot(2,2,3)

bins = np.arange(np.floor(q.min()), np.ceil(q.max()))
plt.hist(q, bins=bins, density=True, histtype="step", color='blue')
plt.xlabel('Temperature (-°C)')
# plt.ylabel('ylabel')

plt.subplot(2,2,4)
plt.step(q, s, color='blue')
plt.xlabel('Temperature (-°C)')
plt.ylim((0, 1.1))
# plt.ylabel('ylabel')

```

```

plt.tight_layout()
plt.subplots_adjust(top=0.94)

plt.savefig('result1.eps', format='eps', dpi=1000)
plt.show()

fig = plt.figure()
fig = plt.figure(figsize=(8.5, 3.5), dpi=100)

ax = fig.add_subplot(1,2,1)

bins = np.arange(np.floor(c.min()),np.ceil(c.max()))
ax.hist(c, bins=bins, density=True, alpha=0.5, color='red')
ax.set_xlabel('Temperature (-°C)')
# plt.ylabel('ylabel')

bins = np.arange(np.floor(q.min()),np.ceil(q.max()))
ax.hist(q, bins=bins, density=True, alpha=0.5, color='blue')
ax.set_xlabel('Temperature (-°C)')
#plt.ylabel('ylabel')

ax2 = fig.add_subplot(1,2,2)

ax2.step(c,e, color='red')
ax2.set_xlabel('Temperature (-°C)')
ax2.set_ylim(0,1.1)
#plt.ylabel('ylabel')

ax2.step(q,s, color='blue')
ax2.set_xlabel('Temperature (-°C)')
ax2.set_ylim(0,1.1)
#plt.ylabel('ylabel')

fig.savefig('result2.jpg', dpi=1000)

```

`fig.show()`



## Appendix C: Supporting information for Chapter 4

### Appendix C-1. Source code for Python script Illuminaanalysis.ipynb

Y. Kamijo, LiGA analysis, (2019), GitHub repository,

<https://github.com/YukiK1201/LiGA/blob/master/Illuminaanalysis.ipynb>

```
import numpy as np
import pandas as pd
import pathlib
import os

# read input data file
dfO = pd.read_excel('normalized_input.xlsx')

dfO.rename(columns={'Unnamed: 0': 'Glycan'},
            inplace=True)
dfO.set_index('Glycan', inplace=True)
dfO

# Read test data file
dfT = pd.read_excel('normalized_test.xlsx')

# Sort columns in order
dfT1 = dfT.iloc[:, [0, 8, 7, 5, 6, 1, 2, 3, 4]]

dfT1.rename(columns={'Unnamed: 0': 'Glycan'}, inplace=True)
dfT1.set_index('Glycan', inplace=True)
dfT1

df1 = dfO.merge(dfT1, on='Glycan', how='outer')
df1

# Drop "???" row
df1 = df1.drop(['???'])

# Drop rows that have "NaN"
df1 = df1.dropna()
df1
```

```

from scipy import stats as st

# set P and R value cut-off
p = 0.1
r = 1.2

Rt = st.ttest_ind(df1.iloc[:,[3,5,7,9]], df1.iloc[:,[4,6,8,10]], axis=1)
pd.options.mode.chained_assignment = None # default='warn'

df1["pde1"] = Rt.pvalue
df1["rde1"] = (df1.iloc[:,[3,5,7,9]].mean(axis = 1)/
              df1.iloc[:,[4,6,8,10]].mean(axis = 1))

df1
df1.to_csv('analyzed.csv')
# Filter by p-value cut-off
dfP = df1[df1["pde1"] <= p]

# Filter by Ratio cut-off
dfPR = dfP[dfP["rde1"] >= r]

# Sort by ratios and save the data
dfPR_hits = dfPR.sort_values(by= ["rde1"], ascending= False)

dfPR_hits
dfPR_hits.to_csv('analyzed_hits.csv')

```

## Appendix C-2. Source code for Matlab script plotONEmaldi.m

J. Maghera, LiGA analysis, (2018), GitHub repository,

<https://github.com/YukiK1201/LiGA/blob/master/plotONEmaldi.m>

```
%%%%%%%%%%%%%%%%%%%%%%%%%%%%%%%%%%%%%%%%%%%%%%%%%%%%%%%%%%%%%%%%%%%%%%%%
%%%%%%%%%%%%%%%%%%%%%%%%%%%%%%%%%%%%%%%%%%%%%%%%%%%%%%%%%%%%%%%%%%%%%%%%
addpath (fullfile('/Volumes/Data/!! OUTLINES/Jasmine -
LiGA/MALDI/'));
%%%%%%%%%%%%%%%%%%%%%%%%%%%%%%%%%%%%%%%%%%%%%%%%%%%%%%%%%%%%%%%%%%%%%%%%
%%%%%%%%%%%%%%%%%%%%%%%%%%%%%%%%%%%%%%%%%%%%%%%%%%%%%%%%%%%%%%%%%%%%%%%%

manual = 0;
filename = '383.txt';
names = 'Tr36';
full_temp = 'Neu5Aca2-6Galb1-4GlcNAcb-Sp';
MW_DBCO = 287; %Use from 315 for "old DBCO" and 287 for new DBCO

XLIM1 = 4000;
XLIM2 = 8000;

%range around the peak for gaussian fitting and baseline fit
% first range is for a larger p8 peak
RANGE0 = 300;
% second range is for the glycan peak
RANGE = 125;

fid = fopen(filename,'r');
disp([names ' glycan is in ' filename ' ' fgetl(fid)...
char(10) fgetl(fid)]);

FORM = '%f %f %*[\n\r]';

AllVar = textscan(fid,FORM);
mass = AllVar{1};
intensity = AllVar{2};

disp(['Read ' num2str( size(mass, 1)) ' lines' ]);
fclose(fid);

IX = find(mass>XLIM1 & mass<XLIM2);

plot_mass = mass(IX);
plot_intensity = intensity(IX);
YMIN = min(plot_intensity);
YMAX = max(plot_intensity);
YH = YMAX-YMIN;
```

```

SCALE = 1000/YH;
plot_intensity = plot_intensity*SCALE;
YH = YH*SCALE;

YMIN = min(plot_intensity);
YMAX = max(plot_intensity);

margin = 0.1;

h = figure(1);
set(h, 'Units', 'normalized', 'position', [0.2 0.6 0.45 0.25] )

% find the full name based on abbreviated name

%%%%%%%%%% PLOT MALDI TRACE AND MAKE IT
PRETTY %%%%%%%%%%%
figure(1);
hold off;
plot(1,1);
hold on;
plot(plot_mass, plot_intensity, '-k');

% add full name of glycan to the title
title([names ' - ' full_temp]);

set(gca,'yscale','lin','xscale','lin',...
'TickDir','out');
ylabel('intensity');
xlabel('M/z');
xlim([4000 8000]);
ylim([YMIN - margin*YH YMAX + margin*YH]);
drawnow;
hold on;

IX2 = find ( plot_intensity == ...
max(plot_intensity(plot_mass>5000 & plot_mass<5500)) );
pVIII = plot_mass(IX2(1));

% define the RANGE and make sure it doesn't exceed the
boundaries

if IX2+RANGE0 > size(plot_intensity,1)
H = size(plot_intensity,1);
else
H = IX2+RANGE0;
end

if IX2-RANGE0 < 1
L = 1;
else
L = IX2-RANGE0;

```

```

end

initial_mass = pVIII;
initial_int = max( plot_intensity(L:H) );

% set the initial width wide enough to prevent fitting to noise.
init_width = RANGE0 / 2;

% fitting starting point and lower bounds
fo = fitoptions('Method','NonlinearLeastSquares',...
'StartPoint',[initial_int initial_mass init_width 1 1],...
'Lower', [initial_int/3 initial_mass-2*RANGE0 init_width/3 -100
-1000]);
ft = fittype('a1*exp(-((x-b1)/c1)^2)+e1*x+f1','options',fo);
f0 = fit(plot_mass(L:H),plot_intensity(L:H),ft);

X = plot_mass(L:H);
MASS_P8 = f0.b1;
MASS_P8_DBCO = MASS_P8 + MW_DBCO;

HEIGHT_P8 = f0.a1;
MAX_P8 = max(f0(X));

plot(X, f0(X), '-r');
plot(X, f0.e1*X + f0.f1, '-b');

% this is where thin vertical red line is drawn and the height
of
% this line is exactly the estimated height of the gaussian peak
% after the slanted baseline correction
line(MASS_P8*[1 1], [MAX_P8, MAX_P8-HEIGHT_P8], 'color','r');

text(MASS_P8*1.01, MAX_P8,...
['M(pVIII)=' num2str(round(MASS_P8)) char(10)...
'H(pVIII)=' num2str(round(HEIGHT_P8))],...
'VerticalAlignment', 'bottom',...
'HorizontalAlignment','left');

text(pVIII, YMIN, 'pVIII', ...
'FontWeight', 'bold',...
'VerticalAlignment', 'top',...
'HorizontalAlignment','center');

line(MASS_P8_DBCO*[1 1], YMIN + [0 0.3*f0.a1], 'color', 'r');
text(MASS_P8_DBCO, YMIN, ['pVIII' char(10) '+DBCO'], ...
'FontWeight', 'bold',...
'VerticalAlignment', 'top',...
'HorizontalAlignment','center');

```

```

%%%%%%%%%% EXTRACT THE FULL NAME AND MAKE GLYCAN
OBJECT %%%%%%%%%%%

sugar = GlycanLeaf.createObj(full_temp);

hold on; plot(1,1);

drawGlycan('input',sugar.String, 'XY', [7500 YMAX],...
'spacing', 150, 'angle', pi);

TEXT = ['MW=' num2str(round(sugar.MW)) char(10)];

DEBUG = 0;
[MW(char(10)),b,c] = sugar.MW;
if DEBUG

for j = 1:numel(sugar.glycans)
TEXT = [TEXT sugar.glycans{j} ...
': ' num2str(round(c(j) )) char(10)];
end
end

text(7500, 0.90*YMAX, TEXT, 'HorizontalAlignment', 'left',...
'VerticalAlignment', 'top');

% set(gca,'xtick',[], 'ytick',[])

%%%%%%%%%%
%%%%%%%%%%
MASS_P8_DBCO_GLY = MASS_P8_DBCO + MW(char(10));

line(MASS_P8_DBCO_GLY*[1 1], YMIN + [0 0.1*HEIGHT_P8], 'color',
'b');

text(MASS_P8_DBCO_GLY, YMIN, '*',...
'FontWeight', 'bold',...
'VerticalAlignment', 'bottom',...
'HorizontalAlignment', 'center');
text(MASS_P8_DBCO_GLY, YMIN, 'P+glycan',...
'FontWeight', 'bold',...
'VerticalAlignment', 'top',...
'HorizontalAlignment', 'center');

drawnow;

repeating = 1;
j=0;

while repeating>0
if manual
choice = questdlg('define a peak?',...
'define a peak?',...
'define a peak','no mo peaks','escape','define a peak');
switch choice
case 'escape', return;

```

```

case 'no mo peaks', repeating = 0; continue;
case 'define a peak',

[x]=ginput(1);

j = j+1;
lineX(j) = x(1);

end
else
j = j+1;
if j==1
% find the main peak
lineX(j) = MASS_P8_DBCO_GLY;

IX = (strcmp('Neu5Ac',sugar.glycans) |...
strcmp('Neu5,9Ac2',sugar.glycans) |...
strcmp('Neu5Gc',sugar.glycans) |...
strcmp('KDN',sugar.glycans) );

repeating = sum(IX);

elseif j==2 && repeating

IX = ~(strcmp('Neu5Ac',sugar.glycans) |...
strcmp('Neu5,9Ac2',sugar.glycans) |...
strcmp('Neu5Gc',sugar.glycans) |...
strcmp('KDN',sugar.glycans) );
Nsialo = sum( ~IX );

[~,~,c]= sugar.MW;

asialoMW = sum(c(IX)) - 18*(sum(IX)-1);

MASS_P8_DBCO_GLY = MASS_P8_DBCO + asialoMW;

lineX(j) = MASS_P8_DBCO_GLY;

line(MASS_P8_DBCO_GLY*[1 1], YMIN + [0 0.1*HEIGHT_P8], 'color',
'b');

text(MASS_P8_DBCO_GLY, YMIN, '*',...
'FontWeight', 'bold',...
'VerticalAlignment', 'bottom',...
'HorizontalAlignment', 'center');
text(MASS_P8_DBCO_GLY, YMIN,...
['-' num2str(Nsialo) 'xSialo'] ,...
'FontWeight', 'bold',...
'VerticalAlignment', 'top',...
'HorizontalAlignment', 'center');

repeating = 0;

end

% find the index of data nearest to the mouse click

```

```

IX2 = max ( find( plot_mass < lineX(j) ));

% define the RANGE and make sure it doesn't exceed the
boundaries

if IX2+RANGE > size(plot_intensity,1)
H = size(plot_intensity,1);
else
H = IX2+RANGE;
end

if IX2-RANGE < 1
L = 1;
else
L = IX2-RANGE;
end

initial_mass = lineX(j);
initial_int = max( plot_intensity(L:H) );

% set the initial width wide enough to prevent fitting to noise.
init_width = RANGE / 2;

fo = fitoptions('Method','NonlinearLeastSquares',...
'StartPoint',[initial_int initial_mass init_width 1 1],...
'Lower', [initial_int/3 initial_mass-2*RANGE init_width/3 -100 -
1000]);
ft = fitype('a1*exp(-((x-b1)/c1)^2)+e1*x+f1','options',fo);

f = fit(plot_mass(L:H),...
plot_intensity(L:H),ft);

X = plot_mass(L:H);
MASS(j) = f.b1;
HEIGHT(j) = f.a1;
MAX(j) = max(f(X));

plot(X, f(X), '-r');
plot(X, f.e1*X + f.f1, '-b');
line(MASS(j)*[1 1], [MAX(j), MAX(j)-HEIGHT(j)], 'color','r');

Delta(j) = round(abs(MASS(j)-MASS_P8_DBCO));
Ratio(j) = round(100*HEIGHT(j) / (HEIGHT(j) + HEIGHT_P8));

if j==1
text(MASS(j)+200, MAX(j)*0.7,...
['M=' num2str(round(MASS(j))) char(10)...
'dM=' num2str(Delta(j)) char(10)...
'R=' num2str(Ratio(j)) '%' char(10)],...
'VerticalAlignment', 'bottom',...
'HorizontalAlignment','left');
elseif j==2
text(MASS(j), MAX(j) + (MAX(j)-HEIGHT(j))*0.1,...
['M=' num2str(round(MASS(j))) char(10)...

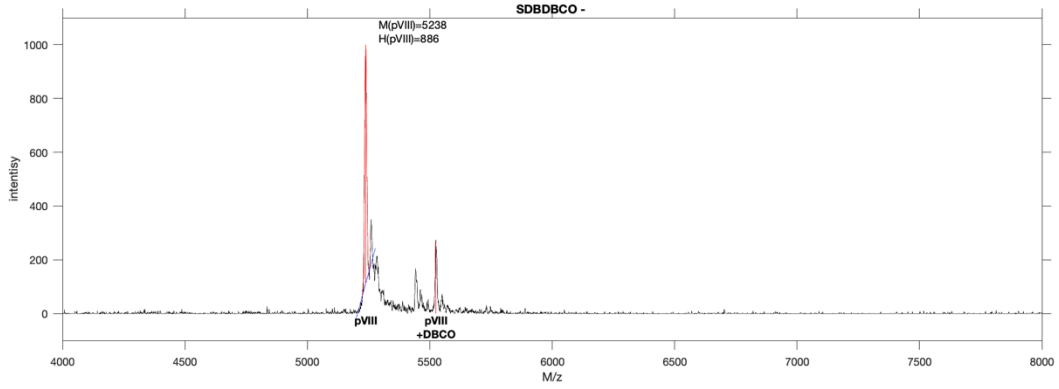
```



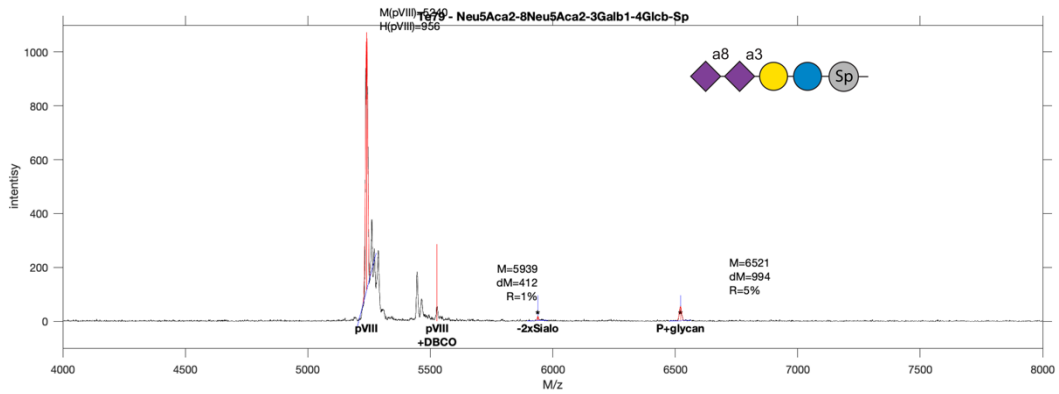
```
'dM=' num2str(Delta(j)) char(10)...  
'R=' num2str(Ratio(j)) '%' char(10)],...  
'VerticalAlignment', 'bottom',...  
'HorizontalAlignment', 'right');  
end  
  
end  
  
end
```

### Appendix C-3. MALDI measurement

#### SDB phage-DBCO conjugate

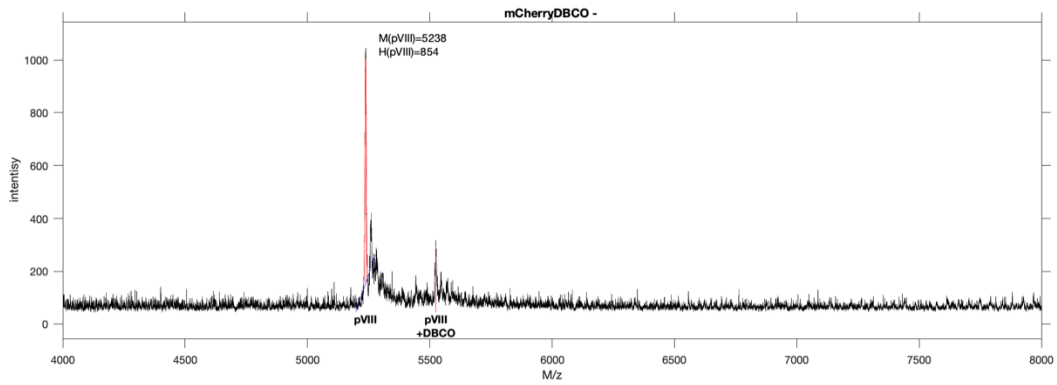


#### SDB phage-Neu5Ac(a2-8)Neu5Ac(a2-3)Gal(b1-4)Glc(b1- conjugate



## Appendix C-4.

### mCherry phage-DBCO conjugate



### mCherry-Gal(a1-4)Gal(b1-4)GlcNAc(b1-3)Gal(b1-4)Glc(b1-

